ABSTRACT

Title of Dissertation: SMART FOAM FOR ACTIVE VIBRATION AND NOISE CONTROL

Wael Nabil Akl, Doctor of Philosophy, 2004

Dissertation Directed By: Professor Amr M. Baz
Department Mechanical Engineering

A new class of smart foams is introduced to simultaneously control the vibration and noise radiation from flexible plates coupled with acoustic cavities. The proposed smart foam consists of a passive foam layer bonded to one surface of an active piezoelectric composite whose other surface is bonded to the surface of the vibrating plate. In this manner, the active piezoelectric composite can control from one side the porosity and the

acoustic absorption characteristics of the foam and from the other side can suppress the vibration of the flexible plate. With such capabilities, the proposed smart foam can simultaneously control structural and acoustic cavity modes over a broad frequency range.

A comprehensive theoretical study of the smart foam elements is introduced, in order to optimize the design and performance of this hybrid actuator. Feedback control of the reflected sound field was numerically and experimentally investigated, using an impedance tube, and showed a great improvement in the sound absorption coefficient.

A finite element model is developed to study the interactions among the foam, the active piezoelectric composite, the flexible plate and an acoustic cavity. The developed finite element model is a reduced 2-dimensional model based on the 1^{st} order shear deformation theory, which was compared with the original 3-dimensional model and it managed to capture all the dynamic characteristics of the foam provided a proper thickness to width ratio is maintained. The model enables the prediction of the plate vibration and the sound pressure level inside the acoustic cavity for a simple PD feedback control strategy of the active piezoelectric composite. It enables also the computation of the acoustic absorption characteristics of the foam. The predictions of the model are also validated experimentally.

The developed theoretical and experimental techniques will provide invaluable tools for the design and application of the proposed smart foam to a wide variety of systems such as passenger cars, helicopter, aircraft cabins and other flexible enclosures, where their operation as quiet platforms is critical to the success of their mission.

SMART FOAM FOR ACTIVE VIBRATION AND NOISE CONTROL

by

Wael Nabil Akl

Dissertation submitted to the Faculty of the Graduate School of the
University of Maryland, College Park in partial fulfillment
of the requirements for the degree of
Doctor of Philosophy
2004

Advisory Committee:

Prof. A. Baz, Chairman / Advisor
Prof. B. Balachandran
Assoc. Prof. N. Wereley
Assoc. Prof. D. Devoe
Asst. Prof. D. Hristu-Varsakelis

© Copyright by

Wael Nabil Akl

2004

ACKNOWLEDGEMENT

I would like to express my deep gratitude to my advisor, Dr. Amr Baz, for his continuous support, patience and encouragement throughout the course of this wok. I would also like to thank my committee members for taking the time to read my dissertation and provide me with valuable comments and suggestions. My thanks also go to the ARO, the sponsor of this research, and for Dr. Gary Anderson, the technical monitor for his invaluable input. In addition I would like to thank all my colleagues and co-workers at the Vibration and Noise Control lab for sustaining a healthy learning environment at the University of Maryland. Finally I would also love to thank my dear parents and wife for supporting me all this period and sustaining me with their love and prayers.

TABLE OF CONTENTS

LIST OF TABLES

LIST OF FIGURES

LIST OF ABBREVIATIONS

AC	Active Control
ACLD	Active Constrained Layer Damping
ANC	Active Noise Control
APDC	Active Piezoelectric Damping Composite
ASAC	Active Structural Acoustic Control
AVC	Active Vibration Control
EMDT	Electro-Magnetic Damping Treatment
FEM	Finite Element Modeling
LQG	Linear Quadratic Gaussian
MCLD	Magnetic Constrained Layer Damping
PCLD	Passive Constrained Layer Damping
PPF	Positive Position Feedback
PVDF	Poly Vinyl Dine Fluoride piezoelectric polymer
PZT	Lead-Zirconium Titanate Piezoelectric ceramics
SPN	Shunted Piezoelectric Network
X-LMS	Filtered Least Mean Square

NOMENCLATURE

A_f	First Lame' constant
b	viscous coupling factor between solid and fluid phases in the foam
B	Adiabatic bulk modulus for the acoustic medium
c	Speed of sound in the acoustic medium
$\left[c^E\right]$	APDC Short-circuit stiffness tensor
[C]	Vector defining the degrees of freedom to which the control effort is applied
D_{APDC_z}	APDC electrical displacement in the z-direction
e_s	Solid phase volumetric strain
e_x	Strain of the foam solid phase in the x-direction
e_y	Strain of the foam solid phase in the y-direction
e_z	Strain of the foam solid phase in the z-direction
e_{zz}	Normal strain in the APDC layer
$\{e_{APDC}\}$	Piezoelectric stress tensor
E'	Viscoelastic storage modulus
E''	Viscoelastic loss modulus
E_{1f}	Young's modulus of the solid phase
E_{2f}	Bulk modulus of elasticity of the fluid inside the pores
E_c	Young's modulus of the constraining layer material
E_p	Young's modulus of the plate material
E_v	Viscoelastic complex modulus
E_z	APDC electrical field in the z-direction
$\mathbf{F_{APDC}}$	Force vector applied by the APDC in the finite element model
F_{s_f}	Force exerted by the acoustic fluid on the foam
F_{s_p}	Force exerted by the acoustic fluid on the plate
g_p	Proportional feedback gain
g_d	Derivative feedback gain
G	Shear modulus for the viscoelastic layer
G'	Shear storage modulus of the viscoelastic layer
G''	Shear loss modulus of the viscoelastic layer
h_1	Thickness of the constraining layer
h_2	Thickness of the APDC layer
h_3	Thickness of the viscoelastic layer
h_4	Thickness of the base plate
h_f	Porosity of the foam
k	Incident acoustic wave number on the foam surface
k_1	Wave number of the first type of irrotational wave in the foam
k_2	Wave number of the second type of irrotational wave in the foam
k_t	Wave number of the rotational wave in the foam
k_x	x-component of the incident wave number

k_y	y-component of the incident wave number
$\mathbf{K_A}$	Acoustic element stiffness matrix
$\mathbf{K_c}$	Constraining layer element stiffness matrix
$\mathbf{K_f}$	Foam element stiffness matrix
K_g	Feedback complex gain.
$\mathbf{K_p}$	Plate element stiffness matrix
$\mathbf{K_{struct}}$	Overall structure element stiffness matrix
$\mathbf{K_v}$	Viscoelastic layer element stiffness matrix
m_{APDC}	Mass per unit volume of the APDC layer
m_c	Mass per unit volume of the constraining layer
m_p	Mass per unit volume of the base plate
m_v	Mass per unit volume of the viscoelastic layer
$\mathbf{M_{1\_f}}$	Fluid phase inertia and inertial coupling term in foam element mass matrix
$\mathbf{M_{1\_s}}$	Solid phase inertia and inertial coupling term in foam element mass matrix
$\mathbf{M_{2\_f}}$	Fluid phase viscous coupling term in foam element mass matrix
$\mathbf{M_{2\_s}}$	Solid phase viscous coupling term in foam element mass matrix
$\mathbf{M_A}$	Acoustic element mass matrix
$\mathbf{M_c}$	Constraining layer element mass matrix
$\mathbf{M_p}$	Plate element mass matrix
$\mathbf{M_{struct}}$	Overall structure element mass matrix
$\mathbf{M_v}$	Viscoelastic layer element mass matrix
N_f	Shear modulus of the foam solid phase
$N_{pb}(x, y, z)$	Shape function for composite plate transverse displacement (w)
$N_{pp}(x, y, z)$	Shape function for composite plate in-plane displacements (u, v)
P	Instantaneous pressure in the acoustic medium at (x,y,z)
P_0	Equilibrium pressure at (x,y,z)
p	Acoustic pressure at (x,y,z)
$\{\boldsymbol{p_e}\}$	Nodal pressure vector
q^2	Foam structure factor, quantifying inertial coupling between solid and fluid phases
Q_f	Coupling between the volume change of the solid and that of the fluid.
$\mathbf{Q_{nc}}$	Non-conservative force
R_f	Constant relating fluid stress and strain
R_{Ref}	Acoustic reflection coefficient from the foam
s_f	Pressure in the fluid phase of the foam
T_{APDC_xz}	APDC mechanical shear stress in xz plane
T_{APDC_z}	APDC mechanical normal stress in the z-direction
u_1	Displacement of the constraining layer in the x-direction
u_2	Displacement of APDC in the x-direction
u_3	Displacement of the viscoelastic layer in the x-direction
u_4	Displacement of the base plate in the x-direction
$\overline{u}_f$	Solid phase displacement vector
u_f	Solid phase displacement in the x-direction

$\overline{U}_f$	Fluid phase displacement vector
U_f	Fluid phase displacement in the x-direction
v_1	Displacement of the constraining layer in the y-direction
v_2	Displacement of the APDC in the y-direction
v_3	Displacement of the viscoelastic layer in the y-direction
v_4	Displacement of the base plate in the y-direction
v_f	Solid phase displacement in the y-direction
V_f	Fluid phase displacement in the y-direction
w_1	Displacement of the constraining layer in the z-direction
w_{1x}	Rotation of the constraining layer in the x-z plane
w_{1y}	Rotation of the constraining layer in the y-z plane
w_2	Displacement of the APDC in the z-direction
w_3	Displacement of the viscoelastic layer in the z-direction
w_4	Displacement of the base plate in the z-direction
w_{4x}	Rotation of the base plate in the x-z plane
w_{4y}	Rotation of the base plate in the y-z plane
w_f	Solid phase displacement in the z-direction
W_f	Fluid phase displacement in the z-direction
$\mathbf{W_{nc\_APDC}}$	Non-conservative work exerted by the APDC
z	Acoustic impedance
$\alpha(\theta)$	Absorption coefficient of the foam as a function of the incident angle
$\overline{\alpha}$	Random incidence absorption coefficient of the foam
$\{\boldsymbol{\delta}_\mathbf{f}\}$	Nodal deflection vector of the foam element
δ_{f_xyz}	Foam deflection vector at any point (x,y,z)
$\{\boldsymbol{\delta}_\mathbf{P}\}$	Nodal deflection vector of the plate composite
$\{\delta_{P\_xyz}\}$	Plate composite deflection vector at any point (x,y,z)
$\boldsymbol{\delta}_\mathbf{struct}$	Overall nodal deflection vector
ε_{33}^{S}	Clamped-body dielectric constant
ε_{APDC}	APDC strain tensor
ε_{APDC_z}	APDC mechanical strain in the z-direction
ε_{cb}	Constraining layer bending strain vector
ε_{cp}	Constraining layer in-plane strain vector
ε_f	Fluid phase volumetric strain
ε_{foam}	Strain vector in the foam
ε_{pb}	Base plate bending strain vector
ε_{pp}	Base plate in-plane strain vector
ε_{vb}	Viscoelastic layer bending strain vector
ε_{vp}	Viscoelastic layer in-plane strain vector
ε_{vs}	Conservative shear strain in the viscoelastic layer
Φ_i	Incident wave's acoustic velocity potential
Φ_r	Reflected wave's acoustic velocity potential
γ_{APDC}	APDC mechanical shear strain in x-z plane

γ_{APDC_y}	Shear angle of the APDC layer in the y-z plane
γ_{vx}	Shear angle of the APDC in x-z plane
γ_{vy}	Shear angle of the APDC in y-z plane
γ_{fxy}	Shear strain in the solid phase of the foam in the xy-plane
γ_{fxz}	Shear strain in the solid phase of the foam in the xz-plane
γ_{fyz}	Shear strain in the solid phase of the foam in the yz-plane
η_v	Viscoelastic loss factor
υ_c	Poisson's ratio of the constraining layer material
υ_f	Poisson's Ratio of the solid phase
υ_p	Poisson's ratio of the plate material
υ_v	Poisson's ratio of the viscoelastic layer material
θ	Wave incident angle
ρ	Instantaneous density of fluid in the acoustic medium at (x,y,z)
ρ_0	Equilibrium density at (x,y,z)
ρ_{1f}	Density of the foam solid phase
ρ_{2f}	Density of the foam fluid phase
σ_{APDC}	APDC stress tensor
σ_{cb}	Constraining layer bending stress vector
σ_{cp}	Constraining layer in-plane stress vector
σ_f	Stress vector in the foam
σ_{fx}	Normal stress in the foam solid phase in the x-direction
σ_{fy}	Normal stress in the foam solid phase in the y-direction
σ_{fz}	Normal stress in the foam solid phase in the z-direction
σ_{pb}	Base plate bending stress vector
σ_{pp}	Base plate in-plane stress vector
σ_{vb}	Viscoelastic layer bending stress vector
σ_{vp}	Viscoelastic layer in-plane stress vector
σ_{vsc}	Conservative shear stress vector in the viscoelastic layer
σ_{vsnc}	Non-conservative shear stress vector in the viscoelastic layer
τ_{fxy}	Shear stress in the solid phase of the foam in the xy-plane
τ_{fxz}	Shear stress in the solid phase of the foam in the xz-plane
τ_{fzy}	Shear stress in the solid phase of the foam in the yz-plane
ω	Excitation angular frequency
$\overline{\omega}$	Rotational strain component in the foam solid phase
$\overline{\Omega}$	Rotational strain component in the foam fluid phase
$[\Omega]$	Acoustic-Structure coupling matrix

CHAPTER 1

BACKGROUND

1.1 INTRODUCTION

In many commercial and military applications, vibration and noise radiation from vibrating systems play an important role in the performance and accuracy of operation of these systems. In manufacturing machinery, for example, the accuracy of machined parts depend to a great extent on the vibration induced either by rotation of the parts or by the inherent nature of the manufacturing operation itself. In military and aerospace applications, the accuracy of target positioning and target identification are highly dependent on the control of vibration of the observation platform. Noise, on the other hand is not only necessary for comfortable operation of commercial equipment (Conover and Ringlee, 1955), but is also essential in military applications to ensure stealth operation. Therefore, considerable attention has been devoted to reducing the vibration and noise of flexible structures using various passive as well as active control treatments.

1.2 OVERVIEW

1.2.1 Passive versus Active Control

In general, passive vibration and noise control are accomplished by taking advantage of specific physical properties of various damping materials in order to enhance the energy dissipation capability of the vibrating structures. Using, for example, viscoelastic materials bonded to the vibrating surface helps in increasing the overall damping characteristics of the resulting composite structure. This leads to a considerable reduction in the vibration over a certain frequency range. Sound absorbing materials bonded to sound radiating surfaces increase also the sound absorption characteristics of these surfaces, and consequently reduce the noise radiation over certain frequency bands.

The major obstacle in using such passive treatments is their limited ability to attenuate low energy and low frequency disturbances. Therefore many techniques have been developed by using active control means, which are suitable for such low-frequency applications, where passive treatment become highly ineffective.

In general, high-frequency disturbances are usually attenuated using passive treatments, whereas low-frequency disturbances cannot be affected except by using active control techniques.

1.2.2 Active Vibration Control

In active vibration control systems, the structural response is automatically modified by applying an external source of power to reduce the vibration. The major components of such systems are the following: a sensor to detect the vibration, an electronic controller to suitably manipulate the signal from the detector, and an actuator to influence the mechanical response of the vibrating structure. Such actuators can be either fully active or semi-active as classified by Fuller et al., (1997). Piezoelectric films, smart composites, and magnetostrictive elements are considered fully active actuating elements. With these types of elements, a secondary vibration response is generated in the structural system to destructively interfere with the disturbance. Semi-active elements act as tunable passive elements to effectively dissipate the vibrational energy from the structure. Electrorheological fluids and shape memory alloys are examples of this category of semi-active elements.

Different types of controllers have been used in active vibration control. Feedback as well as feedforward techniques have been reported in various applications for actively controlling the vibrations of structural systems.

1.2.3 Active Noise Control (ANC)

Generally, the concept of active noise control is based on sensing the noise at certain locations and submitting the measured signal to an external sound source via an appropriate controller, such as a loudspeaker to generate a secondary noise field to cancel

the original noise source. In this approach, feedback as well as feedforward techniques have been applied for noise cancellation. The pioneering work in this area was done by Lueg, (1936), where the external noise in the downstream of a duct is cancelled by generating a destructive sound wave by utilizing an error microphone, a controller, and a loudspeaker. The feedforward technique was first implemented by Conover and Ringlee (1955), where a reference signal is used along with the error microphone used in the work of Lueg.

1.2.4 Active Structural Acoustic Control (ASAC)

The concept of Active Structural Acoustic Control (ASAC) is based on applying active forces to the structure to control only the structural modes, which are efficient sound radiators. This is in contrast to Active Vibration Control (AVC) where the objective is to totally control the vibration of the structure, Fuller (1991).

1.2.5 Smart Foam

For effective vibration and noise reduction at low frequencies, a large amount of passive damping treatments is needed, making such passive methods impractical for a given application below some low-frequency limit. On the other hand, a fully active noise control approach becomes infeasible at high frequencies, due to the extensive computational requirements and associated implementation problems (Smith et al., 1999). Hence, it became obvious that combining the two approaches together can result in

broadband vibration and noise control capabilities. Therefore, hybrid passive/active noise control such as smart foams was implemented, in which the high absorption characteristics of the foam is utilized in the mid to high frequency range, and external sound source coupled to a proper control system is applied to achieve the required attenuation at low frequency range.

1.3 REVIEW OF LITERATURE

1.3.1 Introduction

In vibration control, the emphasis has been placed on hybrid passive/active structure treatments to combine the attractive characteristics of both types and to achieve high damping over a wide frequency range with minimum added weight. A review of individual passive as well as active treatments is necessary to better understand the benefits of hybrid vibration control approaches.

1.3.2 Passive Treatments

Passive treatments have been extensively utilized as a simple and reliable means for damping out the vibrations of different types of structures. These treatments rely in their operation on bonding a viscoelastic layer to the vibrating structure, in a constrained configuration, to attain high damping ratios (Alam and Asnani, 1984). However

extending the application of passive treatments to lower frequencies comes always at the expense of adding considerable weight to the vibrating structures. This poses a serious limitation to their practical use in many applications where the weight is of critical importance as stated by Baz and Ro (1996).

1.3.3 Active Treatments

Active vibration control, on the other hand, overcomes the limitations of the passive treatments, by being effective at low frequency ranges, without adding considerable weight to the vibrating structure. However, the main limitation of using active vibration control alone at higher frequencies stems from the fact that extensive computational requirements are needed for effective implementation of a proper controller. In addition, other drawbacks such as risk of instability due to control spillover and unreliability due to failure of sensors/actuators reduce the reliability of the active control systems.

Active structural vibration control has taken many shapes and forms depending on the type of sensor/actuator used, and on the type of controller implemented. Due to their flexibility and lightweight, piezoelectric actuators have been extensively used in active vibration control. Piezoelectric ceramics such as Lead-Zirconium Titanate (PZT) have been used as films for vibration suppression of beams by Blanguernon et al. (1999), plates by Yang and Chui (1993) and shell structures by Balamurugan and Narayanan (2001). Large force output and fast response are major advantages of using piezoceramic elements in active vibration control. Finite element as well as distributed parameter

models of the resulting composite structure containing the base structure and the embedded piezoelectric layer have been also developed for plates and shells.

More sophisticated applications of piezoelectric films in active-vibration control were also studied like the case of vibration suppression of a spacecraft flexible appendage on a flexible space simulator. Meyer et al. (1998) used both positive position feedback (PPF) as well as Linear Quadratic Gaussian (LQG) algorithms to suppress the vibrations of flexible structures. They found out that the PPF controller resulted in superior damping for single-mode control, while it did not show high effectiveness in the case of multi-mode excitations. LQG on the other hand was proved experimentally to be effective for multi-mode as well as single-mode excitations, but it was not as good as the PPF controller. Piezoelectric films were also used as sensors, utilizing the forward effect in measuring structural displacement in one or two directions as reported by Gu et al. (1994). They utilized two piezoelectric polymer Polyvinyledene Fluoride (PVDF) sensors located at 2 different locations to measure the response of the (3,1) mode of a simply-supported plate. This arrangement was used to replace the classical sensor shaping technique that may be inaccurate and cumbersome. They used feedforward X-LMS control algorithm acting upon a piezoceramic actuator and proved that for on- and off-resonant excitations, the PVDF sensors were superior to accelerometers.

In all these applications, the actuator is used to generate a vibration response to destructively interfere with the original disturbance resulting in vibration attenuation. In another approach shunted piezo-networks are used to dissipate structural vibration energy in a resistive load utilizing the forward piezoelectric effect. Such shunted piezo-networks have been extensively studied by Hagood and von Flotow (1991).

1.3.4 Hybrid passive/active treatments

Combining both passive and active treatments has been reported in literature in different forms utilizing different physical phenomena. Examples of these hybrid treatments include shunted piezoelectric networks (SPN) used by Orsagh and Ghoneim (1999), where a piezoelectric film is used to passively constrain the deformation of a viscoelastic layer that is bonded to a vibrating structure. The film is also used as a part of a shunting circuit, which is actively tuned to improve the damping characteristics of the treatment over a wide operating range. Active Constrained Layer Damping (ACLD) is another approach for hybrid passive/active vibration control (Baz, 1996). It consists of a conventional passive constrained layer damping which is augmented with efficient active control means to control the strain of the constrained layer in response of the structural vibrations. The viscoelastic damping layer is sandwiched between two piezoelectric layers as shown in Figure 1.1. The three-layer composite ACLD when bonded to the beam acts as a smart constraining layer damping treatment with built-in sensing and actuation capabilities (Baz and Ro, 1996; Chen and Baz, 1996). With appropriate strain control, the shear deformation of the viscoelastic damping layer can be increased, the energy dissipation mechanism can be enhanced and the structural vibration can be damped out.

A comprehensive study of the performance characteristics of ACLD was carried out based on closed-form expressions for the energy dissipation characteristics developed therein (Chen and Baz, 1996). Different applications of this type of treatment have been reported in literature.

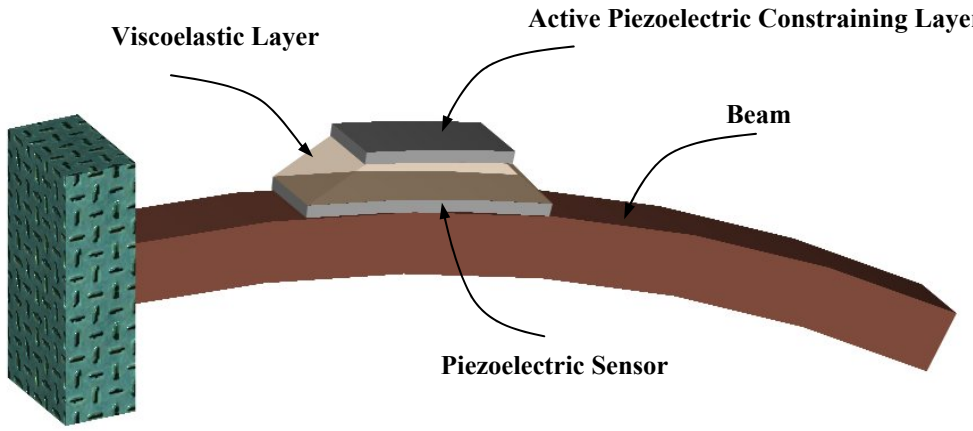

Figure 1.1: Schematic drawing for ACLD.

Shen (1994) used a full ACLD treatment to control the bending vibration of flat plates through the development of a distributed-parameter model to simulate the dynamics of this class of plates. Baz and Ro (1996) studied vibration control of plates using partial treatment with multi-patches of ACLD. A finite element model was developed to simulate the dynamics of plates/ACLD assemblies and experimentally verified. The experiment was conducted on a plate, which is excited by an electromechanical shaker driven by a sinusoidal or white noise signal. The amplitude of the vibration of the free end of the plate is monitored by using a laser sensor, as shown in Figure 1.2.

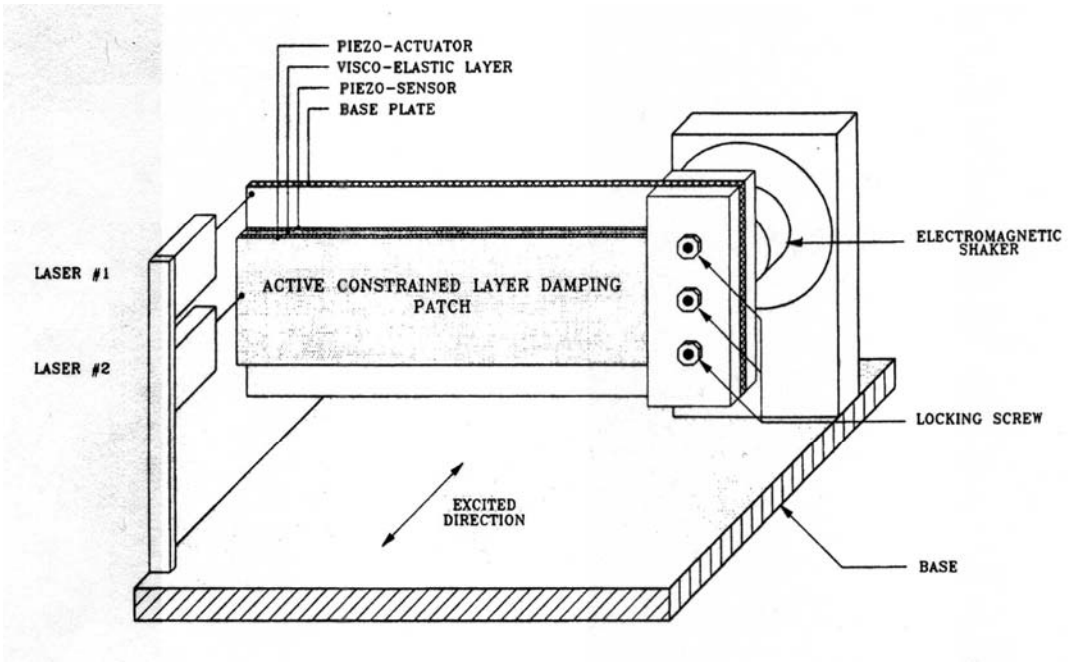

Figure 1.2: Experimental setup of Baz and Ro (1996).

Comparison between the ACLD and other treatments of beams controlled by active control and conventional passive constrained layer damping AC/PCLD has been carried out by Chen and Baz (1996). Based on this study, it is found that the ACLD outperforms AC/PCLD treatments in the case where the longitudinal rigidity of the base structure is higher than that of the piezo actuator, which is the case in most practical applications.

Another class of hybrid passive/active treatment is the Electro-Magnetic Damping Treatment (EMDT) (Oh, et al., 2000), in which viscoelastic damping layers are sandwiched between magnetic layers. The EMDT is an active version of the magnetic constrained layer damping (MCLD) (Ruzzene et al., 2000). The compression damping of the viscoelastic layer is controlled by using electro-magnetic actuators, which have a high control authority. In the EMDT, the damping mechanism is enhanced over the original

passive compression damping treatment. In this type of treatment, Oh et al. (2000) demonstrated the effectiveness of the EMDT as an active compression damping treatment in controlling the vibration of beams both theoretically and experimentally. They studied the vibration attenuation of two different configurations, CC (coil-to-coil) and CM (coil-to-magnet). A schematic representation of both configurations is presented in Figure 1.3. A finite element model for a laminated beam treated with EMDT was developed, and experimentally verified. Both the FEM and the experiments demonstrated considerable effectiveness in damping out the structural vibrations of the base beam.

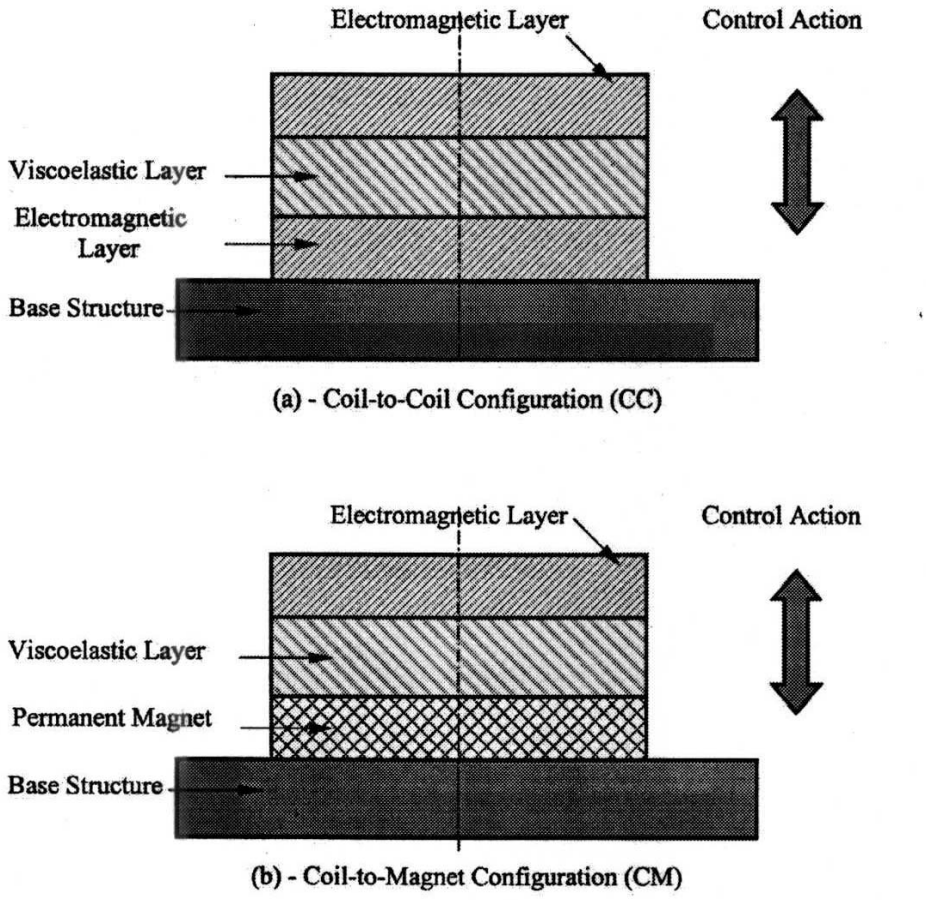

Figure 1.3: Schematic for EMDT configurations as reported by Oh et al. (2000).

By using 1-3 piezoelectric composites, we can have another form of applying hybrid passive/active treatment to vibrating structures for controlling both, structural vibration and associated sound radiation in acoustic cavities (Shields et al., 1998). This type of composites consists of an array of parallel piezoelectric ceramic rods embedded in a polymer matrix as shown in Figure 1.4.

The ceramic rods are poled along their longitudinal axis. When subject to an incident pressure field, the matrix transmits strain to the ceramic rods. This strain is transformed into electrical charge by the direct piezoelectric effect, producing a voltage difference between the electrodes placed at the extremities of the composite patch. Conversely, the application of an alternating current between the electrodes results in straining the ceramic rods and the coupled polymer matrix making the composite suitable to act as an actuator. These composites have found important industrial applications in underwater acoustics, ultrasonic actuators, and sensors for medical diagnostic devices as reported by Smith and Auld (1991) and Smith (1993) in addition to structural vibration and noise control (Shields et al., 1998). To act as sensitive transducers or powerful actuators, the piezoelectric material must efficiently convert the electrical input energy into mechanical energy (i.e. high electromechanical coupling factor). It must also be acoustically matched to bonded structure for optimum coupling of acoustic waves between transducer and the structure. Finally it should posses electric properties, which are compatible with the driving and receiving electronics (dielectric constant) as reported by Smith and Auld (1991). In addition to these requirements, it should not suffer from high electrical or mechanical losses, and not to mention, the additional advantages of lightweight and flexibility, which enable such actuators to be installed on complex structural shapes

(Portis, 1993). Only part of these requirements is present in conventional piezoelectric materials.

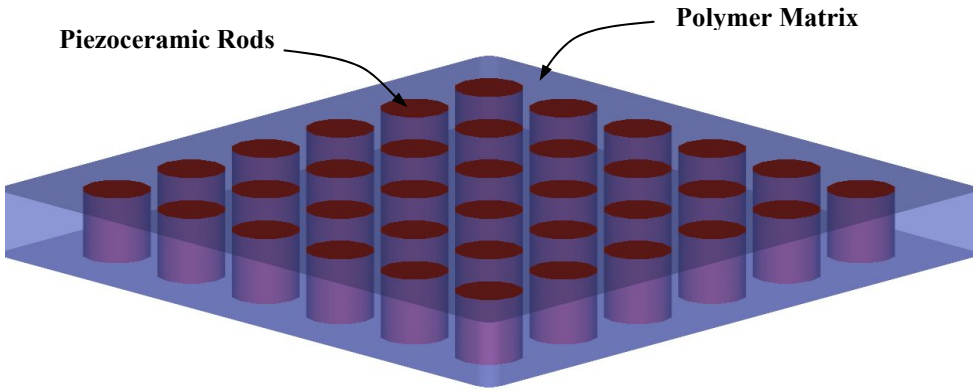

Figure 1.4: "1-3" piezocomposite (90°).

Several attempts for modeling "1-3" piezocomposites have been reported in literature. These attempts can be divided into two categories; the first is modeling the composites for hydrostatic response as developed by Smith (1993) and Avellaneda and Swart (1998). The second is modeling the composites for thickness-mode oscillations, reported by Chan and Unsworth (1989) and Smith and Auld (1991). In these attempts, certain assumptions have been made to facilitate simple modeling of the composite piezoceramic. these assumptions are summarized below:

1. Equal strains in vertical directions. This is true if the following is satisfied:
    - Composite has a fine spatial scale.
    - The polymer width is small compared to the shear wavelength at the driving frequency.

2. The electric field is taken to be the same on both phases (piezo-rods and polymer matrix).
3. The lateral stresses are assumed to be equal in both phases and that any lateral strain in the ceramic is compensated by a complimentary strain in the polymer.
4. The effective dielectric displacement is obtained by averaging over the contributions of the two phases.

However, for the hydrostatic response models developed by Smith (1993) and Avellaneda and Swart (1998), the third assumption was modified in a manner that the overall lateral strain in the composite is obtained through the superposition of the contributions from each phase.

In their research, Chan and Unsworth (1989) developed the thickness-mode oscillation model by using the aforementioned assumptions. They verified their model with experimental investigations by using PZT-7A ceramic and Araldite-D with hardener HY951. They found good agreement between the model data and the measured experimental results.

By using the same approach, Smith (1993) presented his model for thickness mode oscillation. He studied the effect of the ceramic rods periodic spacing on the bandwidth of the piezocomposite. He calculated also important transducer parameter, such as electromechanical coupling factor, specific acoustic impedance and longitudinal bulk velocity. The results obtained in his investigation are in homogeneity with those obtained by Chan (1989). Small variations arise from the different types of ceramic and polymers used in both researches, but the general trend is almost the same.

Extending his model of the "1-3" composites, Smith (1993) developed a model for hydrostatic response. He reported that in piezocomposites with the same fraction ceramic, but with finer spatial space, the axial force in the passive polymer is transferred to the active ceramic, whereas in the coarse spatial scale, much of the force on the polymer simply compresses the passive phase as shown in Figure 1.5. Therefore, a fine spacing should be always used.

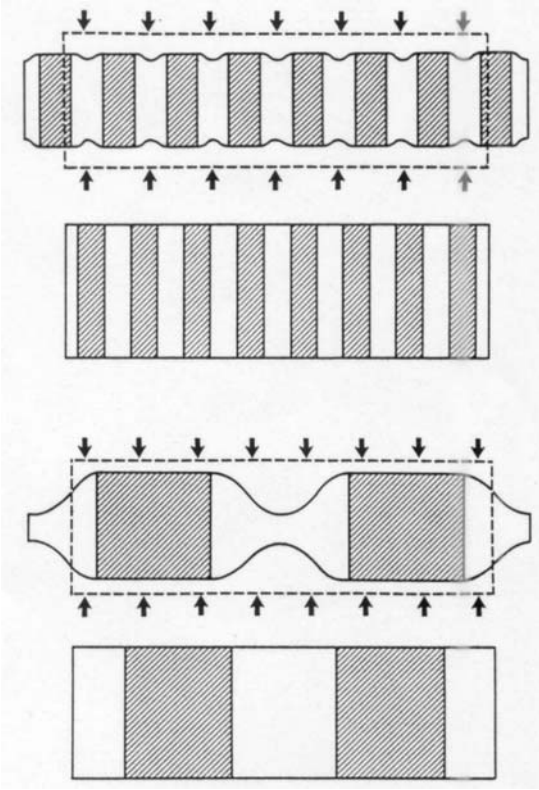

Figure 1.5: Schematic for the effect of spatial space on force transfer in "1-3" composites.

Avellaneda and Swart (1998) developed a detailed model for hydrostatic response of the "1-3" composites. The composite is treated as an equivalent homogeneous continuum or effective medium. This approximation was validated and resulted in good

approximation to the actual material response, provided the composite is made of regularly distributed, slender piezoelectric rods in a homogeneous matrix. Explicit formulae for calculating the hydrostatic parameters are also developed. The effect of Poisson's ratio on the hydrostatic charge coefficient, which is one of the important parameters characterizing the acoustic transducers, was also illustrated.

Detailed investigation for the role of matrix porosity and Poisson's ratio in increasing the piezocomposite transducers sensitivity was accomplished by Swart and Avellaneda (1994). Because of the highly anisotropic nature of piezoelectric materials, it is advantageous to align the most sensitive piezoelectric axis with the direction of the applied stressor electric field. However, for low frequency applications (e.g. underwater acoustics) the applied stress field is largely hydrostatic and consequently most commercial piezoelectrics display a severe degradation sensitivity and electromechanical efficiency. Combining, however, the ceramic with relatively compliant low-density polymers improves the transmission of acoustic energy, and if suitably engineered, can have a much larger sensitivity than a pure piezoelectric device. This is due to the Poisson's ratio effect (Swart and Avellaneda, 1994).

When subjected to a hydrostatic pressure field, uniaxial piezoelectric material suffers from high degradation in sensitivity, because the longitudinal and transverse piezoelectric coefficients are of opposite signs, resulting in overall reduction in hydrostatic piezoelectric coefficient as illustrated in Figure 1.6.

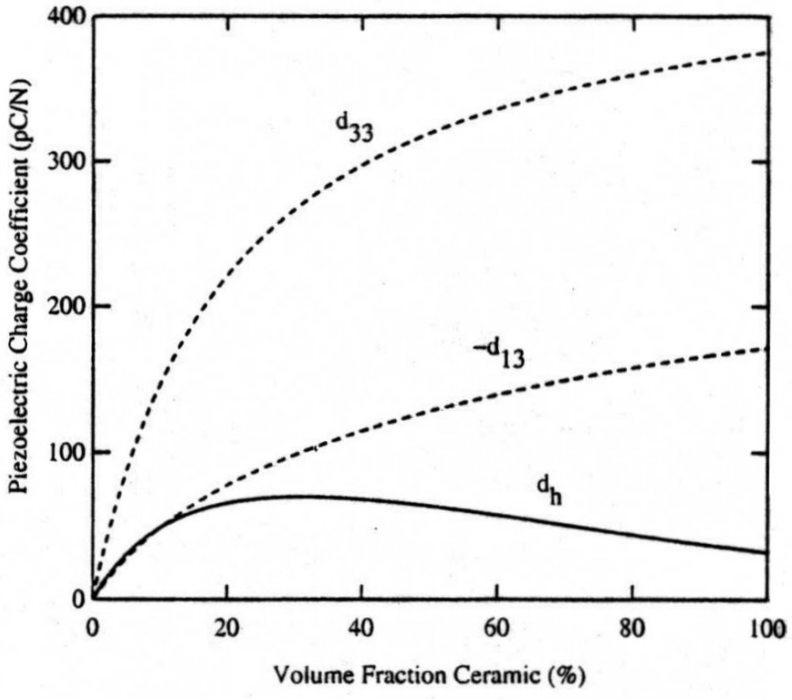

Figure 1.6: Effective hydrostatic piezoelectric constant.

Swart and Avellaneda (1994) showed that the use of a "1-3" PZT-5A polymer composite allows for the possibility of converting an applied hydrostatic field into a predominantly tensile stress on the rods. They also developed a criterion for selecting the polymer material to increase the hydrostatic piezoelectric coefficient, which defines the limit on Poisson's ratio as a function of the ceramic piezoelectric coefficients, along both the longitudinal and transverse directions. They also investigated the effect of adding porosity to the polymer matrix, and it was revealed that increasing porosity results in enhancement in hydrostatic piezoelectric coefficient Figure 1.7, but did not show great improvement for the hydrostatic coupling factor. In addition to their investigation, they considered also the effect of using matrix materials with negative Poisson's ratio and

predicted improvement in sensitivity and electromechanical coupling for all high-contrast polymer/piezoceramic systems.

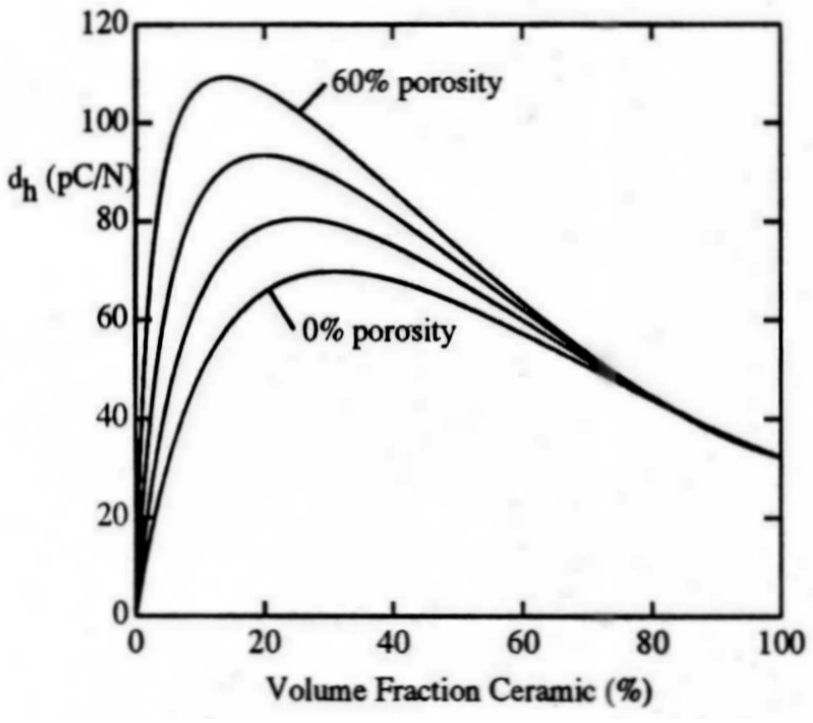

Figure 1.7: Effect of polymer porosity on piezoelectric coefficient.

Effect of polymer characteristics on piezocomposite performance was also investigated by Portis (1993) for structural damping applications. He developed a finite element model for the calculation of the piezocomposite performance. The advantages of the FEM over analytical methods, as reported by Portis, stem from the fact that analytical approach views the composite as a macro system by applying simplifying assumptions, while the FEM describes the detailed response of the composite. This appeared to be true if using a soft polymer, which violates the assumption of the two phases (ceramic and polymer matrix) moving together in the thickness direction. He studied 3 different types of polymer matrices; the first is using conventional rigid epoxy, the second is using soft

urethane, and the third is adding porosity to the soft urethane to increase the compressibility. Using solid epoxy was shown to constrain the displacement of the ceramic rods for the same excitation condition as in the case of the soft urethane. Adding, however, a rigid plate to the composite surface, to simulate a structure upon which the composite is installed, reduces the displacement to values comparable to the first case. Adding porosity to the soft urethane was reported to increase the displacement back to higher levels.

An alternate configuration of Active Piezoelectric Damping Composites (APDC) was introduced by Baz and Tempia (2004). In that configuration, the APDC are provided with piezo-rods that are obliquely embedded across the thickness in order to control both the shear and compression damping characteristics of the composite as shown in Figure 1.8. An analytical model based on the approach of Smith and Auld (1991) was introduced. The model was so modified to take into consideration the effect of the ceramic rods inclination angle. Estimation for the electromechanical coupling factor in both, the shear and the compression modes was also presented. The major thrust of that research was to determine the optimum inclination angle of the ceramic rods to yield the maximum overall electromechanical coupling factor. They found out that an angle of 28° was the optimum value, which corresponds to maximum electromechanical coupling factor as shown in Figure 1.9. It was reported that the overall coupling factor of the APDC at this angle is 16% higher than that of conventional APDC. The investigation was carried out using PZT-5H ceramic rods embedded inside different types of polymers.

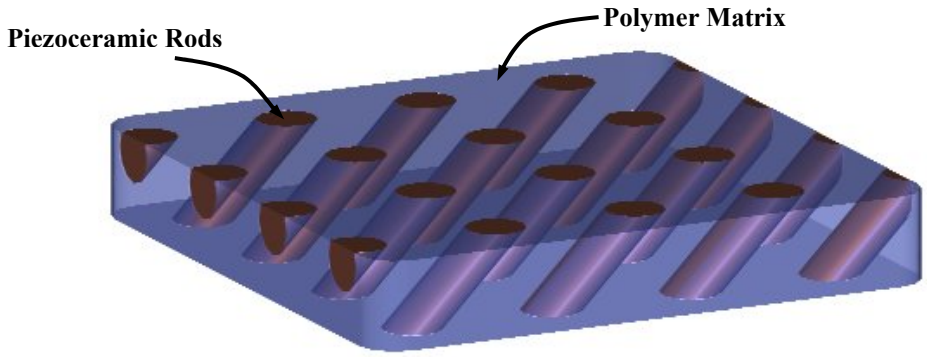

Figure 1.8: 1-3 piezocomposite (45°).

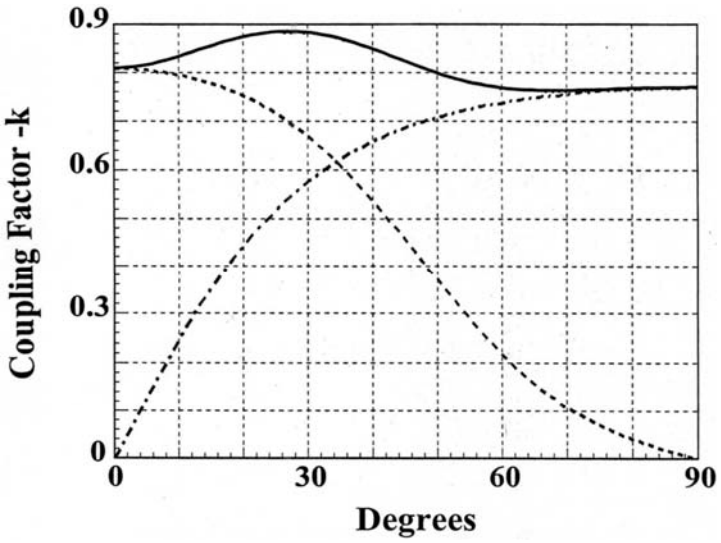

Figure 1.9: Effect of inclination angle on the electromechanical coupling factor. (Baz and Tempia, 1998).

A comprehensive finite element model for the newly proposed configuration of APDC with ceramic rods obliquely embedded in a polymer matrix was developed by Arafa and Baz (2000). They applied their model to the vibration control of a beam with a single patch of APDC, which is constrained from the top with a solid constraining layer. Results obtained in their research show a good improvement in

vibration control of the first two modes of the beam using ceramic rods inclination angle of 30-45°.

1.3.5 Noise Control

Because of the interest in attenuating internal noise levels in aircrafts, moving vehicles and many commercial equipment, noise control has undergone intensive investigations. These investigations involved the theoretical modeling of the mechanisms of sound radiation such as presented by Kinsler, et al. (2000), or in different approaches for reducing the noise level inside cavities.

Noise control can take two different forms. In the first approach, noise attenuation inside the cavities can be obtained by destructive interference of sound pressure waves. This can be achieved by placing a set of sound sources around the primary noise source or at certain locations inside the enclosure, where noise attenuation is required, to generate sound waves attenuating the original noise field. This approach was adopted by Elliot et al. (1990), and criticized by Fuller et al. (1991). In 1990, for example, Elliot et al. controlled actively the in-flight cabin noise induced by the twin turboprops of a passenger aircraft. They used 32 microphone sensors and 16 loudspeakers, placed at various positions within the cabin, as the secondary acoustic sources. A reduction of 13 dB at the blade frequency was reported. In their work, they used LMS adaptive algorithm.

On the other hand, controlling the structural vibration modes, which are efficient sound radiators is another method denoted in literature by “Active Structural Acoustic

Control (ASAC)". Such vibration modes are the low order odd modes, since the even modes form a dipole like radiators, which are inefficient in sound radiation. Fuller et al. (1991), Pan and Hansen (1991) and Clark and Fuller (1992) adopted this method. Fuller et al. (1991) conducted an experimental investigation for comparing both approaches. They discussed the main disadvantage of using active noise control with secondary sound sources, which is mainly the number of acoustic sources needed to control multi-mode radiation. This situation is likely to be of some trouble, when the modal resonant frequencies are high for a fixed sized panel as for example for thicker panels. Thus, a typical control installation may require many acoustic sources particularly when higher panel modes are being excited. It was also reported that it is necessary to create a control pressure distribution very close in phase and amplitude to the noise field radiated from the panel surface, but with a 180° phase shift. This obviously implies the use of many small acoustic sources of appropriate strengths and phases close to the panel surface. Fuller et al. (1991) compared experimentally the performance with a single-point control force applied directly to the vibrating panel to actively suppress the high sound radiating vibration modes, and using one to three secondary acoustic sources to actively attenuate the noise in front of the vibrating panel. It was concluded that the first method is more effective than the second one, even if the sound sources are placed suitably phased array close to the panel surface. The results obtained are justified, because the vibration response of all significant panel modes, non-resonant as well as resonant, was reduced, thus ensuring that the noise radiation was always globally minimized. For the resonantly vibrating panel on the other hand, which are subject to acoustic control using secondary sound sources, the mechanism responsible for a reduction in the radiated sound was

based on altering the radiation impedance seen by the panel and thus reducing the radiated power and changing the directivity pattern. This was achieved with little change in either the phase or the amplitude of the panel vibration.

Pan and Hansen (1991) tried to experimentally verify the theoretical results previously obtained (Pan et al. 1990), where it was concluded that, if the system response is dominated by panel-controlled modes, minimum sound energy is obtained by suppressing the panel vibration. If the system response, however, is dominated by cavity-controlled modes, the control force must be used to adjust the panel velocity distribution so that the real part of the power radiated from the panel into the cavity is minimized. The latter case may result in increasing locally the reactive power flow, leading to increased panel vibration. Pan and Hansen (1991) conducted experiment on a sound cavity formed from thick concrete slabs, and covered by a 6 mm thick aluminum plate. The external sound source was a horn driver that was located above the panel, outside the enclosure. The control was applied using an electromagnetic exciter that was located 2 mm above the panel. The response of the panel-cavity system was examined at two driving frequencies; the first one was at a resonance dominated by a cavity-controlled mode, and the other one was at a resonance dominated by a panel-controlled mode. In the first case, the overall panel vibration level was observed to increase when the control force was used to minimize the sound pressure. On the other hand, when controlling the second frequency, that was a panel-controlled mode, the amplitude of the vibrating panel was reduced when trying to minimize the sound pressure at the interior microphone location.

Using distributed actuators, such as piezoelectric patches instead of point forces acting on a vibrating panel to control the high sound radiating modes, was investigated by

Fuller et al. (1991) and Clark and Fuller (1992). Fuller et al. described the disadvantages of using point forces as control inputs, as being coupled into all possible structural modes, which may lead to a degradation of control performance due to control spillover. This is in addition to the difficulty in applying such control technique outside the laboratory, because of usual space constraints and mounting problems involved with this type of devices. Fuller et al. conducted their experimental investigation on a simply-supported steel plate that was driven with electromagnetic exciters from the back. Vibration response as well as the sound field in front of the panel was measured. Focus was placed on controlling the (1,1) and (3,1) modes, therefore a piezoelectric actuator was bonded at the middle of the panel, to be of highest control authority for these two modes. Good potential of the used actuator in achieving high global sound attenuation was demonstrated.

Clark and Fuller (1992) extended this study by conducting a similar experiment on a steel plate, excited with a steady-state harmonic disturbance generated by a shaker attached from the back and controlled with three piezoelectric patches installed on the front face. Two different configurations of the piezo-patches were investigated. They used filtered X-LMS adaptive control algorithm due to its effectiveness as narrow-band controller, and which in contrast to feedback approaches, requires lower degree of system modeling. On as well as off-resonance cases were studied. For on-resonance cases, only marginal improvement in sound attenuation was observed by increasing the number of piezoelectric actuators, since the acoustic response on resonance is usually dominated by only one mode. For the off-resonance cases on the other hand, increasing the number of control actuators was directly correlated with improvement in sound attenuation. Proper

selection of the position of the actuators was also reported to be essential in achieving good results. Due to its high capability in energy dissipation and its lightweight, the ACLD treatment was utilized for controlling sound radiation from plates into enclosures (Poh et al. 1996). In their research, they used filtered X-LMS adaptive control algorithm in controlling the sound field emitting from an aluminum plate into an acoustic cavity. An external speaker was used to excite the aluminum plate. Error signal required for the LMS algorithm was generated using either an error microphone placed inside the cavity or a laser sensor for plate vibration monitoring. Another microphone was located at the far end of the cavity to test the global attenuation of noise as shown in Figure 1.10. The PCLD/AC treatment was also applied and compared with ACLD results. Results obtained demonstrate the high capability of ACLD treatment in noise attenuation. Convergence time for the case of ACLD was 1.4 seconds in comparison to 20 seconds in the case of PCLD/AC. The control voltage required by ACLD to control the sound radiation was reported to be three times lower than that required by PCLD/AC.

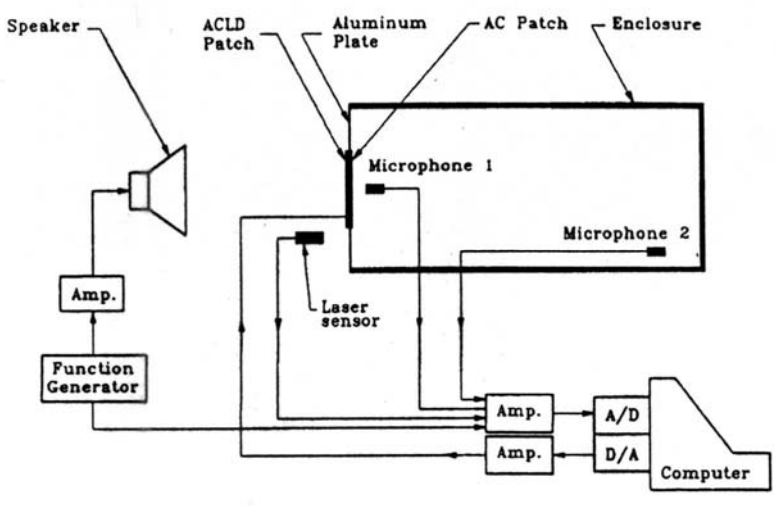

Figure 1.10: Experimental setup as conducted by Poh et al. (1996).

Ro and Baz (1999) extended the above study by developing a finite element model to simulate the dynamics and control of sound radiation of plate/cavity coupled systems using ACLD and PCLD/AC. Derivative feedback control was implemented in the study. The accuracy of the developed finite element model was experimentally validated. The results obtained indicated that ACLD treatments have produced significant attenuation of the structural vibration and sound radiation as shown in Figure 1.11.

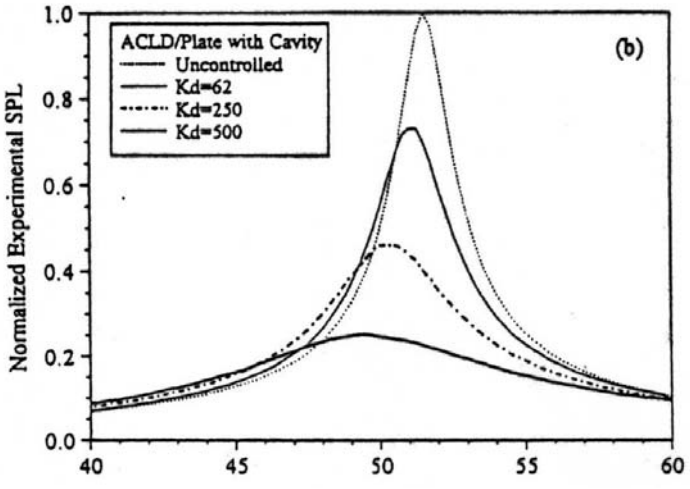

Figure 1.11: SPL attenuation as achieved by Ro and Baz (1999).

In an attempt to utilize another type of hybrid passive/active treatments, Shields et al. (1998) demonstrated the potential and the effectiveness of the APDC treatments in controlling the structural vibrations and associated sound radiation in acoustic cavities. In their study the APDC was used to control vibration and noise radiation below frequencies lower than 100 Hz, which are typical of large flexible structures, such as satellites, aerospace structures and helicopters.

A finite element model that simulates the dynamics and control characteristics of the plate/APDC/cavity system was developed in which both proportional and derivative feedback control were considered. Experimental setup used is illustrated in Figure 1.12. APDCs with hard and soft matrices were examined. It was revealed that the hard matrix composite resulted in more effective attenuation of the vibration and sound radiation than the softer one while using lower control voltages.

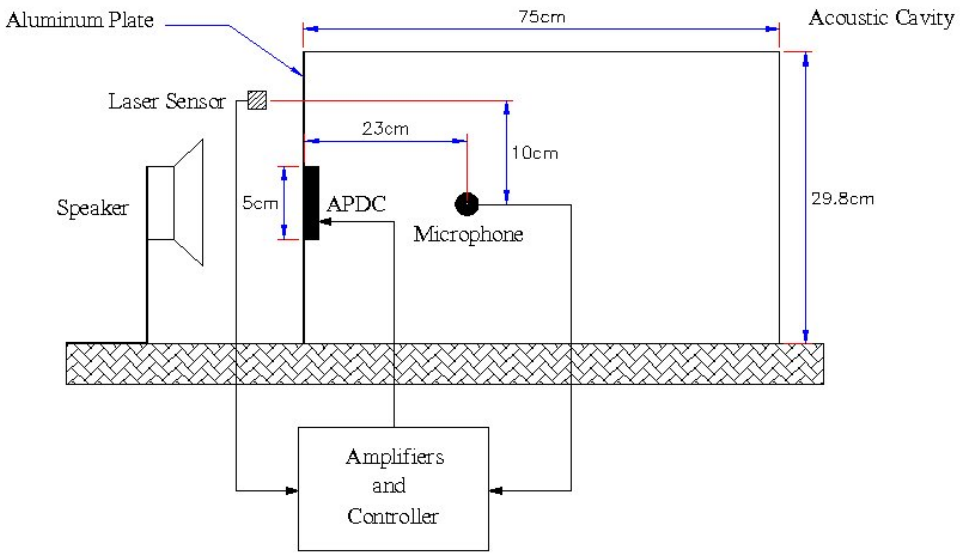

Figure 1.12: Experimental setup as conducted by Shields et al. (1998).

1.3.6 Smart Foam

A review of the modeling and application of impedance tube is carried out because the importance of the impedance tube in assessing the acoustical properties of the smart materials considered in this investigation.

A standard type of the impedance tube is shown in Figure 1.13. It consists of a rigid duct with a speaker located at one end and the material under investigation at the other end. Two microphones are located in-between for measuring the transfer function at two different locations to calculate the different normal incident acoustic properties of the inserted material (ASTM Standards, 1998).

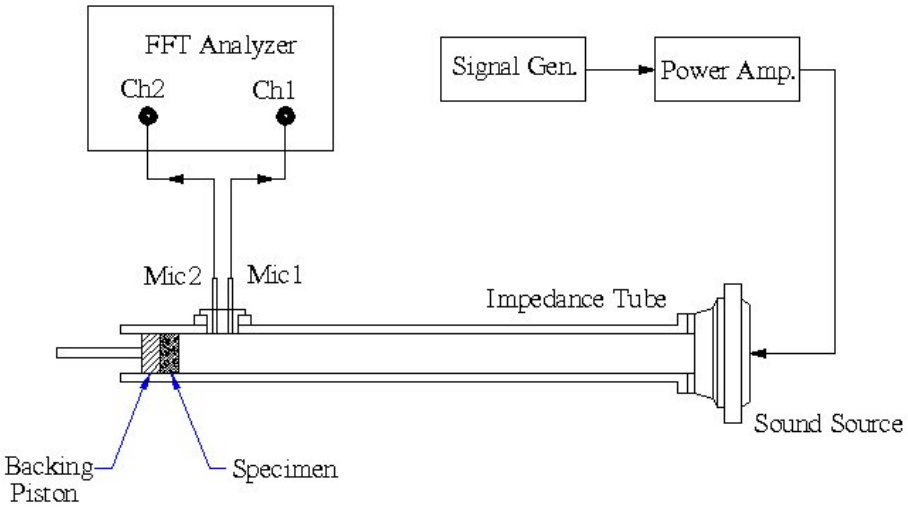

Figure 1.13: Schematic for impedance tube.

The dynamic response of the enclosed acoustic system of the impedance tube is determined by both the governing differential equations and associated boundary conditions. Ducts with idealized, totally reflective boundary conditions can be modeled using a standing wave model with mutually orthogonal modes. However, models of ducts with totally absorbent (nonreflecting) boundary conditions do not resonate, and wave propagation models are frequently used. Actual acoustic systems have non-idealized, partially reflecting boundary conditions, yielding some combination of propagating and

standing wave components in their acoustic pressure response (Hull 1995). The available analytical techniques, as quoted by Hull (1995), do not provide for the possibility that the acoustic response could be obtained as a combination of standing and propagating waves, nor do they consider the effect of partially absorptive boundary conditions on duct models. Therefore a new method for modeling a duct with partially absorptive boundary condition was developed. The system model is a one-dimensional, hard-walled duct excited by a pressure input at one end. The boundary conditions are a pressure release boundary condition at one end and a generalized impedance boundary condition at the other. This is a typical model for the impedance tube, used for estimating acoustic parameters of absorbing materials, such as the absorption coefficient and acoustic impedance as function of wavelength. After developing his model, experimental verification took place, and excellent agreement was reported.

Chung and Blaser (1980-a) presented a method for determining all normal incidence acoustic properties of any material by the measurement of the transfer function between the acoustical pressures at two locations in a tube, where the material under investigation is located. The theory underlying their developed technique involves the decomposition of a broadband stationary random signal into its incident and reflected components using a simple transfer function relation between the acoustic pressures at two locations on the tube wall.

In an extension to their theoretical model representation, Chung and Blaser (1980-b) presented experimental study using the impedance tube, to verify their proposed model. They also presented methods for calibrating the microphones used in the assessment of the transfer function at two different locations along the tube wall. Their research was the

basis upon which the ASTM standard (E1050-98) for testing and estimation of the impedance and absorption characteristics of acoustical materials.

Gentry et al. (1997) utilized smart foam as hybrid active/passive treatment for noise control. The term "Smart foam" stems from the adaptive behavior of passive sound absorbing materials equipped with an actuation element that forces the solid phase of the foam so as to create a perfect impedance match with the incident plane wave, thus causing the sound to be completely absorbed. As described by Gentry et al. (1997), air molecules in the interstices of the porous material oscillate with the frequency of the exciting sound wave. This oscillation results in frictional losses. Changes in the flow direction with multiple expansions and contractions of the flow throughout the irregular pores of the foam result in a loss of momentum in the direction of wave propagation. These phenomena account for most of the energy loss in the high frequency range. However, a porous layer can absorb a large amount of acoustic energy only if its thickness is comparable to the wavelength of the incident sound. Thus, using passive sound absorbing materials is not feasible at low frequency ranges. In their study Gentry et al. (1997) developed a smart foam noise suppression device. The device combines a light weight, distributed active layer and a passive acoustic damping material for the purpose of minimizing structural acoustic radiation. The main difference between the smart foam and the ASAC control methods is that it adaptively modifies the acoustic impedance of the vibrating surface without the use of secondary control inputs which are directly mounted on the structure. The configuration of the smart foam used is illustrated in Figure 1.14.

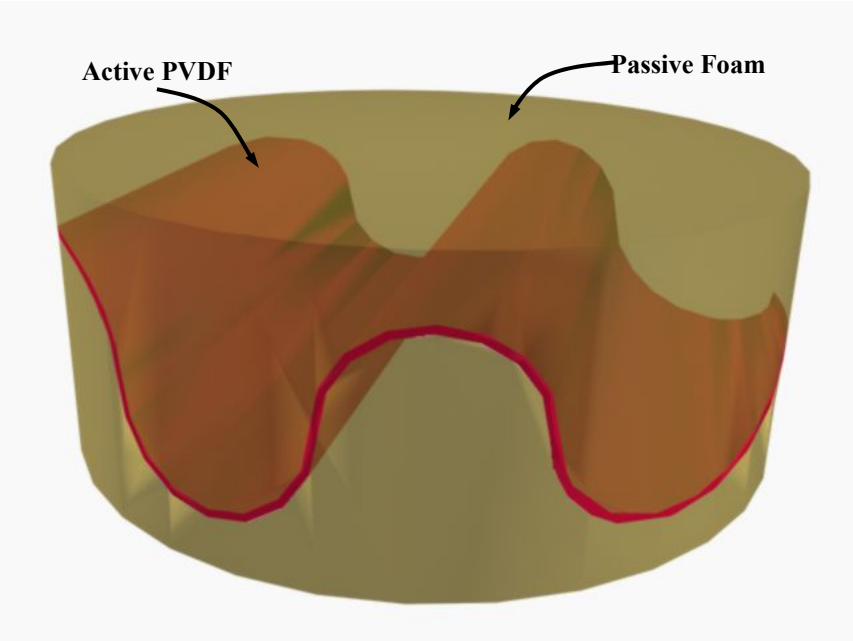

Figure 1.14: Smart foam used by Gentry et al. (1997).

The actuator used by Gentry et al. is an active piezo-polymer (PVDF), which is cylindrically curved to couple the in-plane strain associated with the piezoelectric effect with the out-of plane motion needed to radiate sound from the foam surface. They used their device in controlling sound radiation from a vibrating piston. Feedforward filtered X-LMS controller is used to minimize the signal from a far-field error microphone. Electrical connections to the PVDF layer were optimized for maximum sound radiation. Harmonic as well as broadband control was investigated, and global cancellation of harmonic and broadband noise induced by the vibrating piston was achieved.

Although good results regarding noise control were reported using the suggested method, nothing was revealed about the vibration of the piston itself. Thus, it was not evident if the developed smart foam is capable of structural vibration as well as noise control or not.

Guigou and Fuller (1998) investigated the previously suggested smart foam in reducing sound radiation from a vibrating plate with the use of adaptive feedforward and feedback controllers for different disturbance frequency bandwidths. An error microphone was located in close proximity of the smart foam provides the error signal to be minimized. For the feedforward controller, two different reference signals were implemented. First signal was sent to the piezoceramic actuator exciting the plate and second signal was the output of an accelerometer attached to the plate, which is more realistic in practice. For on- and off-resonance harmonic excitation, the adaptive feedback system performed as well as the adaptive feedforward control system. For band-limited excitation, both controllers showed good results when the band was limited to 600±50 Hz, since it contained only one resonance frequency and it was well predictable. However increasing the bandwidth to 200 to 400 Hz resulted in performance degradation of the feedback controller. Using the accelerometer signal as the reference signal was less efficient than using the actuating signal.

Two different boundary conditions are applied to a porous material to achieve best sound absorption characteristics were reported in literature. Guicken and Lorenz (1984) as quoted by Smith et al. (1999), applied a hybrid noise absorption system, in which a porous plate is placed inside an impedance tube a small distance away from a control speaker located at the end of the tube. The signal sensed by a reference microphone in front of the panel was sent to the control speaker to minimize the sound pressure sensed by a second microphone directly behind the plate. This pressure release condition on the back surface of the panel led to nearly perfect absorption over a frequency range from 100 to 600 Hz.

Furstoss et al. (1997) performed a theoretical study to determine the optimal impedance at the back face of a porous layer to prevent reflections at the front surface of the surface, for oblique and normal sound incidence.

Therefore, it was the objective of Smith et al. (1999) to compare experimentally between both types of boundary conditions regarding the performance and control effort in a 100-1000 Hz broadband frequency range. They described the pressure-release boundary condition of being local, while impedance matching condition induces more than a localized effect. The experimental setup used consists of an impedance tube, equipped with a disturbance generation speaker mounted at one end and another control speaker mounted on the other end behind the absorbing layer and air cavity as illustrated in Figure 1.15. Filtered X-LMS algorithm was used and the sensitivity of the hybrid absorbing system relative to the cavity depth and the thickness of the foam sample was studied. Average absorption coefficient over the selected frequency range was revealed to be higher with impedance matching than with pressure release with less control effort needed. They also reported that the impedance matching condition is less sensitive to cavity depth as well as foam thickness than pressure release boundary condition.

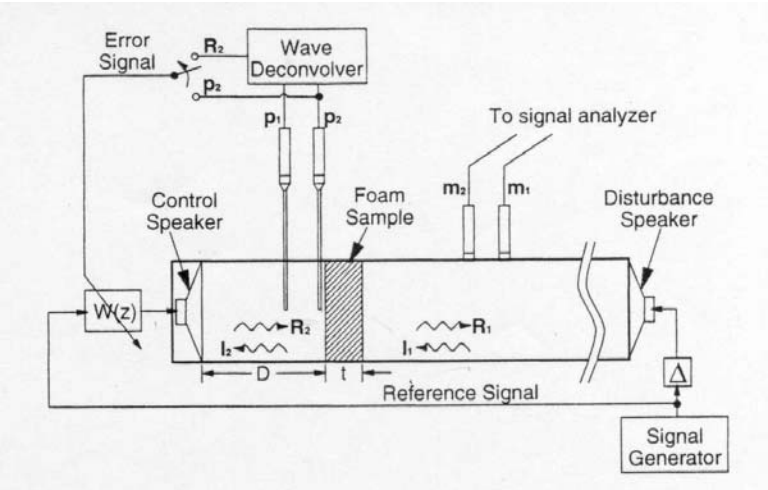

Figure 1.15: Experiment setup as conducted by Furstoss et al. (1997).

Combining X-LMS feedforward control algorithm with feedback loop demonstrated its effectiveness, when properly used, for active noise control under both transient and stationary disturbances, when applied to a three dimensional enclosures using an actively controlled foam as reported by Y. Kim et al. (2002). The purpose of including the feedback controller was to increase the convergence rate of the adaptive feedforward controller. Experimental studies were also conducted and showed good agreement with the proposed hybrid control algorithm.

In an attempt to model elastic plates covered with porous materials, N. Dauchez et al. (2003) studied the different dissipation mechanisms in bonding a foam layer to a thin simply-supported aluminum plate excited by a point force. They found out that thermal dissipation can be easily neglected compared to structural and viscous dissipation losses. Viscous damping on the other hand was found to be the dominant dissipation mechanism for soft foam, while structural damping became more significant for stiffer types of the porous layer.

A theoretical study investigating the control effort and displacements required for introducing forces to the front layer of an absorptive foam material to result in increased absorption was performed by Bolton and Green (1993). Partially reticulated foams with high flow resistivity were shown to have good properties for low required control effort at low frequencies. The configuration analyzed by Bolton and Green, as described in Figure 1.16, consists of a rigidly backed foam slab with normal and tangential force components applied to the slab surface. The value of these forces is estimated to achieve perfect sound absorption of the incident sound field.

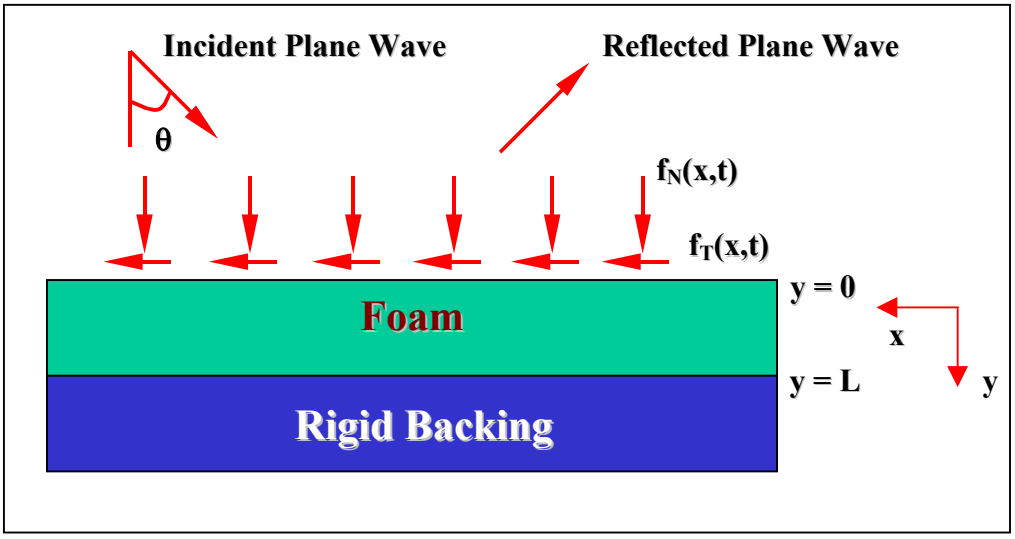

Figure 1.16: Forced foam configuration. (Bolton and Green, 1993).

Several attempts for numerically predicting the behavior of foam in closed cavities were recorded in literature. Among these attempts, is the work of Kang and Bolton (1995) which presented a finite element model for a two-dimensional foam layer backed with a rigid wall and exposed to an acoustic cavity. Also, Dauchez et al. (2003) solved this problem by considering the foam to consist only of solid phase and the viscoelastic dissipation to be the major source or damping. Coupling the foam with a flexible plate and using multilayer plate theory, the damping effect of the foam on the flexible plate is predicted. However, the acoustic characteristics of the foam are not accounted for. Kang et al. (1999) extended the work of Kang and Bolton (1994) using axisymmetric formulation rather than using Cartesian coordinate system. Atalla et al. (1998) replaced the fluid displacement degrees of freedom of the foam, as first introduced by Biot (1956), by a single pressure degree of freedom. This made it easier to couple the foam with acoustic cavities. However the 3-dimensional form of the model was still maintained. On

the other hand, Zienkiewicz (1982) and Simon (1986) have both previously noted, as quoted by Kang and Bolton (1996), that this type of formulation can only be used when the fluid phase acceleration terms are negligible, which is not usually satisfied in acoustical problems,

Hence, still the only way to couple the 3-dimensional foam model to a 2-dimensional model of an elastic structure is to introduce the flexural rigidity of the elastic structure in the boundary condition set for the foam and generate the appropriate coupling matrices. Using this method results in much higher computational effort because of the 3-dimensional nature of the finite element model of the foam layer.

1.4. STATEMENT OF THE PROBLEM

The limitations of passive vibration and noise control treatments arise from their limited performance at low frequency zones, which are characterized by the low disturbance energy. On the other hand, using purely active control techniques is infeasible at high frequencies due to limited actuation bandwidth. Therefore, combining the two techniques results in an effective means for controlling broadband excitations. Very few attempts have been reported for combining noise and vibration control treatments using hybrid actuators. Among these attempts is the use of Active Structural Acoustic Control techniques, which involve mainly vibration control of the highly sound emitting modes, without affecting the cavity modes. Therefore, in the case of trying to reduce the noise transmitted through a panel into a cavity due to one of the cavity modes

by actively modifying the velocity distribution of the panel, such that the real part of the power radiated from the panel into the cavity is minimized, higher level of panel vibration is observed (Pan and Hansen, 1991). Therefore, there is a definite need for devising a new class of hybrid passive / active actuation system that can simultaneously control effectively the vibration and sound radiation.

1.5 PROPOSED HYBRID ACTUATOR

Based on the aforementioned review of the current available types of actuators, a new hybrid passive / active actuator for vibration and noise control applications is proposed. This actuator combines the advantages of the passive elements, being efficient at high frequency ranges and the benefits of the active elements at low frequency zones.

The passive elements used are viscoelastic material for vibration damping of structures and polyurethane foam for noise attenuation inside cavities. The active elements used herein is a set of APDC elements with 45° oblique piezo rods.

Construction of the proposed actuator is as illustrated in Figure 1.17, where a viscoelastic layer is bonded to the surface of the structure in order to reduce passively its structural vibration. To increase the energy dissipation of the viscoelastic material, forces are applied externally to its top layer to increase the shear strain, resulting in higher damping characteristics. This is similar to the mechanisms employed in the Active Constrained Layer Damping (ACLD) technique developed by Baz, (1996). The applied force is generated using a set of APDC patches. As shown in Figure 1.17, the APDC

patches are placed on top of the viscoelastic layer in pairs, in such a way that the obliquely embedded piezo rods are facing each other. With this setup, the net force exerted on the viscoelastic layer is in form of an external tensile force, when the piezo rods expand outwards, and compressive force, when they contract inwards. In order to apply this mechanism efficiently, a constraining layer is bonded to the top of the APDC patches forming a reaction support to ensure that most of the displacement of the piezo-rods is transferred to the viscoelastic layer.

The second passive element used in the proposed hybrid actuator is polyurethane foam for noise attenuation purposes. The foam is characterized by its high absorption coefficient at high frequencies. To extend the capabilities of the foam to lower frequency regions, external displacement field is required to actively move the foam in the transverse direction, to modify its boundary conditions facing the acoustic medium, in order to improve sound absorption techniques. The external displacement applied to the foam is generated by the vertical component of the APDC patches as described in Figure 1.17.

Finally, combining all these elements together in one arrangement as shown in Figure 1.18 presents a new class of actuators, which is hybrid between passive and active elements. The actuator will also be effective in simultaneously suppressing structural vibration and attenuating noise radiation.

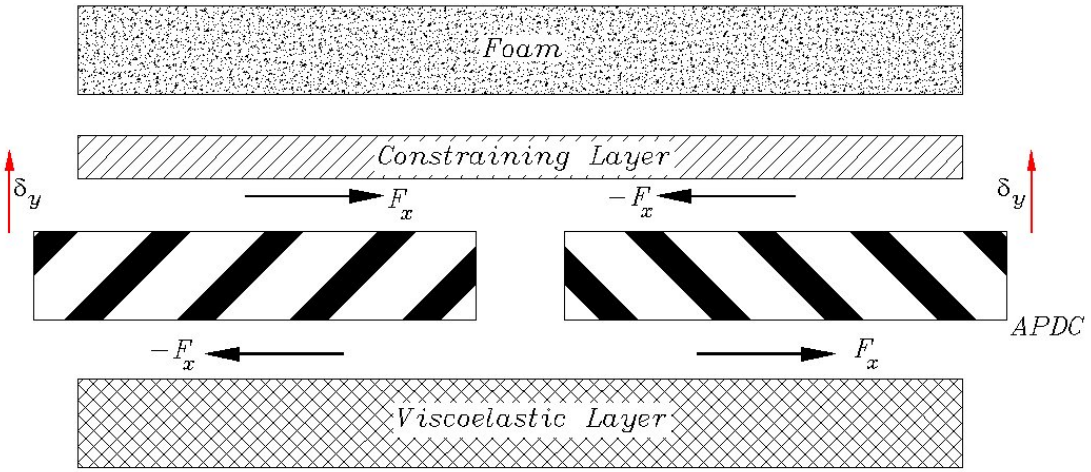

Figure 1.17: Free body diagram of the proposed configuration.

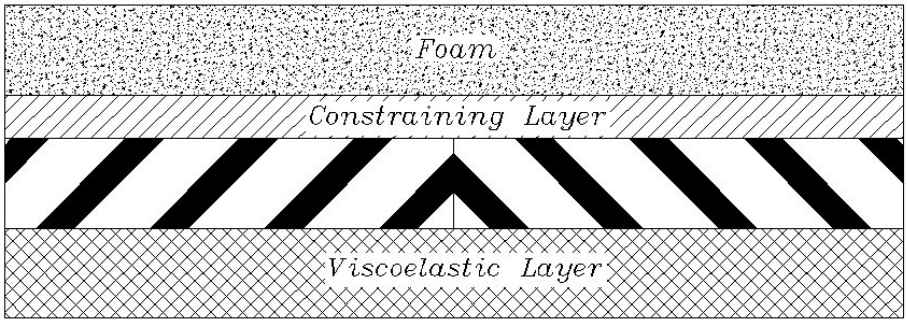

Figure 1.18: Schematic drawing of the proposed actuator configuration

1.6 SCOPE OF THE PRESENT WORK

Since the main objective of the current investigation is to develop a hybrid passive / active control treatment to simultaneously attenuate the vibration and the noise inside acoustic cavities due to both structure and cavity modes over a broad range of frequencies, the following approach has been adopted:

1. Investigating the use of the APDC actuators with inclined piezo rods in conjunction with viscoelastic layer to control structural vibration. In this regard, the in-plane strain component of the APDC actuators will be utilized to shear a viscoelastic layer resulting in higher energy dissipation.
2. Studying the absorption characteristics of the polyurethane foam for noise reduction in an acoustic cavity, by applying proper control techniques upon using the transverse components of the APDC actuator to actively control the exposed foam.
3. Combining the APDC, viscoelastic layer and polyurethane foam in a single configuration to act as a hybrid actuator.
4. Developing a finite element model for a flexible plate coupled with an acoustic cavity treated with such an actuator in order to investigate the different parameters affecting the performance, control gains, number of actuators used and actuator location.
5. Verifying the developed model experimentally.

1.7 SUMMARY:

In this chapter, a review of the different vibration and noise control techniques has been presented. Passive vibration and noise attenuation approaches as well as the active and hybrid techniques for overcoming the limitations of the former passive approaches

have been introduced. Among the hybrid techniques presented here, is the Active Constrained Layer Damping (ACLD) technique, where an active element is utilized to shear a layer of viscoelastic material bonded to the structure surface to increase the energy dissipation. Also the use of Active Piezoelectric Damping Composites (APDC) as an actuator in vibration control was briefly discussed. Smart foam, on the other hand, is used as a hybrid passive / active element for noise radiation attenuation. Finally the main research problem is formulated, and a newly developed hybrid passive / active actuator for simultaneous vibration and noise radiation attenuation was proposed.

CHAPTER 2

THEORETICAL STUDY

2.1. POLYURETHANE FOAM

A porous material in general is one with interconnected pores that run through. Thus, for Polyurethane foams, the popular model by Biot (1956) is based on dividing the porous material into two separate phases, the solid phase (called the frame and represents the solid portion of the foam) and the fluid phase, which represents the medium inside the pores. Inertial as well as viscous coupling exists between these two phases.

The model is also defined in terms of macroscopically measurable physical properties of the fluid and solid phases. Generally, foam models depend on the assumptions made for the solid phase of being either rigid or elastic. In the rigid assumption, the solid phase does not move significantly compared to the fluid medium. This may be due to the physical nature of the solid phase material, or due to its high volume density. In this case, only one longitudinal wave is assumed to propagate through the foam, which is the one that moves in the fluid part. In the elastic assumption, on the other hand, foam can support several wave types simultaneously; longitudinal as well as shear waves.

The objective of the model used here, which was previously developed by Shiau (1991), is to estimate the wave numbers for the different wave types propagating through the foam and the relationship between stresses and displacements in the different phases. Knowing such information, based on the physical properties of the porous material, can

result in an accurate estimate of the acoustic behavior of the porous material.

Hence, a brief description of this model of elastic porous materials is necessary before we account for the active control of the foam in order to enhance its acoustic properties, specially the acoustic absorption coefficient.

2.1.1. Overview of the modeling approach

The derivation of the theoretical value of the absorption coefficient involves the following steps:

1. Defining the stress-strain relationships and dynamic equations for both phases.
2. These relationships are then combined to yield three wave equations for the longitudinal and transverse components of the waves.
3. Finally a two-dimensional model for the porous foam is developed, which is appropriate for the prediction of the oblique incidence sound reflection of plane waves through finite depth and infinite lateral extend, leading finally to the estimation of the required absorption coefficient.

2.1.2. Stress-Strain Relationships

From Biot (1956), the relationship governing the stress in the x-, y- and z-directions acting on the frame and solid and fluid strains are given as:

$$\sigma_{fx} = 2N_f e_x + A_f e_s + Q_f \varepsilon_f , \quad (2.1)$$

$$\sigma_{fy} = 2N_f e_y + A_f e_s + Q_f \varepsilon_f , \quad (2.2)$$

and

$$\sigma_{fz} = 2N_f e_z + A_f e_s + Q_f \varepsilon_f \quad (2.3)$$

where:

- $e_s = \nabla . \bar{u}_f$ is the solid volumetric strain and $\bar{u}_f$ is the solid displacement vector.
- $e_x = \frac{\partial u_f}{\partial x}, e_y = \frac{\partial v_f}{\partial y}, e_z = \frac{\partial w_f}{\partial z}$, u_f, v_f and w_f are the x-, y- and z-components of the displacement vector of the solid.
- $\varepsilon_f = \nabla . \bar{U}_f$ is the fluid volumetric strain with $\bar{U}_f$ denoting the fluid vector displacement.
- $N_f = \frac{E_{1f}}{2(1+\upsilon_f)}$ is the shear modulus with E_{1f} denoting the in vacuo Young's modulus of the solid phase and υ_f is its Poisson's ratio.
- $A_f = \frac{\upsilon_f E_{1f}}{(1+\upsilon_f)(1-2\upsilon_f)}$ is the first Lame' constant.
- $Q_f=(1-h_f)E_{2f}$ represents the coupling between the volume change of the solid and that of the fluid, h_f is the porosity and E_{2f} is the bulk modulus of elasticity of the fluid inside the pores.

A schematic drawing for the foam backed from one side with a rigid wall, and exposed from the other side to incident plain wave is illustrated in Figure 2.1.

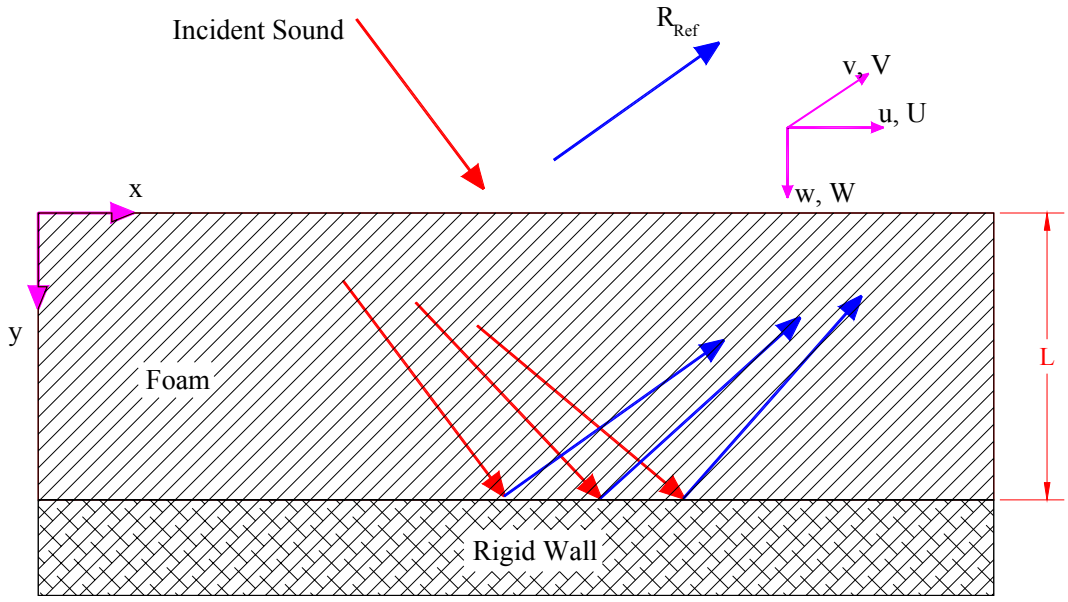

Figure 2.1: Schematic of the foam exposed to incident plane wave.

It is clear that the solid stress in each direction depends on the solid strain in that direction, solid strain in the other directions (Poisson's effect) and the fluid strain.

The pressure on the fluid, on the other hand, can be expressed as:

$$s_f = R_f \varepsilon_f + Q_f e_s \tag{2.4}$$

where, $R_f = h_f E_{2f}$ is a constant relating fluid stress and strain.

The shear stress on the solid phase is expressed as:

$$\tau_{fxy} = \tau_{fyx} = N_f \gamma_{fxy}, \tag{2.5}$$

$$\tau_{fxz} = \tau_{fzx} = N_f \gamma_{fxz}, \tag{2.6}$$

and

$$\tau_{fyz} = \tau_{fzy} = N_f \gamma_{fyz}. \tag{2.7}$$

where,

$$\gamma_{fxy} = \frac{\partial u_f}{\partial y} + \frac{\partial v_f}{\partial x},\ \gamma_{fxz} = \frac{\partial u_f}{\partial z} + \frac{\partial w_f}{\partial x},\ \gamma_{fyz} = \frac{\partial v_f}{\partial z} + \frac{\partial w_f}{\partial y}$$

2.1.3. Dynamic Relationships

The differential equations governing the motion of the solid phase, as presented by Biot (1956) are given by:

$$\frac{\partial \sigma_{fx}}{\partial x} + \frac{\partial \tau_{fyx}}{\partial y} + \frac{\partial \tau_{fzx}}{\partial z} =$$

$$\rho_{1f} \frac{\partial^2 u_f}{\partial t^2} + \rho_{2f}(q^2 - 1)\frac{\partial^2}{\partial t^2}(u_f - U_f) + b\frac{\partial}{\partial t}(u_f - U_f), \tag{2.8}$$

$$\frac{\partial \tau_{fxy}}{\partial x} + \frac{\partial \sigma_{fy}}{\partial y} + \frac{\partial \tau_{fzy}}{\partial z} =$$

$$\rho_{1f} \frac{\partial^2 v_f}{\partial t^2} + \rho_{2f}(q^2 - 1)\frac{\partial^2}{\partial t^2}(v_f - V_f) + b\frac{\partial}{\partial t}(v_f - V_f), \tag{2.9}$$

and $$\frac{\partial \tau_{fxz}}{\partial x} + \frac{\partial \tau_{fyz}}{\partial y} + \frac{\partial \sigma_{fz}}{\partial z} =$$

$$\rho_{1f} \frac{\partial^2 w_f}{\partial t^2} + \rho_{2f}(q^2 - 1)\frac{\partial^2}{\partial t^2}(w_f - W_f) + b\frac{\partial}{\partial t}(w_f - W_f). \qquad (2.10)$$

Noting that:

1. The net force per unit volume acting on an incremental solid volume is balanced by acceleration of the solid (first term on the RHS), inertial coupling force proportional to the relative acceleration of the two phases (second term on the RHS) and viscous coupling force proportional to the relative velocity of the two phases (third term on the RHS).
2. ρ_{1f} is the bulk density of the solid phase.
3. ρ_{2f} is the bulk density of the fluid phase.
4. Inertial coupling force is the result of momentum transfer between the solid and fluid resulting from pore tortuosity, which is quantified by "the structure factor, q^2".
5. b is a viscous coupling factor that can be related to macroscopic flow resistivity of the porous material.

Similarly the differential equations governing the motion of the fluid phase are given by:

$$\frac{\partial s_f}{\partial x} = \rho_{2f} \frac{\partial^2 U_f}{\partial t^2} + \rho_{2f}(q^2 - 1)\frac{\partial^2}{\partial t^2}(U_f - u_f) + b\frac{\partial}{\partial t}(U_f - u_f), \qquad (2.11)$$

$$\frac{\partial s_f}{\partial y} = \rho_{2f}\frac{\partial^2 V_f}{\partial t^2} + \rho_{2f}(q^2-1)\frac{\partial^2}{\partial t^2}(V_f - v_f) + b\frac{\partial}{\partial t}(V_f - v_f), \qquad (2.12)$$

and

$$\frac{\partial s_f}{\partial z} = \rho_{2f}\frac{\partial^2 W_f}{\partial t^2} + \rho_{2f}(q^2-1)\frac{\partial^2}{\partial t^2}(W_f - w_f) + b\frac{\partial}{\partial t}(W_f - w_f). \qquad (2.13)$$

2.1.4. Wave Equations

In order to define the relationships between the displacements and strain for solid as well as fluid phases as presented by Shiau (1991), three effective mass coefficients (ρ_{11}^*, ρ_{12}^*, ρ_{22}^*) are defined. They relate the stress field to the acceleration of the fluid and solid phases, taking into account both the inertial coupling and the viscous damping caused by the relative motion of the two phases.

Manipulating equations (2.8-2.13) and representing the result in a vector form, then the displacements and strain for both solid as well as fluid phases (assuming harmonic excitation with frequency "ω") can be expressed by the following formulae:

$$N_f\nabla^2\bar{u}_f + \nabla\left[(A_f + N_f)e_s + Q_f\varepsilon_f\right] = -\omega^2\left(\rho_{11}^*\bar{u}_f + \rho_{12}^*\bar{U}_f\right), \qquad (2.14)$$

and

$$\nabla\left[Q_f e_s + R_f\varepsilon_f\right] = -\omega^2\left(\rho_{12}^*\bar{u}_f + \rho_{22}^*\bar{U}_f\right) \quad . \qquad (2.15)$$

where,

- $\rho_{11}^* = \rho_{11} + \dfrac{b}{j\omega}$
- $\rho_{11} = \rho_{1f} + \rho_a$, effective mass of the solid moving in the fluid.

- $\rho_{12}^{*} = \rho_{12} - \dfrac{b}{j\omega}$
- $\rho_{12} = -\rho_a$ is a mass coupling parameter between fluid and solid.
- $\rho_{22}^{*} = \rho_{22} + \dfrac{b}{j\omega}$
- $\rho_{22} = \rho_{2f} + \rho_a$, effective fluid mass within the pores.
- $\rho_a = \rho_{2f}\left(q^2 - 1\right)$, is an additional mass proportional to the fluid mass moving with the solid.
- $\rho_{11}, \rho_{12}, \rho_{22}$ are mass coefficients which account for the effects of non-uniform relative fluid flow through pores.
- $\rho_{11}^{\bullet}, \rho_{12}^{\bullet}, \rho_{22}^{\bullet}$ are the counterparts of $\rho_{11}, \rho_{12}, \rho_{22}$ when allowance is made for viscous energy dissipation resulting from the relative motion between the solid and the fluid phases of foam.

The solid and fluid displacement components may be expressed as the sum of irrotational and divergence-free components, $\overline{u}_f = \overline{u}_l + \overline{u}_t$ and $\overline{U}_f = \overline{U}_l + \overline{U}_t$, where the subscript "*l*" is for irrotational components and "*t*" is for divergence-free component. Then,

$$\nabla.\overline{u}_f = \nabla.\overline{u}_l = e_s,\ \nabla.\overline{U}_f = \nabla.\overline{U}_l = \varepsilon_f,\ \nabla \times \overline{u}_f = \nabla \times \overline{u}_t = \overline{\omega}$$

Applying the divergence operation to equations (2.14, 2.15) gives

$$\nabla^2(P_f e_s + Q_f \varepsilon_f) = -\omega^2(\rho_{11}^* e_s + \rho_{12}^* \varepsilon_f), \tag{2.16}$$

and $$\nabla^2(Q_f e_s + R_f \varepsilon_f) = -\omega^2(\rho_{12}^* e_s + \rho_{22}^* \varepsilon_f). \tag{2.17}$$

where, $P_f = A_f + 2N_f$

Further manipulations of the above equations result in:

$$Q\nabla^2\varepsilon_f + \omega^2\rho_{12}^*\varepsilon_f = -P_f\nabla^2 e_s - \omega^2\rho_{11}^* e_s, \tag{2.18}$$

and $$R_f\nabla^2\varepsilon_f + \omega^2\rho_{22}^*\varepsilon_f = -Q_f\nabla^2 e_s - \omega^2\rho_{12}^* e_s. \tag{2.19}$$

Solving equations (2.18) and (2.19) for $\nabla^2\varepsilon_f$ and ε_f results in:

$$\nabla^2\varepsilon_f = \frac{(\rho_{12}^* Q_f - \rho_{22}^* P_f)\nabla^2 e_s + \omega^2\left[\left(\rho_{12}^*\right)^2 - \rho_{11}^*\rho_{22}^*\right]e_s}{\left(\rho_{22}^* Q_f - \rho_{12}^* R_f\right)}, \tag{2.20}$$

and $$\varepsilon_f = \frac{(P_f R_f - Q_f^2)\nabla^2 e_s + \omega^2\left[\rho_{11}^* R_f - \rho_{12}^* Q_f\right]e_s}{\omega^2\left(\rho_{22}^* Q_f - \rho_{12}^* R_f\right)}. \tag{2.21}$$

Equating equation (2.20) with the Laplacian of equation (2.21) results in:

$$\nabla^4 e_s + A_1\nabla^2 e_s + A_2 e_s = 0 \tag{2.22}$$

where,

$$A_1 = \frac{\omega^2(\rho_{11}^* R_f - 2\rho_{12}^* Q_f + \rho_{22}^* P_f)}{P_f R_f - Q_f^2}, \quad A_2 = \frac{\omega^4\left[\rho_{11}^*\rho_{22}^* - (\rho_{12}^*)^2\right]}{P_f R_f - Q_f^2}$$

Equation (2.22) governs the propagation of dilatational waves in the solid phase. Once e_s is calculated, ε_f can also be estimated from (2.21). Since equation (2.22) is a fourth order partial differential equation, then there has to be 2 dilatational waves propagating through the solid phase with the following wave numbers,

$$k_{1,2}^2 = \frac{A_1 \pm \sqrt{A_1^2 - 4A_2}}{2}$$

Applying the curl operation on (2.14), (2.15) results in:

$$-\omega^2(\rho_{11}^*\overline{\omega} + \rho_{12}^*\overline{\Omega}) = N_f \nabla\overline{\omega}\,, \tag{2.23}$$

and

$$-\omega^2(\rho_{12}^*\overline{\omega} + \rho_{22}^*\overline{\Omega}) = 0\,. \tag{2.24}$$

The wave equation governing the rotational wave is given by:

$$\nabla^2\overline{\omega} + k_t^2\overline{\omega} = 0 \tag{2.25}$$

where,

$$k_t^2 = \frac{\omega^2}{N_f}\left[\rho_{11}^* - (\rho_{12}^*)^2 \Big/ \rho_{22}^*\right]$$

2.1.5. Calculation of the wave numbers

Assuming the velocity potential of the incident wave to take the following form:

$$\Phi_i = e^{-j(k_x x + k_y y)} \tag{2.26}$$

where,

$k = \omega/c$ is the incident wave number.

$k_x = k\cos(\theta)$ is the x-component of the wave number k,

$k_y = k\sin(\theta)$ is the y-component of the wave number k,

and θ = the incident wave angle.

Since the foam is assumed to extend infinitely in the x-direction, all the resulting wave components will encounter the term of $e^{-k_x x}$ in the solution.

Therefore a solution for the waves propagating in the x-y plane, as presented by Shiau, (1991), can be given as:

For solid phase:

Longitudinal waves:

$$e_s = e^{-jk_x x}\left(C_1 e^{-k_{1y} y} + C_2 e^{k_{1y} y} + C_3 e^{-k_{2y} y} + C_4 e^{k_{2y} y}\right) \tag{2.27}$$

shear waves : $$\overline{\omega} = e^{-jk_x x}\left(C_5 e^{-k_{ty} y} + C_6 e^{k_{ty} y}\right) \tag{2.28}$$

For fluid phase:

Longitudinal waves:

$$\varepsilon_f = e^{-jk_x x}\left(b_1 C_1 e^{-k_{1y}y} + b_1 C_2 e^{k_{1y}y} + b_2 C_3 e^{-k_{2y}y} + b_2 C_4 e^{k_{2y}y}\right) \quad (2.29)$$

shear waves: $$\overline{\Omega} = g e^{-jk_x x}\left(C_5 e^{-k_{ty}y} + C_6 e^{k_{ty}y}\right) \quad (2.30)$$

where,

$$k_{1,2y}^2 = k_{1,2}^2 - k_x^2,$$

$$k_{ty}^2 = k_t^2 - k_x^2,$$

$$b_i = a_1 - a_2 k_i^2,\ a_1 = \frac{\rho_{11}^* R_f - \rho_{12}^* Q_f}{\rho_{22}^* Q_f - \rho_{12}^* R_f},\quad a_2 = \frac{P_f R_f - Q_f^2}{\omega^2\left(\rho_{22}^* Q_f - \rho_{12}^* R_f\right)}$$

The constants C_1 through C_6 are determined by the application of the proper boundary conditions.

The displacements u, v, U, V and the stresses σ_{fy}, s_f and τ_{fxy} are then given as:

$$u_f = jk_x e^{-jk_x x}\left(\frac{C_1}{k_1^2}e^{-k_{1y}y} + \frac{C_2}{k_1^2}e^{k_{1y}y} + \frac{C_3}{k_2^2}e^{-k_{2y}y} + \frac{C_4}{k_2^2}e^{k_{2y}y}\right) -$$

$$j\frac{k_{ty}}{k_t^2}e^{-jk_x x}\left(C_5 e^{-k_{ty}y} - C_6 e^{k_{ty}y}\right), \quad (2.31)$$

$$v_f = jk_x e^{-jk_x x}\left(\frac{k_{1y}}{k_1^2}C_1 e^{-k_{1y}y} - \frac{k_{1y}}{k_1^2}C_2 e^{k_{1y}y} + \frac{k_{2y}}{k_2^2}C_3 e^{-k_{2y}y} - \frac{k_{2y}}{k_2^2}C_4 e^{k_{2y}y}\right) +$$

$$j\frac{k_x}{k_t^2}e^{-jk_x x}\left(C_5 e^{-k_{ty}y} + C_6 e^{k_{ty}y}\right), \quad (2.32)$$

$$U_f = jk_x e^{-jk_x x}\left(b_1 \frac{C_1}{k_1^2} e^{-k_{1y} y} + b_1 \frac{C_2}{k_1^2} e^{k_{1y} y} + b_2 \frac{C_3}{k_2^2} e^{-k_{2y} y} + b_2 \frac{C_4}{k_2^2} e^{k_{2y} y} \right) - jg \frac{k_{ty}}{k_t^2} e^{-jk_x x}\left(C_5 e^{-k_{ty} y} - C_6 e^{k_{ty} y} \right), \tag{2.33}$$

$$V_f = jk_x e^{-jk_x x}\left(b_1 \frac{k_{1y}}{k_1^2} C_1 e^{-k_{1y} y} - b_1 \frac{k_{1y}}{k_1^2} C_2 e^{k_{1y} y} + b_2 \frac{k_{2y}}{k_2^2} C_3 e^{-k_{2y} y} - b_2 \frac{k_{2y}}{k_2^2} C_4 e^{k_{2y} y} \right) + jg \frac{k_x}{k_t^2} e^{-jk_x x}\left(C_5 e^{-k_{ty} y} + C_6 e^{k_{ty} y} \right), \tag{2.34}$$

$$\sigma_{fy} = e^{-jk_x x}\begin{pmatrix} \left(2N \frac{k_{1y}^2}{k_1^2} + A + b_1 Q \right) C_1 e^{-k_{1y} y} + \left(2N \frac{k_{1y}^2}{k_1^2} + A + b_1 Q \right) C_2 e^{k_{1y} y} \\ + \left(2N \frac{k_{2y}^2}{k_2^2} + A + b_2 Q \right) C_3 e^{-k_{2y} y} + \left(2N \frac{k_{2y}^2}{k_2^2} + A + b_2 Q \right) C_4 e^{k_{2y} y} \\ + 2N \frac{k_x k_{ty}}{k_t^2} \left(C_5 e^{-k_{ty} y} - C_6 e^{k_{ty} y} \right) \end{pmatrix} \tag{2.35}$$

$$s_f = e^{-jk_x x}\begin{pmatrix} (Q + b_1 R) C_1 e^{-k_{1y} y} + (Q + b_1 R) C_2 e^{k_{1y} y} + \\ (Q + b_2 R) C_3 e^{-k_{2y} y} + (Q + b_2 R) C_4 e^{k_{2y} y} \end{pmatrix} \tag{2.36}$$

and $$\tau_{fxy} = e^{-jk_x x} N \begin{pmatrix} \frac{2k_x k_{1y}}{k_1^2} \left(C_1 e^{-k_{1y} y} - C_2 e^{k_{1y} y} \right) + \\ \frac{2k_x k_{2y}}{k_2^2} \left(C_3 e^{-k_{2y} y} - C4 e^{k_{2y} y} \right) + \\ \frac{\left(k_x^2 - k_{ty}^2 \right)}{k_t^2} \left(C_5 e^{-k_{ty} y} + C_6 e^{k_{ty} y} \right) \end{pmatrix}. \tag{2.37}$$

2.1.6. Absorption Coefficient

The prediction of the plain wave absorption coefficient α at any incident angle θ can be calculated based on the reflection coefficient R_{Ref} utilizing the following formula:

$$\alpha(\theta) = 1 - \left| R_{\mathrm{Re}\, f} \right|^2 \tag{2.38}$$

and the random incidence absorption coefficient $\overline{\alpha}$ is calculated from:

$$\overline{\alpha} = 2\int_0^{\theta} \alpha(\xi)\sin(\xi)\cos(\xi)d\xi \tag{2.39}$$

2.1.7. Applying Boundary Conditions

The boundary conditions applied here correspond to foam backed from one side with a rigid wall and exposed from the other side to an incident plain wave with a velocity potential $\Phi_i = e^{-j(k_x x + k_y y)}$.

Hence, the velocity potential in the acoustic field is the summation of the incident and reflected ones:

$$\Phi = \Phi_i + \Phi_r = e^{-jk_x x}\left(e^{-jk_y y} + R_{\mathrm{Re}\, f} e^{jk_y y}\right) \tag{2.40}$$

Table (2.1) summarizes the boundary conditions associated with the smart foam in its controlled and uncontrolled modes of operation.

	y=0	**y=L**
Uncontrolled	$-h_f\ p = s_f$	$u_f = 0$
	$-(1-h_f)p=\sigma_{fy}$	$v_f = 0$
	$\frac{\partial v_f}{\partial t} = j\omega(1-h)v_f + j\omega h_f V_f$	$V_f = 0$
	$\tau_{fxy} = 0$	
Controlled	$-h_f\ p = s_f$	$u_f = K_{px}.\Phi_r$
	$-(1-h_f)p=\sigma_{fy}$	$v_f = K_{py}.\Phi_r$
	$\frac{\partial v_f}{\partial t} = j\omega(1-h_f)v_f + j\omega h_f V_f$	$V_f = K_{py}.\Phi_r$
	$\tau_{fxy} = 0$	

Table 2.1: Boundary conditions for controlled and uncontrolled cases
("*p*" is the acoustic pressure at the boundary)

The control approach utilized here employs a proportional feedback of the reflected component of the velocity potential. Here, K_{px} and K_{py} are the feedback control gains. This control strategy aims at minimizing the reflected velocity potential by maximizing the absorption coefficient of the smart foam.

2.2. VISCOELASTIC MATERIAL

Viscoelastic materials are such materials that exhibit viscous as well as elastic characteristics. Several models have been introduced for describing the behavior of these materials. The most accurate among these models is the Golla-Hughes-MacTavish (GHM) model, which is suitable for finite element analysis. The viscoelastic material, due to its nature, is characterized by a complex modulus $E_v = E'(1+i\eta_v)$, which takes the damping characteristics into consideration, where E' is the storage modulus (for elastic behavior) and η_v is the loss factor. Each of the storage modulus and the loss factor is frequency as well as temperature-dependent. Therefore in this analysis, when considering the conservative and non-conservative potential energy, interpolating functions relating E' and η_v to the frequency are employed. The parameters of the interpolating functions are obtained from the experimental behavior for the viscoelastic material under consideration.

2.3. ACTIVE PIEZOELECTRIC DAMPING COMPOSITES (APDC)

In the APDC, piezo-ceramic rods are obliquely embedded in a 3-dimentional-polymer matrix. Polarization of the rods is carried out along their length.

Two types of stresses can be assumed to exist in this piezoelectric composite. The first one is the normal stress acting along the z-direction, and the other one is shearing stress acting along the x-direction. These two stresses result from the inclination of the piezo-rods.

The following advantages can be observed from this type of stress-strain configuration:

- Compression as well as shear strains occur in the polymer matrix, resulting in higher energy dissipation in the APDC.
- Lateral motion of the APDC surface can be utilized to control vibration of the base structure.

The constitutive equations for the APDC represented in matrix form can be given as:

$$\begin{Bmatrix} T_{APDC\_z} \\ T_{APDC\_xz} \\ D_{APDC\_z} \end{Bmatrix} = \begin{bmatrix} \left[c^E\right] & -\{e_{APDC}\} \\ \{e_{APDC}\}^T & \varepsilon_{33}^S \end{bmatrix} \begin{Bmatrix} e_{zz} \\ \gamma_{APDC} \\ E_z \end{Bmatrix} \tag{2.41}$$

where,

T_{APDC_xz} is the APDC mechanical shear stress in xz plane,

T_{APDC_z} is APDC mechanical normal stress in the z-direction,

E_z is APDC electrical field in the z-direction,

$\left[c^E\right]$ is the short-circuit stiffness tensor of size (2×2),

$\{e_{APDC}\}$ is the piezoelectric stress tensor of size (2×1),

and ε_{33}^S is the clamped-body dielectric constant.

A complete derivation of these quantities is presented by Baz and Tempia (2004), where the analysis is based on the "Thickness Mode" assumptions made by Smith and Auld (1991).

2.4. ACOUSTIC CAVITY

In this section, a brief description of the equations describing the behavior of an inviscid, irrotational fluid is presented.

For fluids other than perfect gases, the relationship between the pressure p and density ρ fluctuations can be expressed by a Taylor's series expansion as follows:

$$P = P_0 + \left(\frac{\partial P}{\partial \rho}\right)_{\rho_0} (\rho - \rho_0) + \frac{1}{2}\left(\frac{\partial^2 P}{\partial \rho^2}\right)_{\rho_0} (\rho - \rho_0)^2 + \ldots \tag{2.42}$$

where the subscript "o" denotes reference values.

If the fluctuations are small, then using the first term only as an approximation for *(p-ρ)* relationship, yields

$$P - P_0 = p \approx B\frac{\rho - \rho_0}{\rho_0} \tag{2.43}$$

where, $B = \rho_0 \left(\frac{\partial P}{\partial \rho} \right)_{\rho_0} = c^2 \rho_0$ is defined as the adiabatic bulk modulus.

Three sets of equations are required, to govern the acoustic wave propagation inside the cavity. These equations are:

1. Continuity of mass equation.
2. Force balance.
3. Equation of state.

Continuity of Mass Equation

$$\left[-\frac{\partial}{\partial x}(\rho u_x) - \frac{\partial}{\partial y}(\rho u_y) - \frac{\partial}{\partial z}(\rho u_z) \right] d(Vol) = \frac{\partial \rho}{\partial t} d(Vol) \tag{2.44}$$

$$\text{or} \quad \frac{\partial \rho}{\partial t} + \vec{\nabla}.(\rho \vec{u}) = 0 \tag{2.45}$$

Equation (2.45) defines the mass continuity through a volume "*dV*" of the fluid.

Force Balance Equation

$$df_x = -\frac{\partial p}{\partial x} dxdydz, \tag{2.46}$$

$$df_y = -\frac{\partial p}{\partial y} dxdydz, \tag{2.47}$$

$$\text{and} \quad df_z = -\frac{\partial p}{\partial z} dxdydz. \tag{2.48}$$

or $$d\vec{f} = -\nabla p\, d(Vol) = m\vec{a} \tag{2.49}$$

where, $\vec{a}$ is the fluid finite volume acceleration which is given by:

$$\vec{a} = \frac{\partial \vec{u}}{\partial t} + (\vec{u}.\nabla)\vec{u} \tag{2.50}$$

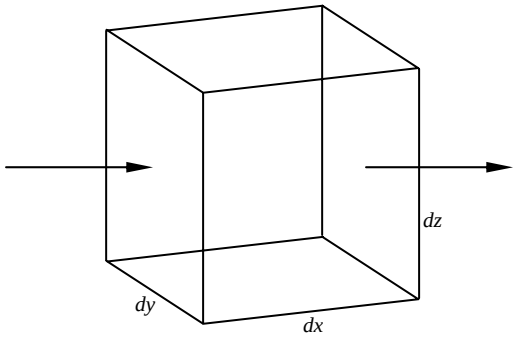

Fig. (2.2) Mass flow through finite volume

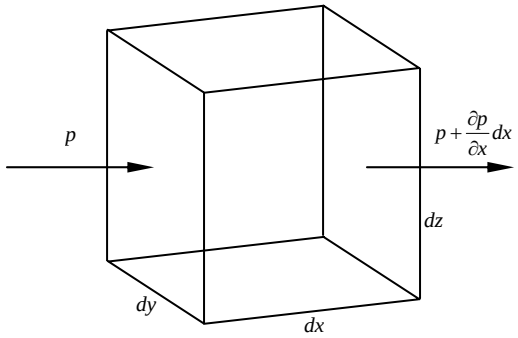

Fig. (2.3) Force equilibrium in finite volume

Substituting for the acceleration into the force balance equation results in:

$$\rho\left[\frac{\partial \vec{u}}{\partial t} + (\vec{u}.\nabla)\vec{u}\right] = -\nabla p\,. \tag{2.51}$$

Linearizing equation (2.51) about ρ_0 leads to the following relationship:

$$\rho\frac{\partial \vec{u}}{\partial t} = -\nabla p\,. \tag{2.52}$$

Simple manipulation of equation (2.52), utilizing the definition of the adiabatic bulk modulus, yields the following wave equation:

$$\nabla^2 p = \frac{1}{c^2}\frac{\partial^2 p}{\partial t^2}. \tag{2.53}$$

where, "c" is the acoustic wave speed defined as: $c = \sqrt{B/\rho_0}$

2.5. IMPEDANCE TUBE

The impedance tube is an apparatus used for measuring normal acoustic properties of different materials. As illustrated in Figure 2.4, it consists of a solid metal tube with a sound source, usually a speaker, installed at one end and the test specimen backed with a rigid piston mounted on the other end. It is also equipped with two microphones placed at a specific spacing along the tube, to measure the acoustic pressure inside the tube at these two locations.

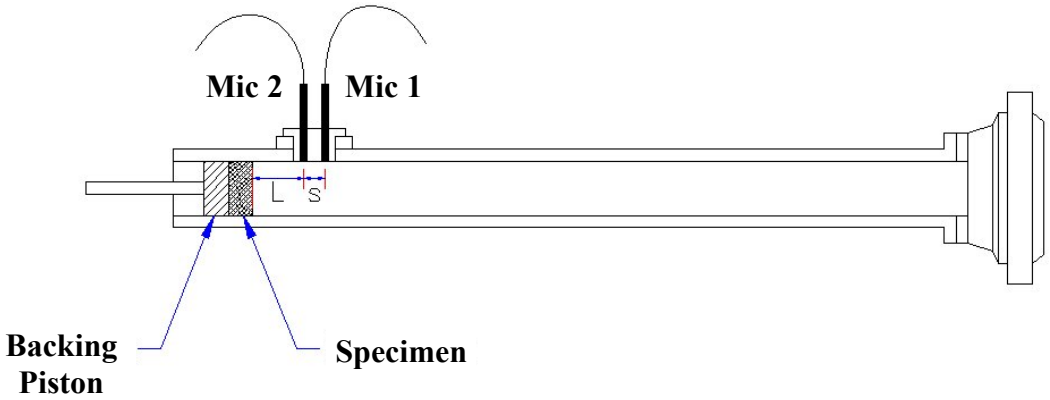

Figure 2.4: Schematic of the impedance tube as presented in ASTM Standards 1050-98.

The method used for estimating all the normal incidence acoustic properties uses a measurement of the transfer function between the acoustical pressures at two locations in the tube. The theory underlying this method involves the decomposition of a broadband stationary random signal into its incident and reflected components. This wave decomposition leads to the determination of the complex reflection coefficient from the acoustic properties such as the acoustic impedance and the sound absorption coefficient. This theory was developed by Chung and Blaser (1980-a).

Let $p_1(t)$ and $p_2(t)$ be the random acoustic pressures at the first and second microphone locations, respectively. Each pressure can be written as the sum of its incident and reflected components,

$$p_1(t) = p_{1i}(t) + p_{1r}(t) \tag{2.54}$$

The following convolution integrals with impulsive responses r_1, r_2, h_i, h_r and h_{12} are introduced to relate their respective random acoustic pressures,

$$p_{1r}(t) = \int_0^\infty r_1(\tau)\, p_{1i}(t-\tau)\, d\tau\,, \tag{2.55}$$

$$p_{2r}(t) = \int_0^\infty r_2(\tau)\, p_{2i}(t-\tau)\, d\tau\,, \tag{2.56}$$

$$p_{2i}(t) = \int_0^\infty h_i(\tau)\, p_{1i}(t-\tau)\, d\tau\,, \tag{2.57}$$

$$p_{2r}(t) = \int_0^\infty h_r(\tau)\, p_{1r}(t-\tau)\, d\tau \,, \tag{2.58}$$

and

$$p_2(t) = \int_0^\infty h_{12}(\tau)\, p_1(t-\tau)\, d\tau \tag{2.59}$$

where, r_1, r_2 : the impulsive responses corresponding to the reflected wave evaluated at the first and the second microphone locations, respectively.

h_i, h_r : the impulsive responses corresponding to the incident and the reflected waves, respectively.

and h_{12} : the impulsive response corresponding to the combined incident and reflected waves evaluated between the two microphone locations.

From equations (2.54), (2.55) and (2.59):

$$p_{2i}(t) + p_{2r}(t) = \int_0^\infty h_{12}(\tau)\left[p_{1i}(t-\tau) + p_{1r}(t-\tau)\right] d\tau \tag{2.60}$$

From equations (2.58), (2.59) and (2.60):

$$\int_0^\infty p_{1i}(t-\tau)\left[h_{12}(\tau) - h_i(\tau)\right] d\tau = \int_0^\infty p_{1r}(t-\tau)\left[h_r(\tau) - h_{12}(\tau)\right] d\tau \tag{2.61}$$

Multiplying both sides of equation (2.61) by $p_{1i}(t-\alpha)$ and taking the expected value yields:

$$E\left\{\int_0^\infty p_{1i}(t-\tau)\,p_{1i}(t-\alpha)\left[h_{12}(\tau)-h_i(\tau)\right]d\tau\right\}=$$

$$E\left\{\int_0^\infty p_{1r}(t-\tau)\,p_{1i}(t-\alpha)\left[h_r(\tau)-h_{12}(\tau)\right]d\tau\right\} \tag{2.62}$$

or $$\int_0^\infty E\left\{p_{1i}(t-\tau)\,p_{1i}(t-\alpha)\left[h_{12}(\tau)-h_i(\tau)\right]\right\}d\tau=$$

$$\int_0^\infty E\left\{p_{1r}(t-\tau)\,p_{1i}(t-\alpha)\left[h_r(\tau)-h_{12}(\tau)\right]\right\}d\tau \tag{2.63}$$

but, $$E\left\{p_{1i}(t-\tau)\,p_{1i}(t-\alpha)\right\}=R_{1i1i}(\alpha-\tau) \tag{2.64}$$

and $$E\left\{p_{1r}(t-\tau)\,p_{1i}(t-\alpha)\right\}=R_{1i1r}(\alpha-\tau) \tag{2.65}$$

where R_{1i1i}, R_{1i1r} are the auto-and cross-correlation functions, respectively.

Substituting equations (2.64), (2.65) into (2.63) and taking the Fourier transforms results in:

$$\frac{S_{1i1r}(f)}{S_{1i1i}(f)}=\frac{\int_0^\infty\left[h_{12}(\tau)-h_i(\tau)\right]e^{-j2\pi f\tau}d\tau}{\int_0^\infty\left[h_r(\tau)-h_{12}(\tau)\right]e^{-j2\pi f\tau}d\tau} \tag{2.66}$$

where, $S_{1i1i}(f)$, the Fourier transform of $R_{1i1i}(\eta)$ is the auto-spectral density of the incident

pressure component at the first microphone. Similarly, $S_{1i1r}(f)$ is the cross spectral density between the incident and reflected pressure components at the same microphone location.

Equation (2.66) represents the definition of the complex reflection coefficient at the first microphone location $R_1(f)$.

Further manipulations result in the following expression for the complex reflection coefficient:

$$R_1(f) = \frac{H_{12}(f) - H_i(f)}{H_r(f) - H_{12}(f)} \tag{2.67}$$

where H_i, H_r and H_{12} are acoustical transfer functions corresponding to impulsive responses h_i, h_r and h_{12}, respectively.

Assuming plane-wave propagation and neglecting losses at the tube wall, we may express H_i, H_r by,

$$H_i(f) = e^{-jks} \quad , \quad H_r(f) = e^{jks} \tag{2.68}$$

where "k" is the wave number, and "s" is the microphone spacing as shown in Figure 2.5.

The reflection coefficient "R_{Ref}" on the surface of a test material, which is not at the microphone location can be calculated from :

$$R_{\mathrm{Re}\,f} = R_1 e^{j2kl} \tag{2.69}$$

where "l"is the spacing between the specimen surface and the first microphone location.

The complex acoustic impedance can be accordingly calculated from:

$$\frac{z}{\rho c} = \frac{1 + R_{\mathrm{Re}\,f}}{1 - R_{\mathrm{Re}\,f}} = j\frac{H_{12}\sin(kl) - \sin[k(l-s)]}{\cos[k(l-s)] - H_{12}\cos(kl)} \tag{2.70}$$

The sound absorption coefficient is expressed as:

$$\alpha = 1 - \left|R_1\right|^2 \tag{2.71}$$

Based on this derivation for the complex reflection coefficient and correspondingly the acoustic impedance and the absorption coefficient, the ASTM Standard E-1050 (1998) was built.

2.6. SUMMARY

This chapter has been focused on presenting the theoretical aspects of modeling foam, viscoelastic material, APDC, acoustic cavity, and the impedance tube. The foam as a 2-dimensional model supports the propagation of three types of waves; two irrotational waves traveling in the direction of the finite thickness and another rotational wave, which occurs due to viscosity coupling between the solid and fluid phases. By using this model, the absorption coefficient of the foam, when exposed to an acoustic medium can be calculated after accounting for the boundary conditions imposed on both foam surfaces.

Modifying the boundary conditions, using proper feedback approach, can be used to improve the absorption characteristics of the foam.

Viscoelastic material, on the other hand, was modeled using the complex modulus approach, which facilitates including its dissipative characteristics in the modeling of vibration damping in flexible structures. Basic equations governing the wave propagation inside an acoustic cavity is also presented, to be further utilized, when fluid-structure interaction is modeled. The active element, which is the APDC, was briefly discussed, and its constitutive equations were presented, taking into consideration the inclination of the embedded piezo rods and their effect of the types of stresses and strains present in this material. Finally a comprehensive derivation of the equations governing the calculation of the absorption coefficient in an impedance tube was presented. The impedance tube is the standard equipment used for determining acoustic properties of absorption materials. In this study, the absorption coefficient of the hybrid actuator is experimentally estimated using the impedance tube. Therefore the understanding of the theory of the impedance tubes is necessary.

CHAPTER 3

FINITE ELEMENT MODELING

3.1. FINITE ELEMENT MODELING OF PLATE-VISCOELASTIC-APDC COMPOSITE

Investigation of the effect of combining the actuation characteristic of Active Piezoelectric Damping Composites (APDC) with a viscoelastic layer, mounted on the surface of a plate, for vibration attenuation as well as noise reduction when including polyurethane foam on top of the composite is carried out using the model shown in Figure 3.1.

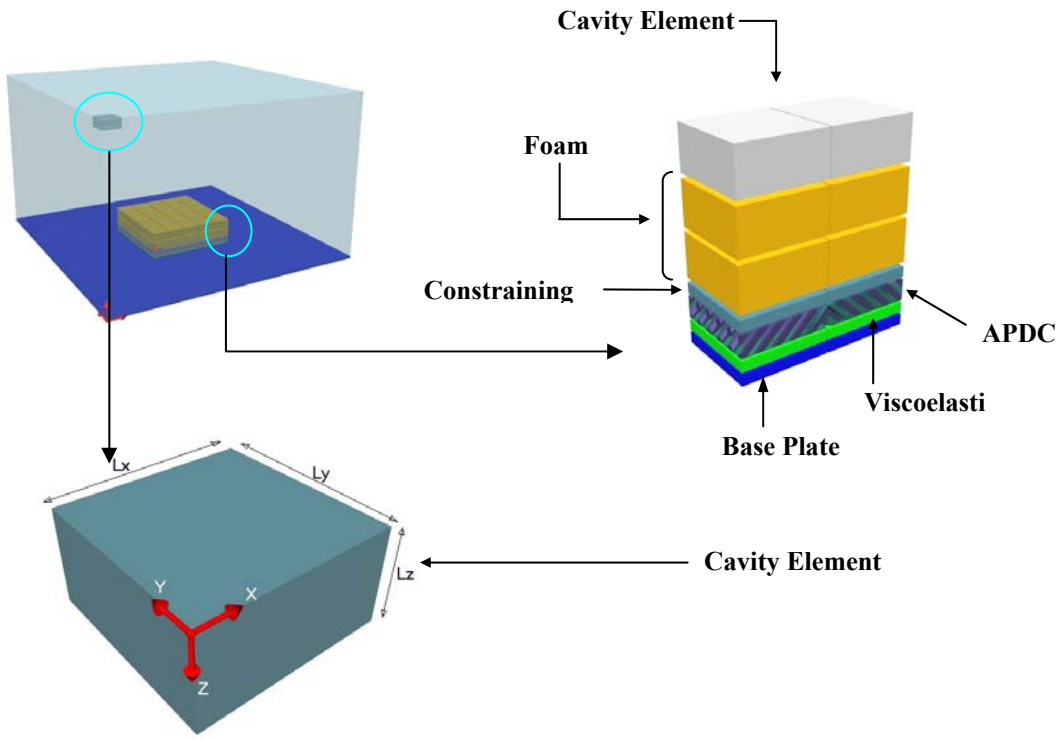

Figure 3.1: Finite element model of the plate composite coupled to acoustic cavity.

3.1.1. System Kinematics

The kinematics of the 4-layer composite as illustrated in Figure 3.2, is based on the following assumptions:

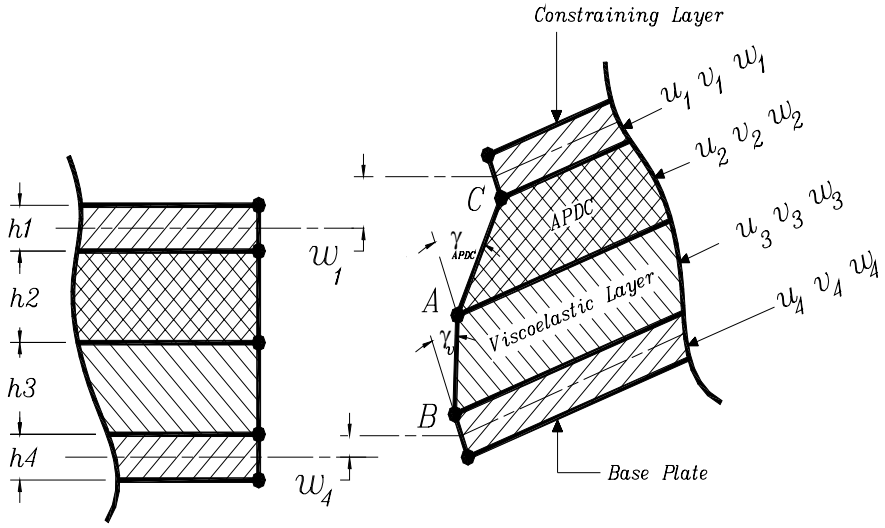

Figure 3.2: Kinematics of the plate composite.

1. In the viscoelastic layer, energy dissipation considered is due to shear as well as longitudinal in-plane strains.
2. Harmonic excitation is considered.
3. For the APDC layer the transverse deflection is assumed to vary linearly along its thickness.
4. The plate is assumed to have 5 degrees of freedom (u_4, v_4, w_4, w_{4x}, w_{4y})

representing the longitudinal displacement in x, y-directions, transverse displacement in the z-direction and rotations about y, x-axes respectively.

5. The constraining layer is assumed to have also 5 different degrees of freedom (u_1, v_1, w_1, w_{1x}, w_{1y}) independent of those of the plate.
6. The viscoelastic layer is assumed to have two independent degrees of freedom (u_3, v_3) in addition to the angles of rotation (γ_{vx}, γ_{vy}) which are dependent on the plate's degrees of freedom.

The next step involves the representation of all the different variables in the system, such as (u_2, v_2, w_2, γ_{APDC}, γ_{vx}, γ_{vy}) in terms of the 12 independent degrees of freedom of the system.

3.1.1.1 APDC Layer

The kinematics of the APDC layer are illustrated in the free body diagram shown in Figure 3.3, from which the following relationships are extracted:

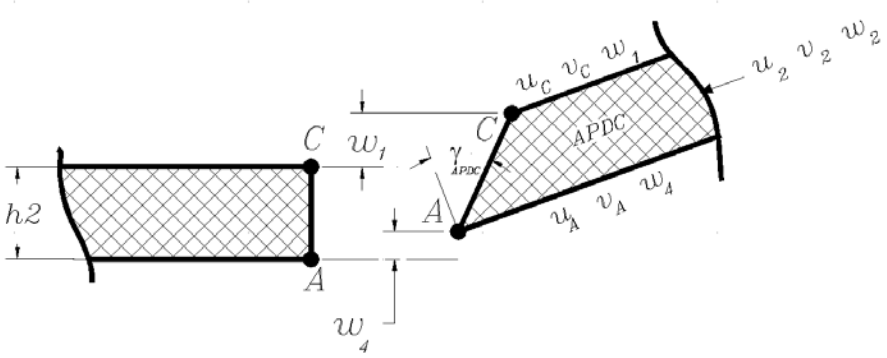

Figure 3.3: Kinematics of the APDC layer.

$$u_C = u_1 + \frac{h_1}{2} w_{1x} \tag{3.1}$$

but $$\frac{u_A - u_C}{h_2} = \frac{w_{1x} + w_{4x}}{2} - \gamma_{APDC} \tag{3.2}$$

hence, $$\gamma_{APDC} = \frac{1}{h_2}\left[(u_1 - u_c) + \frac{h_1 + h_2}{2} w_{1x} + w_{4x}\frac{h_2}{2}\right], \tag{3.3}$$

and $$w_2 = \frac{w_1 + w_4}{2} + \frac{w_1 - w_4}{h_2} z \tag{3.4}$$

3.1.1.2 Viscoelastic Layer

The kinematics of the viscoelastic layer is illustrated by the free body diagram shown in Figure 3.4. The following relationships are extracted:

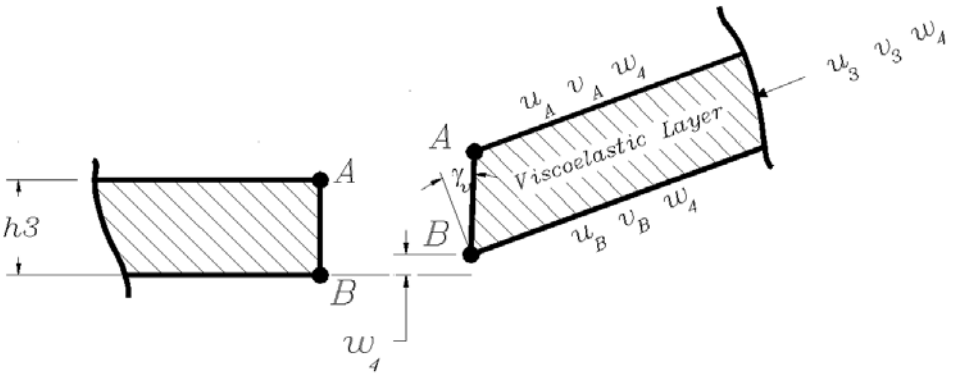

Figure 3.4: Kinematics of the viscoelastic layer

$$u_B = u_4 - \frac{h_4}{2} w_{4x}, \qquad v_B = v_4 - \frac{h_4}{2} w_{4y} \tag{3.5}$$

$$u_B - u_A = u_4 - u_A - \frac{h_4}{2} w_{4x}, \quad v_B - v_A = v_4 - v_A - \frac{h_4}{2} w_{4y} \tag{3.6}$$

but $$w_{4x} - \gamma_{vx} = \frac{u_B - u_A}{h3}, \qquad w_{4y} - \gamma_{vy} = \frac{v_B - v_A}{h3} \tag{3.7}$$

hence, $$\gamma_{vx} = \frac{1}{h_3}\left[(u_A - u_4) + \frac{h_4 + 2h_3}{2} w_{4x}\right] \tag{3.8}$$

and $$\gamma_{vy} = \frac{1}{h_3}\left[(v_A - v_4) + \frac{h_4 + 2h_3}{2} w_{4y}\right] \tag{3.9}$$

Since $u_3 = \frac{u_B + u_A}{2}$ and substituting u_B from (3.5), u_A can be calculated as follows:

$$u_A = 2u_3 - u_4 + \frac{h_4}{2} w_{4x} \tag{3.10}$$

and $$v_A = 2v_3 - v_4 + \frac{h_4}{2} w_{4y} \tag{3.11}$$

Substituting for the values of u_A and v_A in equations (3.3), (3.10) and (3.11), gives

$$\gamma_{APDC} = \frac{1}{h_2}\left(u_1 - 2u_3 + u_4 + \frac{(h_2 - h_4)}{2} w_{4x} + \frac{h_1 + h_2}{2} w_{1x}\right), \tag{3.12}$$

$$\gamma_{vx} = \frac{1}{h_3}\left(2(u_3 - u_4) + (h_3 + h_4) w_{4x}\right), \tag{3.13}$$

and $$\gamma_{vy} = \frac{1}{h_3}\left(2(v_3 - v_4) + (h_3 + h_4) w_{4y}\right) \tag{3.14}$$

Finally, $$u_2 = \frac{u_A + u_C}{2} = \frac{1}{2}\left(2u_3 + u_1 - u_4 + \frac{h_4}{2} w_{4x} + \frac{h_1}{2} w_{1x}\right), \tag{3.15}$$

$$v_2 = \frac{v_A + v_C}{2} = \frac{1}{2}\left(2v_3 + v_1 - v_4 + \frac{h_4}{2} w_{4y} + \frac{h_1}{2} w_{1y}\right) \tag{3.16}$$

3.1.2. Degrees of Freedom and Shape Functions

The composite plate element is considered to be a rectangular shell element with 4 nodes as shown in Figure 3.5. Each node has 12 degrees of freedom including u_1, v_1, w_1, w_{1x}, w_{1y} describing the longitudinal displacement of the constraining layer in the x, y-directions and the transverse deflection in the z-direction as well as rotations about the y- and x-axes respectively, u_4, v_4, w_4, w_{4x} and w_{4y} describing the same quantities for the base plate and u_3, v_3 describing the longitudinal in-plane-displacement of the viscoelastic layer.

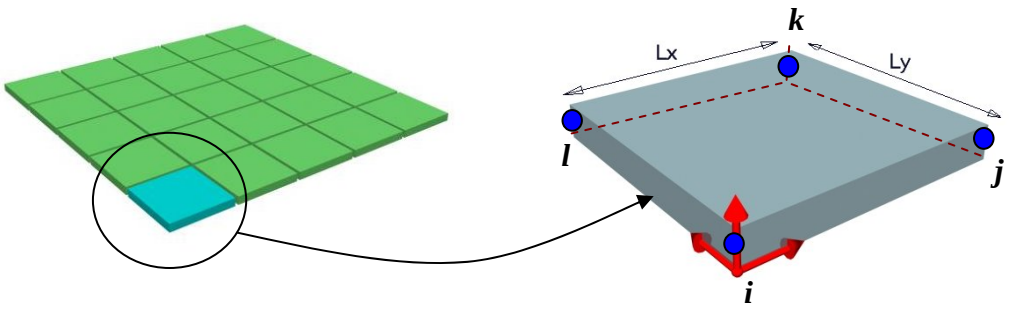

Figure 3.5: Plate element.

The deflection vector for any point (x,y,z) inside the element is defined as:

$$\delta_{P\_xyz} = \begin{pmatrix} u_1 & v_1 & w_1 & w_{1x} & w_{1y} & u_4 & v_4 & w_4 & w_{4x} & w_{4y} & u_3 & v_3 \end{pmatrix}^T \qquad (3.17)$$

Therefore for a 4-node element, the overall nodal deflection vector is a (48×1) vector $\{\delta_P\}$ defined as follows:

$$\{\boldsymbol{\delta}_{\mathbf{P}}\} = \left(\delta_{P\_i} \quad \delta_{P\_j} \quad \delta_{P\_k} \quad \delta_{P\_l}\right)^T \tag{3.18}$$

where, *i, j,… , l* are the 4 nodes per element and,

$$\boldsymbol{\delta}_{\mathbf{P\_nn}} = (u_{1\_nn} \quad v_{1\_nn} \quad w_{1\_nn} \quad w_{1x\_nn} \quad w_{1y\_nn} \quad u_{4\_nn} \quad v_{4\_nn} \quad w_{4\_nn} \quad w_{4x\_nn} \quad w_{4y\_nn} \quad u_{3\_nn} \quad v_{3\_nn})^T$$

represents the deflection vector at node "*nn*".

The corresponding element shape functions are chosen to be:

$$N_{pp}(x,y,z) = (1 \quad x \quad y \quad xy), \tag{3.19}$$

and

$$N_{pb}(x,y,z) = \left(1 \quad x \quad y \quad x^2 \quad xy \quad y^2 \quad x^3 \quad x^2y \quad xy^2 \quad y^3 \quad x^3y \quad xy^3\right) \tag{3.20}$$

where, subscript "*pp*" denotes in-plane displacements (*u,v*) and "*pb*" defines transverse displacement (*w*).

The shape functions for the different degrees of freedom are defined as, N_{u1}, N_{v1}, N_{w1}, N_{u4}, N_{v4}, N_{w4}, N_{u3}, N_{v3}.

Hence, the spatial distribution of the different displacements are assumed to take the following form,

$$u_1 = a_1 + a_2 x + a_3 y + a_4 xy, \tag{3.21}$$

$$v_1 = a_5+a_6\,x+a_7\,y+a_8\,xy, \tag{3.22}$$

$$w_1 = a_9+a_{10}\,x+a_{11}\,y+a_{12}\,x^2+a_{13}\,x.y+a_{14}\,y^2+a_{15}\,x^3+a_{16}\,x^2y+ a_{17}\,xy^2+a_{18}\,y^3+a_{19}\,x^3y+a_{20}\,xy^3, \tag{3.23}$$

$$u_4 = a_{21}+a_{22}\,x+a_{23}\,y+a_{24}\,xy, \tag{3.24}$$

$$v_4 = a_{25}+a_{26}\,x+a_{27}\,y+a_{28}\,xy, \tag{3.25}$$

$$w_4 = a_{29}+a_{30}\,x+a_{31}\,y+a_{32}\,x^2+a_{33}\,x.y+a_{34}\,y^2+a_{35}\,x^3+a_{36}\,x^2y+ a_{37}\,xy^2+a_{38}\,y^3+a_{39}\,x^3y+a_{40}\,xy,^3 \tag{3.26}$$

$$u_3 = a_{41}+a_{42}\,x+a_{43}\,y+a_{44}\,xy \tag{3.27}$$

and $$v_3 = a_{45}+a_{46}\,x+a_{47}\,y+a_{48}\,xy. \tag{3.28}$$

where the constants $\{a_1, a_2, \ldots, a_{48}\}$ are determined in terms of the 48 components of the nodal degrees of freedom vector $\{\boldsymbol{\delta_P}\}$.

Accordingly the deflection vector $\{\delta_{P\_xyz}\}$ may be expressed in terms of the nodal degrees of freedom vector as follows,

$$\{\delta_{P\_xyz}\} = \begin{bmatrix} N_{u1} & & & & & & & & & & & \\ & N_{v1} & & & & & & & & & & \\ & & N_{w1} & & & & & & & & & \\ & & & N_{w1x} & & & & & & & & \\ & & & & N_{w1y} & & & & & & & \\ & & & & & N_{u4} & & & & & & \\ & & & & & & N_{v4} & & & & & \\ & & & & & & & N_{w4} & & & & \\ & & & & & & & & N_{w4x} & & & \\ & & & & & & & & & N_{w4y} & & \\ & & & & & & & & & & N_{u3} & \\ & & & & & & & & & & & N_{v3} \end{bmatrix} [A_{coeff\_P}]\{\delta_P\} \tag{3.29}$$

where $[A_{coeff\_P}]$ is the (48×48) spatial interpolating matrix corresponding to u_1, v_1, w_1, w_{1x}, w_{1y}, u_4, v_4, w_4, w_{4x}, w_{4y}, u_3, v_3.

3.1.3. Conservative Energy Equations of the Plate, Constraining and Viscoelastic Layers

The energy of the composite plate consists of the kinetic and strain energies due to in-plane and bending strains of the base plate, constraining and viscoelastic layers as well as the shear strain in the viscoelastic material.

3.1.3.1 Strain Energy due to in-plane and bending strains

$$\mathbf{P.E._1} = \mathbf{P.E.}|_{\mathbf{PLate}} + \mathbf{P.E.}|_{\mathbf{Constraining\ Layer}} + \mathbf{P.E.}|_{\mathbf{Viscoelastic\ Layer}}, \tag{3.30}$$

with $$\mathbf{P.E.}|_{\mathbf{PLate}} = \frac{1}{2}\int_V \left(\sigma_{pp}^T \cdot \varepsilon_{pp} + \sigma_{pb}^T \cdot \varepsilon_{pb}\right) dV\,, \tag{3.31}$$

$$\mathbf{P.E.}|_{\mathbf{Constraining\ Layer}} = \frac{1}{2}\int_V \left(\sigma_{cp}^T \cdot \varepsilon_{cp} + \sigma_{cb}^T \cdot \varepsilon_{cb}\right) dV\,, \tag{3.32}$$

and $$\mathbf{P.E.}|_{\mathbf{Viscoelastic\ Layer}} = \frac{1}{2}\int_V \left(\sigma_{vp}^T \cdot \varepsilon_{vp} + \sigma_{vb}^T \cdot \varepsilon_{vb}\right) dV\,; \tag{3.33}$$

where,

- "$\sigma_{pp}, \sigma_{cp}, \sigma_{vp}$" are the in-plane stress vectors of size (3×1) of the plate, constraining and viscoelastic layers defined as:

$$\sigma_{pp} = \left(\sigma_{ppx} \quad \sigma_{ppy} \quad \tau_{ppxy}\right)^T\,, \tag{3.34}$$

$$\sigma_{cp} = \left(\sigma_{cpx} \quad \sigma_{cpy} \quad \tau_{cpxy}\right)^T, \tag{3.35}$$

and $$\sigma_{vp} = \left(\sigma_{vpx} \quad \sigma_{vpy} \quad \tau_{vpxy}\right)^T; \tag{3.36}$$

where,

σ_{ppx}, σ_{cpx}, σ_{vpx} : normal stresses in the x-direction of the plate, constraining and viscoelastic layer due to in-plane strain,

σ_{ppy}, σ_{cpy}, σ_{vpy} : normal stresses in the y-direction of the plate, constraining and viscoelastic layer due to in-plane strain,

and τ_{ppxy}, τ_{cpxy}, τ_{vpxy}: shear stresses in the xy plane of the plate, constraining and viscoelastic layer due to in-plane strain.

- "ε_{pp}, ε_{cp}, ε_{vp}" are the in-plane strain vectors of size (3×1) of the plate, constraining and viscoelastic layer defined as:

$$\varepsilon_{pp} = \left(\frac{\partial u_4}{\partial x} \quad \frac{\partial v_4}{\partial y} \quad \frac{\partial u_4}{\partial y} + \frac{\partial v_4}{\partial x} \right)^T, \tag{3.37}$$

$$\varepsilon_{cp} = \left(\frac{\partial u_1}{\partial x} \quad \frac{\partial v_1}{\partial y} \quad \frac{\partial u_1}{\partial y} + \frac{\partial v_1}{\partial x} \right)^T, \tag{3.38}$$

and $$\varepsilon_{vp} = \left(\frac{\partial u_3}{\partial x} \quad \frac{\partial v_3}{\partial y} \quad \frac{\partial u_3}{\partial y} + \frac{\partial v_3}{\partial x} \right)^T; \tag{3.39}$$

- "$\sigma_{pb}, \sigma_{cb}, \sigma_{vb}$" are the bending stress vectors of size (3×1) of the plate, constraining and viscoelastic layer defined as:

$$\sigma_{pb} = \left(\sigma_{pbx} \quad \sigma_{pby} \quad \tau_{pbxy} \right)^T, \tag{3.40}$$

$$\sigma_{cp} = \left(\sigma_{cbx} \quad \sigma_{cby} \quad \tau_{cbxy} \right)^T, \tag{3.41}$$

and $\sigma_{vp} = \left(\sigma_{vbx} \quad \sigma_{vby} \quad \tau_{vbxy}\right)^T$; (3.42)

where,

σ_{pbx}, σ_{cbx}, σ_{vx} : normal stresses in the x-direction of the plate, constraining and viscoelastic layer due to bending strain,

σ_{pby}, σ_{cby}, σ_{vby} : normal stresses in the y-direction of the plate, constraining and viscoelastic layer due to bending strain,

and τ_{pbxy}, τ_{cbxy}, τ_{vbxy} : shear stresses in the xy plane of the plate, constraining and viscoelastic layer due to bending strain.

- "ε_{pb}, ε_{cb}, ε_{vb}" are the bending strain vectors of size (3×1) of the plate, constraining and viscoelastic layer defined as:

$$\varepsilon_{pb} = z\left(\frac{\partial^2 w_4}{\partial x^2} \quad \frac{\partial^2 w_4}{\partial y^2} \quad \frac{2\partial^2 w_4}{\partial x \partial y}\right)^T, \tag{3.43}$$

$$\varepsilon_{cb} = z\left(\frac{\partial^2 w_1}{\partial x^2} \quad \frac{\partial^2 w_1}{\partial y^2} \quad \frac{2\partial^2 w_1}{\partial x \partial y}\right)^T, \tag{3.44}$$

and $$\varepsilon_{vb} = z\left(\frac{\partial^2 w_4}{\partial x^2} \quad \frac{\partial^2 w_4}{\partial y^2} \quad \frac{2\partial^2 w_4}{\partial x \partial y}\right)^T. \tag{3.45}$$

The relationships between "σ_{pp}, σ_{pb}", "σ_{cp}, σ_{cb}" and "σ_{cp}, σ_{cb}" and their corresponding strain vectors are defined in terms of three (3×3) symmetric matrices (D_p, D_c, D_v) denoting the stress-strain relationships given by:

$$D_{ii} = \frac{E_{ii}}{1-\upsilon_{ii}^2}\begin{pmatrix} 1 & \upsilon_{ii} & 0 \\ \upsilon_{ii} & 1 & 0 \\ 0 & 0 & \dfrac{1-\upsilon_{ii}}{2} \end{pmatrix} \tag{3.46}$$

Note that the subscript "*ii*" = "*p*" for the plate, "*c*" for the constraining layer and "*v*" for the viscoelastic layer. Also E_{ii} and υ_{ii} denote Young's modulus and Poisson's ratio respectively for layer "*ii*".

Now, let

$$N_{pp\_xyz}(x,y,z) \equiv \left(N_{u4\_x} \quad N_{v4\_y} \quad N_{u4\_y} + N_{v4\_x}\right), \tag{3.47}$$

$$N_{pb\_xyz}(x,y,z) \equiv \left(N_{w4\_xx} \quad N_{w4\_yy} \quad 2N_{w4\_xy}\right), \tag{3.48}$$

$$N_{cp\_xyz}(x,y,z) \equiv \left(N_{u1\_x} \quad N_{v1\_y} \quad N_{u1\_y} + N_{v1\_x}\right), \tag{3.49}$$

$$N_{cb\_xyz}(x,y,z) \equiv \left(N_{w1\_xx} \quad N_{w1\_yy} \quad 2N_{w1\_xy}\right), \tag{3.50}$$

$$N_{vp\_xyz}(x,y,z) \equiv \left(N_{u3\_x} \quad N_{v3\_y} \quad N_{u3\_y} + N_{v3\_x}\right), \tag{3.51}$$

and $$N_{vb\_xyz}(x,y,z) \equiv \left(N_{w4\_xx} \quad N_{w4\_yy} \quad 2N_{w4\_xy}\right); \tag{3.51}$$

where,

$N_{(\_xx)}$ is defined as $\dfrac{\partial^2 N_{(\,)}}{\partial x^2}$,

$N_{(\_yy)}$ is defined as $\dfrac{\partial^2 N_{(\,)}}{\partial y^2}$,

and $N_{(\_xy)}$ is defined as $\dfrac{\partial^2 N_{(\,)}}{\partial x \partial y}$

Then, the conservative strain energy of the plate, constraining and viscoelastic layers due to in-plane and bending stresses can therefore be expressed as:

$$\mathbf{P.E._1} = \mathbf{P.E.}\big|_{\mathbf{Plate}} + \mathbf{P.E.}\big|_{\mathbf{Constraining\ Layer}} + \mathbf{P.E.}\big|_{\mathbf{Viscoelastic\ Layer}} =$$

$$\frac{1}{2}\{\boldsymbol{\delta}_{\mathbf{P}}\}^T \left[A_{coeff\_P}\right]^T \left(I_1 + I_2 + I_3 + I_4 + I_5 + I_6\right)\left[A_{coeff\_P}\right]\{\boldsymbol{\delta}_{\mathbf{P}}\} \tag{3.52}$$

where,

$$I_1 = \int_{-\frac{h_4}{2}}^{\frac{h_4}{2}} \int_y \int_x \left(\left[N_{pp\_xyz}\right]^T \cdot D_p^T \cdot \left[N_{pp\_xyz}\right]\right) dxdydz\,,$$

$$I_2 = \int_{-\frac{h_4}{2}}^{\frac{h_4}{2}} \int_y \int_x \left(z^2 \left[N_{pb\_xyz}\right]^T \cdot D_p^T \cdot \left[N_{pb\_xyz}\right]\right) dxdydz\,,$$

$$I_3 = \int_{h_2+h_3+\frac{h_4}{2}}^{h_1+h_2+h_3+\frac{h_4}{2}} \int_y \int_x \left(\left[N_{cp\_xyz}\right]^T \cdot D_c^T \cdot \left[N_{cp\_xyz}\right]\right) dxdydz\,,$$

$$I_4 = \int_{h_2+h_3+\frac{h_4}{2}}^{h_1+h_2+h_3+\frac{h_4}{2}} \int_y \int_x \left(z^2 \left[N_{cb\_xyz}\right]^T \cdot D_c^T \cdot \left[N_{cb\_xyz}\right]\right) dxdydz\,,$$

$$I_5 = \int_{\frac{h_4}{2}}^{h_3+\frac{h_4}{2}} \int_y \int_x \left(\left[N_{vp\_xyz}\right]^T \cdot D_v^T \cdot \left[N_{vp\_xyz}\right]\right) dxdydz\,,$$

and $$I_6 = \int_{\frac{h_4}{2}}^{h_3+\frac{h_4}{2}} \int_y \int_x \left(z^2 \left[N_{vb\_xyz}\right]^T \cdot D_v^T \cdot \left[N_{vb\_xyz}\right]\right) dxdydz$$

3.1.3.2 Strain Energy due to shear strain in viscoelastic layer

$$\mathbf{P.E._2} = \mathbf{P.E._S}\big|_{\mathbf{Viscoelastic\ Layer}} = \frac{1}{2}\int_V \left(\sigma_{vsc}^T \cdot \varepsilon_{vs}\right) dV \tag{3.53}$$

where,

- "σ_{vsc}" is the shear stress vectors of size (2×1) of the viscoelastic layer given by:

$$\sigma_{vsc} = \begin{pmatrix} \sigma_{vscx} & \sigma_{vscy} \end{pmatrix}^T \tag{3.54}$$

where,

σ_{vscx},: conservative shear stress in the x-direction of the viscoelastic layer.

σ_{vscy}: conservative shear stress in the y-direction of the viscoelastic layer.

- "ε_{vs}" is the shear strain vector of size (2×1) of the viscoelastic layer given by:

$$\varepsilon_{vs} = \begin{pmatrix} \gamma_{vx} & \gamma_{vy} \end{pmatrix}^T \tag{3.55}$$

The relationship between "σ_{vcs}" and the corresponding strain vector is defined in terms of the shear storage modulus (G'), such that $\sigma_{vcs} = G'\varepsilon_{vs}$

Utilizing equations (3.16) and (3.17), the shear strain components γ_{vx} and γ_{vy} can be determined in terms of the shape functions. Hence, the following terms are defined:

$$N_{vs\_xyz}(x, y, z) \equiv \begin{pmatrix} N_{vs\_1} & N_{vs\_2} \end{pmatrix}, \tag{3.56}$$

$$N_{vs\_1} = \frac{1}{h_3}\left(2\left(u_3 - u_4\right) + \left(h_3 + h_4\right)w_{4x}\right), \tag{3.57}$$

and

$$N_{vs\_2} = \frac{1}{h_3}\left(2\left(v_3 - v_4\right) + \left(h_3 + h_4\right)w_{4y}\right); \tag{3.58}$$

where,

$N_{(\_x)}$ is defined as $\dfrac{\partial N_{(\,)}}{\partial x}$,

and $N_{(\_y)}$ is defined as $\frac{\partial N_{(\,)}}{\partial y}$

The conservative shear strain energy in the viscoelastic material can therefore be expressed as:

$$\mathbf{P.E._2} = \frac{1}{2}\{\boldsymbol{\delta}_\mathbf{P}\}^T \left[A_{coeff\_P}\right]^T G'(I_7)\left[A_{coeff\_P}\right]\{\boldsymbol{\delta}_\mathbf{P}\} \tag{3.59}$$

where, $I_7 = \int_{\frac{h_4}{2}}^{h_3+\frac{h_4}{2}} \int_y \int_x \left(\left[N_{vs\_xyz}\right]^T \cdot \left[N_{vs\_xyz}\right]\right) dxdydz$

3.1.3.3 Strain Energy of the APDC

$$\mathbf{P.E._3} = \frac{1}{2}\int_V \sigma_{APDC}^T . \varepsilon_{APDC}\, dV \tag{3.60}$$

where

- σ_{APDC} is the stress vector in the APDC layer
- ε_{APDC} is the corresponding (2×1) strain vector defined as

$$\varepsilon_{APDC} = (e_{zz} \quad \gamma_{APDC})^T \tag{3.61}$$

where

$e_{zz} = \frac{\partial w_2}{\partial z}$: the normal strain in the APDC layer,

and γ_{APDC} : the shear strain in the APDC.

The stress σ_{APDC} is related to the mechanical strain ε_{APDC} and electric field E_z through the following constitutive equation:

$$\sigma_{APDC} = \left[c^E\right]\{\varepsilon_{APDC}\} - \{e_{APDC}\}E_z \tag{3.62}$$

where,

$\left[c^E\right]$ serves as the short-circuit stiffness tensor for the APDC,

and $\{e_{APDC}\}$ serves as the piezoelectric strain tensor.

A complete derivation for the different components in the constitutive equation for the APDC is given by Baz and Tempia (2004).

Let,

$$N_{APDC\_xyz}(x,y,z) \equiv \quad \left(N_{APDC\_1} \quad N_{APDC\_2}\right), \tag{3.63}$$

$$N_{APDC\_1} = \frac{1}{h_2}\left[N_{w1} - N_{w4}\right], \tag{3.64}$$

and $$N_{APDC\_2} = \frac{1}{h_2}\left[N_{u1} - 2N_{u3} + N_{u4} + \frac{h_2 - h_4}{2}N_{w4\_x} + \frac{h_1 + h_2}{2}N_{w1\_x}\right] \tag{3.65}$$

Hence, the strain and stress tensors can be expressed in terms of the shape functions and the nodal deflection vector as following :

$$\varepsilon_{APDC} = N_{APDC\_xyz} \cdot A_{coeff\_P} \cdot \{\boldsymbol{\delta}_{\mathbf{P}}\}, \tag{3.66}$$

and $\sigma_{APDC} = \left[c^E\right] N_{APDC\_xyz} . A_{coeff\_P} . \{\boldsymbol{\delta}_{\mathbf{P}}\} - \{e_{APDC}\} E_Z$. (3.67)

Accordingly, the total strain energy of the APDC is expressed as follows:

$$\mathbf{P.E._3} = \frac{1}{2} \{\boldsymbol{\delta}_{\mathbf{P}}\}^T A_{coeff\_P}^T (I_8) A_{coeff\_P} \{\boldsymbol{\delta}_{\mathbf{P}}\} \tag{3.68}$$

where, $I_8 = \int_V N_{APDC\_xyz}^T \left[c^E\right]^T . N_{APDC\_xyz} \, dV$

The non-conservative work exerted by the APDC can also be formulated as follows:

$$\mathbf{W_{nc\_APDC}} = E_Z \{e_{APDC}\}^T \left(\int_V N_{APDC\_xyz} \, dV \right) A_{coeff\_P} \{\boldsymbol{\delta}_{\mathbf{P}}\} \tag{3.69}$$

3.1.3.4 Kinetic Energy due to in-plane, bending and shear strains

The kinetic energy for the composite plate is defined as:

$$\mathbf{K.E.} = \frac{1}{2} \int_V m \left(\delta_{p\_xyz}^{\bullet} \right)^2 dV \tag{3.70}$$

Representation of the kinetic energy in terms of the shape functions and nodal deflection vector yields the following relationship:

$$\mathbf{K.E.} = \mathbf{K.E.}\big|_{\mathbf{Plate}} + \mathbf{K.E.}\big|_{\mathbf{Constraining\,Layer}} + \mathbf{K.E.}\big|_{\mathbf{Viscoelastic\,Layer}} + \mathbf{K.E.}\big|_{\mathbf{APDC}} =$$

$$\frac{1}{2}\left\{\dot{\boldsymbol{\delta}}_{\mathbf{P}}\right\}^T \left[A_{coeff\_P}\right]^T \left(I_1 + I_2 + I_3 + I_4 + I_5 + I_6 + I_7 + I_8\right)\left[A_{coeff\_P}\right]\left\{\dot{\boldsymbol{\delta}}_{\mathbf{P}}\right\} \tag{3.71}$$

where,

$$I_1 = m_p \int_{-\frac{h_4}{2}}^{\frac{h_4}{2}} \int_y \int_x \left(\left[N_{pp\_xyz}\right]^T \cdot \left[N_{pp\_xyz}\right]\right) dxdydz\,,$$

$$I_2 = m_p \int_{-\frac{h_4}{2}}^{\frac{h_4}{2}} \int_y \int_x \left(\left[N_{pb\_xyz}\right]^T \cdot \left[N_{pb\_xyz}\right]\right) dxdydz\,,$$

$$I_3 = m_c \int_{h_2+h_3+\frac{h_4}{2}}^{h_1+h_2+h_3+\frac{h_4}{2}} \int_y \int_x \left(\left[N_{cp\_xyz}\right]^T \cdot \left[N_{cp\_xyz}\right]\right) dxdydz\,,$$

$$I_4 = m_c \int_{h_2+h_3+\frac{h_4}{2}}^{h_1+h_2+h_3+\frac{h_4}{2}} \int_y \int_x \left(\left[N_{cb\_xyz}\right]^T \cdot \left[N_{cb\_xyz}\right]\right) dxdydz$$

$$I_5 = m_v \int_{\frac{h_4}{2}}^{h_3+\frac{h_4}{2}} \int_y \int_x \left(\left[N_{vp\_xyz}\right]^T \cdot \left[N_{vp\_xyz}\right]\right) dxdydz\,,$$

$$I_6 = m_v \int_{\frac{h_4}{2}}^{h_3+\frac{h_4}{2}} \int_y \int_x \left(\left[N_{vb\_xyz}\right]^T \cdot \left[N_{vb\_xyz}\right]\right) dxdydz$$

$$I_7 = m_v \int_{\frac{h_4}{2}}^{h_3+\frac{h_4}{2}} \int_y \int_x \left(\left[N_{vs\_xyz}\right]^T \cdot \left[N_{vs\_xyz}\right]\right) dxdydz\,,$$

and $$I_8 = m_{APDC} \int_{h_3+\frac{h_4}{2}}^{h_2+h_3+\frac{h_4}{2}} \int_y \int_x \left(\left[N_{APDC\_xyz}\right]^T \cdot \left[N_{APDC\_xyz}\right]\right) dxdydz\,.$$

3.1.4. Work done due to non-conservative (dissipative) forces in the viscoelastic layer

The non-conservative work ($\mathbf{W_{nc\_v}}$) exerted by the viscoelastic layer arises from the losses defined by the stress-strain relationships for the viscoelastic material ($\sigma_v = K_v \cdot \varepsilon_v$), where K_v is the complex modulus. In this study, the energy dissipation due to bending stresses is neglected compared to that of the shear strain. The same assumption was adopted by Baz (1996), whereby the shear modulus for such material is defined as $G = G' + iG''$, where G' is the shear storage modulus and G'' is the shear loss modulus defined as $G'' = \eta_v G'$, where η_v is the loss factor. Under these conditions the non-conservative work ($\mathbf{W_{nc\_v}}$) is given by:

$$\mathbf{W_{nc\_v}} = \frac{1}{2}\int_V \left(\sigma_{vsnc}^T \cdot \varepsilon_{vs}\right) dV \tag{3.72}$$

where "σ_{vsnc}" is the non-conservative shear stress vector of size (2×1) in the viscoelastic layer defined as:

$$\sigma_{vsnc} = \left(\sigma_{vsncx} \quad \sigma_{vsncy}\right)^T \tag{3.73}$$

where,

σ_{vsncx},: non-conservative shear stress in the x-direction in the viscoelastic layer,

and σ_{vsncy} : non-conservative shear stress in the y-direction in the viscoelastic layer.

The relationships between "σ_{vncs}" and the corresponding strain vector is defined in

terms of the shear loss modulus (G''), such that $\sigma_{vncs} = iG''\varepsilon_{vs}$.

Hence, the non-conservative work done due to shear of the viscoelastic material can therefore be expressed as:

$$\mathbf{W_{nc\_v}} = \frac{1}{2}\{\boldsymbol{\delta}_\mathbf{P}\}^T \left[A_{coeff\_P}\right]^T (I_9)\left[A_{coeff\_P}\right]\{\boldsymbol{\delta}_\mathbf{P}\} \tag{3.74}$$

where, $I_9 = iG''\int_{\frac{h_4}{2}}^{h_3+\frac{h_4}{2}} \int_y \int_x \left(\left[N_{vs\_xyz}\right]^T \cdot \left[N_{vs\_xyz}\right]\right) dxdydz$

3.1.5. Element Stiffness and Mass Matrices

Lagrange's equations of motion can be developed using the following extended Hamilton's principle (Baruh, 1998):

$$\int_{t_1}^{t_2} \left(\delta\left(\mathbf{K.E.}(\boldsymbol{\delta}_\mathbf{P}^\bullet)\right) - \delta\left(\mathbf{P.E.}(\boldsymbol{\delta}_\mathbf{P})\right) + \delta\left(\mathbf{W_{nc}}(\boldsymbol{\delta}_\mathbf{P})\right)\right) dt =$$

$$\int_{t_1}^{t_2} \delta\left(\mathbf{L}(\boldsymbol{\delta}_\mathbf{P}, \boldsymbol{\delta}_\mathbf{P}^\bullet)\right) dt + \int_{t_1}^{t_2} \delta\left(\mathbf{W_{nc}}(\boldsymbol{\delta}_\mathbf{P})\right) dt = 0 \tag{3.75}$$

where, $\mathbf{L}(\boldsymbol{\delta}_\mathbf{P}, \boldsymbol{\delta}_\mathbf{P}^\bullet)$ is the Lagrangian defined as $\mathbf{K.E.}(\boldsymbol{\delta}_\mathbf{P}^\bullet) - \mathbf{P.E.}(\boldsymbol{\delta}_\mathbf{P})$, and $\mathbf{W_{nc}} = \mathbf{W_{nc\_v}} + \mathbf{W_{nc\_APDC}}$ is the non-conservative work exerted by the viscoelastic layer and the APDC respectively. The variation of the non-conservative work $\delta\mathbf{W_{nc}}$ is given by:

$$\delta \mathbf{W_{nc}} = \mathbf{Q_{nc}}\delta(\boldsymbol{\delta}_\mathbf{P}) =$$

$$\left[A_{coeff\_P}\right]^T iG''\left(\int_{\frac{h_4}{2}}^{h_3+\frac{h_4}{2}} \int_y \int_x \left(\left[N_{vs\_xyz}\right]^T \cdot \left[N_{vs\_xyz}\right]\right) dxdydz\right) \cdot \left[A_{coeff\_P}\right] \{\boldsymbol{\delta}_\mathbf{P}\} \delta(\boldsymbol{\delta}_\mathbf{P}) -$$

$$E_Z \{g_{APDC}\}^T \left(\int_{Vol} N_{APDC\_xyz}\, d(Vol)\right) \left[A_{coeff\_P}\right] \delta(\boldsymbol{\delta}_\mathbf{P}) \tag{3.76}$$

The variation of the Lagrangian "$\delta\mathbf{L}$" can also be determined and combined with $\delta\mathbf{W_{nc}}$ to obtain the following Lagrange's equation of the system:

$$\frac{\partial \mathbf{L}}{\partial(\boldsymbol{\delta}_\mathbf{P})} - \frac{d}{dt}\frac{\partial \mathbf{L}}{\partial\left(\dot{\boldsymbol{\delta}}_\mathbf{P}\right)} = -\mathbf{Q_{nc}} \tag{3.77}$$

This yields the following system of differential equations of motion:

$$\left(\mathbf{M_p} + \mathbf{M_c} + \mathbf{M_v}\right)\{\ddot{\boldsymbol{\delta}}_\mathbf{P}\} + \left(\mathbf{K_p} + \mathbf{K_c} + \mathbf{K_v}\right)\{\boldsymbol{\delta}_\mathbf{P}\} = -\mathbf{Q_{nc}} \tag{3.78}$$

where,

$$\mathbf{K_p} = \left[A_{coeff\_P}\right]^T \int_{-\frac{h_4}{2}}^{\frac{h_4}{2}} \int_y \int_x \begin{pmatrix} \left[N_{pp\_xyz}\right]^T \cdot D_{pp}^T \cdot \left[N_{pp\_xyz}\right] + \\ z^2 \left[N_{pb\_xyz}\right]^T \cdot D_{pb}^T \cdot \left[N_{pb\_xyz}\right] \end{pmatrix} dxdydz \cdot \left[A_{coeff\_P}\right], \tag{3.79}$$

$$\mathbf{M_p} = \left[A_{coeff\_P}\right]^T \int_{-\frac{h_4}{2}}^{\frac{h_4}{2}} \int_y \int_x \begin{pmatrix} \left[N_{pp\_xyz}\right]^T \cdot \left[N_{pp\_xyz}\right] + \\ \left[N_{pb\_xyz}\right]^T \cdot \left[N_{pb\_xyz}\right] \end{pmatrix} dxdydz \cdot \left[A_{coeff\_P}\right], \tag{3.80}$$

$$\mathbf{K_c} = \left[A_{coeff\_P}\right]^T \int_{h_2+h_3+\frac{h_4}{2}}^{h_1+h_2+h_3+\frac{h_4}{2}} \int_y \int_x \begin{pmatrix} \left[N_{cp\_xyz}\right]^T \cdot D_{cp}^T \cdot \left[N_{cp\_xyz}\right] + \\ z^2 \left[N_{cb\_xyz}\right]^T \cdot D_{cb}^T \cdot \left[N_{cb\_xyz}\right] \end{pmatrix} dxdydz \cdot \left[A_{coeff\_P}\right], \tag{3.81}$$

$$\mathbf{M_c} = \left[A_{coeff\_P}\right]^T \int_{h_2+h_3+\frac{h_4}{2}}^{h_1+h_2+h_3+\frac{h_4}{2}} \int_y \int_x \begin{pmatrix} \left[N_{cp\_xyz}\right]^T \cdot \left[N_{cp\_xyz}\right] + \\ \left[N_{cb\_xyz}\right]^T \cdot \left[N_{cb\_xyz}\right] \end{pmatrix} dxdydz \cdot \left[A_{coeff\_P}\right], \tag{3.82}$$

$$\mathbf{K_v} = \left[A_{coeff\_P}\right]^T \int_{\frac{h_4}{2}}^{h_3+\frac{h_4}{2}} \int_y \int_x \left(\begin{matrix} \left[N_{vp\_xyz}\right]^T \cdot D_v^T \cdot \left[N_{vp\_xyz}\right] + \\ z^2 \left[N_{vb\_xyz}\right]^T \cdot D_v^T \cdot \left[N_{vb\_xyz}\right] \end{matrix} \right) dxdydz \cdot \left[A_{coeff\_P}\right], \tag{3.83}$$

$$\text{and } \mathbf{M_v} = \left[A_{coeff\_P}\right]^T \int_{\frac{h_4}{2}}^{h_3+\frac{h_4}{2}} \int_y \int_x \left(\begin{matrix} \left[N_{vp\_xyz}\right]^T \cdot \left[N_{vp\_xyz}\right] + \\ \left[N_{vb\_xyz}\right]^T \cdot \left[N_{vb\_xyz}\right] \end{matrix} \right) dxdydz \cdot \left[A_{coeff\_P}\right]. \tag{3.84}$$

The $\mathbf{K_i}$ and $\mathbf{M_i}$ are the element stiffness and mass matrices for the base plate ($i=p$), constraining ($i=c$) and viscoelastic layers ($i=v$) respectively.

Also $$\mathbf{Q_{nc}} = \left(\mathbf{K_{nc\_v}}\right)\left\{\boldsymbol{\delta}_\mathbf{P}\right\} + E_z\left\{\mathbf{F_{APDC}}\right\} =$$

$$\left[A_{coeff\_P}\right]^T iG'' \left(\int_{\frac{h_4}{2}}^{h_3+\frac{h_4}{2}} \int_y \int_x \left(\left[N_{vs\_xyz}\right]^T \cdot \left[N_{vs\_xyz}\right]\right) dxdydz \right) \left[A_{coeff\_P}\right] \left\{\boldsymbol{\delta}_\mathbf{P}\right\} -$$

$$E_z \left\{g_{APDC}\right\}^T \left(\int_{Vol} N_{APDC\_xyz}\, d(Vol) \right) \left[A_{coeff\_P}\right] \tag{3.85}$$

is the non-conservative force exerted by the viscoelastic layer and the APDC.

3.2. FINITE ELEMENT MODELING OF POLYURETHANE FOAM

Biot (1956) developed a 3-dimensional model for porous materials used in sound absorption such as polyurethane foam. In that model, Biot used 3-dimensional stress analysis of the foam taking into consideration the solid-fluid coupling losses due to either, momentum change of the fluid particles in the foam, or the frictional losses

between the fluid and solid phases due to fluid viscosity.

The detailed theoretical derivation for the wave propagation in polyurethane foam was presented by Shiau (1991). In that derivation, only the 2-dimensional case is considered by assuming infinite long foam extending in the x direction with finite depth in the y-direction.

Using the same approach in the finite element modeling of the foam will result in considerable modeling difficulty when coupled to a 2-dimensional structure such as a plate. Such difficulty will exist whether the plate is modeled using either classical plate theory, which is valid for thin plates, or first-order shear deformation theory, which is suitable for thick plates. This difficulty arises from the incompatibility of the degrees of freedom of both the 3- and 2-dimensional structural elements. Therefore a 2-dimensional model of the foam was developed to facilitate the coupling with various 2-dimensional structures.

The aforementioned 2-dimensional model is based on the first-order shear deformation theory. The foam element is therefore considered to be a 2-dimensional quad element with 7 degrees of freedom per node as shown in Figure 3.6. These degrees of freedom include u_f, v_f, w_f, ϕ_{fx}, ϕ_{fy} describing the solid phase displacements in the x, y and z-directions as well as rotations about the y and x-axis respectively, and U_f, V_f, describing the fluid displacement in the x- and y-directions.

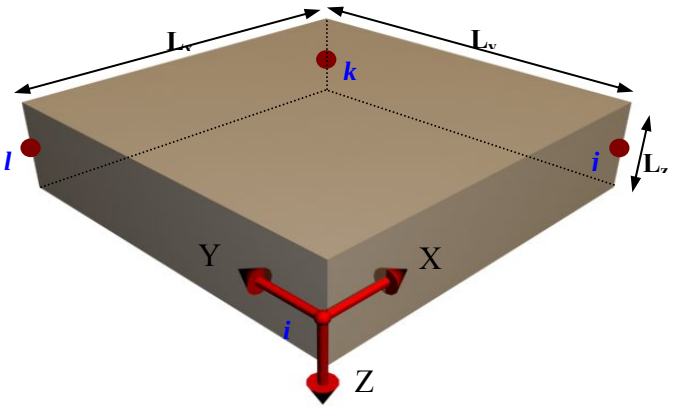

Figure 3.6: Foam quad element.

The following assumptions were adopted:

1. Normal strain in the z-direction of the solid phase is neglected $\left(\frac{\partial w_f}{\partial z} = 0\right)$.
2. Normal strain in the z-direction of the fluid phase is neglected $\left(\frac{\partial W_f}{\partial z} = 0\right)$.
3. A correlation between the transverse displacement of the fluid and solid phases exist.

The deflection vector for any point (x,y,z) inside the element is defined as:

$$\delta_{f\_xyz} = \begin{pmatrix} u_f & v_f & w_f & \phi_{fx} & \phi_{fy} & U_f & V_f \end{pmatrix}^T \tag{3.86}$$

Therefore, for the 4-node element, the overall nodal deflection vector is a (28×1) vector $\{\delta_f\}$ defined as:

$$\{\boldsymbol{\delta}_{\mathbf{f}}\} = \begin{pmatrix} \delta_{f\_i} & \delta_{f\_j} & \delta_{f\_k} & \delta_{f\_l} \end{pmatrix}^T \tag{3.87}$$

where: i, j, k and l are the 4 nodes per element and

$\delta_{f\_nn} = \begin{pmatrix} u_{nn} & v_{nn} & w_{nn} & \phi_{xnn} & \phi_{ynn} & U_{nn} & V_{nn} \end{pmatrix}^T$ represents the deflection vector at node "*nn*". The corresponding element shape function is chosen to be:

$$N_{foam}(x, y, z) = \begin{pmatrix} 1 & x & y & xy \end{pmatrix} \tag{3.88}$$

This shape function is the same for all seven DOF's, and it will be denoted as N_{uf}, N_{vf}, N_{wf}, $N_{\phi fx}$, $N_{\phi fy}$, N_{Uf}, and N_{Vf} corresponding to each DOF of the foam element.

Hence, the spatial distribution of the different displacements are assumed to take the following form,

$$u_f = a_1 + a_2\, x + a_3\, y + a_4\, x.y, \tag{3.89}$$

$$v_f = a_5 + a_6\, x + a_7\, y + a_8\, x.y, \tag{3.90}$$

$$w_f = a_9 + a_{10}\, x + a_{11}\, y + a_{12}\, x.y, \tag{3.91}$$

$$\phi_{fx} = a_{13} + a_{14}\, x + a_{15}\, y + a_{16}\, x.y, \tag{3.92}$$

$$\phi_{fy} = a_{17} + a_{18}\, x + a_{19}\, y + a_{20}\, x.y, \tag{3.93}$$

$$U_f = a_{21} + a_{22}\, x + a_{23}\, y + a_{24}\, x.y, \tag{3.94}$$

and $$V_f = a_{25} + a_{26}\, x + a_{27}\, y + a_{28}\, x.y, \tag{3.95}$$

where the constants $\{a_1, a_2, \ldots, a_{28}\}$ are to be determined in terms of the 28 components of the nodal degrees of freedom vector $\{\boldsymbol{\delta}_{\mathbf{f}}\}$.

Accordingly, the deflection vector $\{\delta_{f\_xyz}\}$ may be expressed in terms of the nodal degrees of freedom vector as follows,

$$\left\{\delta_{f\_xyz}\right\}=\begin{bmatrix} N_{uf} & & & & & & & \\ & N_{vf} & & & & & & \\ & & N_{wf} & & & & & \\ & & & N_{\phi fx} & & & & \\ & & & & N_{\phi fy} & & & \\ & & & & & N_{Uf} & & \\ & & & & & & N_{Vf} & \end{bmatrix}\left[A_{coeff\_f}\right]\{\delta_f\} \qquad (3.96)$$

where $[A_{coeff_f}]$is the (28×28) spatial interpolating matrix corresponding to u_f, v_f, w_f, ϕ_{fx}, ϕ_{fy}, U_f, and V_f.

3.2.1. Element Stiffness Matrix:

The element stiffness matrix is calculated from the potential energy of the element, which is defined as:

$$\mathbf{P.E.}\Big|_{\mathbf{Foam}} = \frac{1}{2}\int_V \sigma_f^T \cdot \varepsilon_{foam}\, dV \qquad (3.97)$$

where "σ_f" is the stress vector of size (6×1) induced in the foam and is defined as:

$$\sigma_f = \begin{pmatrix}\sigma_{fx} & \sigma_{fy} & \tau_{xy} & \tau_{xz} & \tau_{yz} & s_f\end{pmatrix}^T \qquad (3.98)$$

where:

σ_{fx} : normal stress in the solid phase in the x-direction,

σ_{fy} : normal stress in the solid phase in the y-direction,

τ_{fxy} : shear stress in the solid phase in the xy plane,

τ_{fxz} : shear stress in the solid phase in the xz plane,

τ_{fyz} : shear stress in the solid phase in the yz plane,

s_f : force per unit area acting on the fluid phase,

and "ε_{foam}" is a strain vector of size (6×1) and is defined as:

$$\begin{Bmatrix} e_{fx} \\ e_{fy} \\ \gamma_{fxy} \\ \gamma_{fxz} \\ \gamma_{fyz} \\ \varepsilon_{fv} \end{Bmatrix} = \begin{Bmatrix} \dfrac{\partial u_f}{\partial x} + z\dfrac{\partial \phi_{fx}}{\partial x} \\ \dfrac{\partial v_f}{\partial x} + z\dfrac{\partial \phi_{fy}}{\partial y} \\ \dfrac{\partial u_f}{\partial x} + \dfrac{\partial v_f}{\partial x} + z\left(\dfrac{\partial \phi_{fx}}{\partial y} + \dfrac{\partial \phi_{fy}}{\partial x}\right) \\ \phi_{fx} + \dfrac{\partial w_f}{\partial x} \\ \phi_{fy} + \dfrac{\partial w_f}{\partial y} \\ \dfrac{\partial U_f}{\partial x} + \dfrac{\partial V_f}{\partial y} \end{Bmatrix} \tag{3.99}$$

where:

e_{fx} : normal strain of the solid phase in the x-direction,

e_{fy} : normal strain of the solid phase in the y-direction,

γ_{fxy} : shear strain of the solid phase in the xy plain,

γ_{fxz} : shear strain of the solid phase in the xz plain,

γ_{fyz} : shear strain of the solid phase in the yz plain,

$\varepsilon_{fv} = \nabla \cdot \overline{U}_f$: fluid volumetric strain,

and $\overline{U}_f$: fluid displacement vector.

The stress vector "$\sigma_f = D_f \cdot \varepsilon_f$", where D_f is a (6×6) symmetric matrix defining the stress-strain relationships and is defined as:

$$D_f = \begin{bmatrix} \frac{E}{(1-\upsilon^2)} & \frac{\upsilon E}{(1-\upsilon^2)} & 0 & 0 & 0 & Q \\ \frac{\upsilon E}{(1-\upsilon^2)} & \frac{E}{(1-\upsilon^2)} & 0 & 0 & 0 & Q \\ 0 & 0 & \frac{E}{2(1+\upsilon)} & 0 & 0 & 0 \\ 0 & 0 & 0 & \frac{E}{2(1+\upsilon)} & 0 & 0 \\ 0 & 0 & 0 & 0 & \frac{E}{2(1+\upsilon)} & 0 \\ Q & Q & 0 & 0 & 0 & R \end{bmatrix} \tag{3.100}$$

Now, let $N_{f\_xyz}(x, y, z) =$

$$\{N_{uf\_x} + z\, N_{\phi fx\_x} \quad N_{vf\_y} + z\, N_{\phi fy\_y} \quad N_{uf\_y} + N_{vf\_x} + z\left(N_{\phi fx\_y} + N_{\phi fy\_x}\right) \quad N_{\phi fx} + N_{wf\_x} \quad N_{\phi fy} + N_{wf\_y} \quad N_{Uf\_x} + N_{Vf\_y}\}^T \tag{3.101}$$

where $N_{(\_x)}$ is defined as $\frac{\partial N_{(\,)}}{\partial x}$ and similarly $N_{(\_y)}$, $N_{(\_z)}$.

Then, the potential energy can be expressed as:

$$\mathbf{P.E.}\big|_{\mathbf{Foam}} = \frac{1}{2}\{\boldsymbol{\delta}_\mathbf{f}\}^\mathbf{T}\left[A_{coeff\_f}\right]^T \int_V \left[N_{f\_xyz}\right]^T \cdot D_f^T \cdot \left[N_{f\_xyz}\right] dV \cdot \left[A_{coeff\_f}\right]\{\boldsymbol{\delta}_\mathbf{f}\} \tag{3.102}$$

and the element stiffness matrix can be easily shown to be equal to:

$$\mathbf{K_f} = \left[A_{coeff\_f}\right]^T \left(\int_V \left[N_{f\_xyz}\right]^T . D_f^T . \left[N_{f\_xyz}\right] dV \right) \left[A_{coeff\_f}\right] \tag{3.103}$$

It should be noted that the inclusion of transverse shear strains in the equations presents computational difficulties when the side-to-thickness ratio of the foam is large (i.e., when the foam becomes thin). For thin plate-like structures, the transverse shear strains ($e_{xz}=\phi_x+\partial_{wf}/\partial_x$ and $e_{yz}=\phi_y+\partial_{wf}/\partial_y$) are negligible, and consequently the element stiffness matrix becomes extremely stiff. This phenomenon is called shear locking and can be overcome using reduced order integration for the parts containing both the shear strains.

3.2.2. Element Mass Matrix:

The element mass matrix can be calculated from the relationship governing the dynamics of the solid and fluid phases of the foam, which is expressed as follows:

$$\sum \left. \frac{Force}{unit\,volume} \right|_{x-direction} = C_1 \cdot \ddot{x} + C_2 \cdot \dot{x} \tag{3.104}$$

The first term on the RHS corresponds to the inertial effect of each of the solid and fluid phases in addition to the inertial coupling in-between. The second term represents

the viscous coupling between the solid and fluid phases, which depends on the velocity and not the acceleration as the first part.

The dynamic relations for the solid and fluid phases of the foam, which relate the forces acting on an incremental volume of the foam to its resulting motion, are defined as follows (Shiau, 1991):

For solid phase:

$$\frac{\partial \sigma_x}{\partial x}+\frac{\partial \tau_{yx}}{\partial y}+\frac{\partial \tau_{zx}}{\partial z}=\rho_1\frac{\partial^2 u_f}{\partial t^2}+\rho_2(q^2-1)\frac{\partial^2}{\partial t^2}(u_f-U_f)+b\frac{\partial}{\partial t}(u_f-U_f), \quad (3.105)$$

$$\frac{\partial \tau_{xy}}{\partial x}+\frac{\partial \sigma_y}{\partial y}+\frac{\partial \tau_{zy}}{\partial z}=\rho_1\frac{\partial^2 v_f}{\partial t^2}+\rho_2(q^2-1)\frac{\partial^2}{\partial t^2}(v_f-V_f)+b\frac{\partial}{\partial t}(v_f-V_f), \quad (3.106)$$

and $$\frac{\partial \tau_{xz}}{\partial x}+\frac{\partial \tau_{yz}}{\partial y}+\frac{\partial \sigma_z}{\partial z}=\rho_1\frac{\partial^2 w_f}{\partial t^2}+\rho_2(q^2-1)\frac{\partial^2}{\partial t^2}(w_f-W_f)+b\frac{\partial}{\partial t}(w_f-W_f). \quad (3.107)$$

For fluid phase:

$$\frac{\partial s}{\partial x}=\rho_2\frac{\partial^2 U_f}{\partial t^2}+\rho_2(q^2-1)\frac{\partial^2}{\partial t^2}(U_f-u_f)+b\frac{\partial}{\partial t}(U_f-u_f), \quad (3.108)$$

$$\frac{\partial s}{\partial y}=\rho_2\frac{\partial^2 V_f}{\partial t^2}+\rho_2(q^2-1)\frac{\partial^2}{\partial t^2}(V_f-v_f)+b\frac{\partial}{\partial t}(V_f-v_f), \quad (3.109)$$

and $$\frac{\partial s}{\partial z}=\rho_2\frac{\partial^2 W_f}{\partial t^2}+\rho_2(q^2-1)\frac{\partial^2}{\partial t^2}(W_f-w_f)+b\frac{\partial}{\partial t}(W_f-w_f) \quad (3.110)$$

Noting that:

6. Inclusion of W_f (transverse fluid displacement) in the equations of motion is due to the fact that, although normal strain in the z-direction of the fluid phase is neglected, fluid motion in the z-direction still exists in a constant manner across the thickness.
7. The net force per unit volume acting on an incremental solid volume is balanced by the acceleration of the solid phase (first term on RHS of equation 3.105 to 3.107), inertial coupling force proportional to the relative acceleration of the two phases (second term on RHS) and viscous coupling force proportional to the relative velocity of the two phases (third term on RHS).
8. ρ_1 is the bulk density of the solid phase.
9. ρ_2 is the bulk density of the fluid phase.
10. Inertial coupling force is the result of momentum transfer between the solid and fluid resulting from pore tortuosity, which is quantified by "the structure factor, q^2".
11. b is a viscous coupling factor that can be related to macroscopic flow resistivity of the porous material.

Accordingly, the mass distributed over the volume can be expressed as follows:

For the solid phase:

$$\mathbf{M_{1\_s}} = \int_V \left[\begin{array}{l} \rho_1 \left(u_f^T u_f + v_f^T v_f + w_f^T w_f \right) + \\ \rho_a \left(\begin{array}{l} \left(u_f - U_f \right)^T \left(u_f - U_f \right) + \left(v_f - V_f \right)^T \left(v_f - V_f \right) + \\ \left(w_f - W_f \right)^T \left(w_f - W_f \right) \end{array} \right) \end{array} \right] dV \,, \tag{3.111}$$

and $$\mathbf{M_{2\_s}} = b \int_V \left[\begin{array}{l} \left(u_f - U_f \right)^T \left(u_f - U_f \right) + \left(v_f - V_f \right)^T \left(v_f - V_f \right) + \\ \left(w_f - W_f \right)^T \left(w_f - W_f \right) \end{array} \right] dV \tag{3.112}$$

where, $\rho_a = \rho_2 (q^2 - 1)$.

In terms of the shape functions, the above equations reduce to:

$$\begin{array}{l} \mathbf{M_{1\_s}} = \left[A_{coeff} \right]^T \int_V \rho_1 \left(N_{uf}^T \cdot N_{uf} + N_{vf}^T \cdot N_{vf} + N_{wf}^T \cdot N_{wf} \right) + \\ \rho_a \left(\begin{array}{l} \left(N_{uf} - N_{Uf} \right)^T \left(N_{uf} - N_{Uf} \right) + \\ \left(N_{vf} - N_{Vf} \right)^T \left(N_{vf} - N_{Vf} \right) + \\ \left(N_{wf} - N_{Wf} \right)^T \left(N_{wf} - N_{Wf} \right) \end{array} \right) dV \left[A_{coeff} \right], \end{array} \tag{3.113}$$

and $$\mathbf{M_{2\_s}} = \left[A_{coeff} \right]^T b \int_V \left(\begin{array}{l} \left(N_{uf} - N_{Uf} \right)^T \left(N_{uf} - N_{Uf} \right) + \\ \left(N_{vf} - N_{Vf} \right)^T \left(N_{vf} - N_{Vf} \right) + \\ \left(N_{wf} - N_{Wf} \right)^T \left(N_{wf} - N_{Wf} \right) \end{array} \right) dV \left[A_{coeff} \right]. \tag{3.114}$$

For the fluid phase:

$$\mathbf{M_{1\_f}} = \int_V \begin{bmatrix} \rho_{21}\left(U_f^T U_f + V_f^T V_f + W_f^T W_f\right) + \\ \rho_a \begin{pmatrix} \left(U_f - u_f\right)^T \left(U_f - u_f\right) + \left(V_f - v_f\right)^T \left(V_f - v_f\right) + \\ \left(W_f - w_f\right)^T \left(W_f - w_f\right) \end{pmatrix} \end{bmatrix} dV, \tag{3.115}$$

$$\mathbf{M_{2\_f}} = b\int_V \begin{bmatrix} \left(U_f - u_f\right)^T \left(U_f - u_f\right) + \left(V_f - v_f\right)^T \left(V_f - v_f\right) + \\ \left(W_f - w_f\right)^T \left(W_f - w_f\right) \end{bmatrix} dV. \tag{3.116}$$

In terms of the shape functions, the above equations reduce to:

$$\begin{aligned} \mathbf{M_{1\_f}} = &\left[A_{coeff}\right]^T \int_V \rho_2 \left(N_{Uf}^T \cdot N_{Uf} + N_{Vf}^T \cdot N_{Vf} + N_{Wf}^T \cdot N_{Wf}\right) + \\ &\rho_a \begin{pmatrix} \left(N_{Uf} - N_{uf}\right)^T \left(N_{Uf} - N_{uf}\right) + \\ \left(N_{Vf} - N_{vf}\right)^T \left(N_{Vf} - N_{vf}\right) + \\ \left(N_{Wf} - N_{wf}\right)^T \left(N_{Wf} - N_{wf}\right) \end{pmatrix} dV \left[A_{coeff}\right], \end{aligned} \tag{3.117}$$

and $$\mathbf{M_{2\_f}} = \left[A_{coeff}\right]^T b \int_V \begin{pmatrix} \left(N_{Uf} - N_{uf}\right)^T \left(N_{Uf} - N_{uf}\right) + \\ \left(N_{Vf} - N_{vf}\right)^T \left(N_{Vf} - N_{vf}\right) + \\ \left(N_{Wf} - N_{wf}\right)^T \left(N_{Wf} - N_{wf}\right) \end{pmatrix} dV \left[A_{coeff}\right]. \tag{3.118}$$

Therefore, the equation of motion of the foam can be expressed as:

$$\left(\mathbf{M_{1\_s}} + \mathbf{M_{1\_f}}\right)\left\{\ddot{\boldsymbol{\delta}}_\mathbf{f}\right\} + \left(\mathbf{M_{2\_s}} + \mathbf{M_{2\_f}}\right)\left\{\dot{\boldsymbol{\delta}}_\mathbf{f}\right\} + \left(\mathbf{K_f}\right)\left\{\boldsymbol{\delta}_\mathbf{f}\right\} = f_f \tag{3.119}$$

where "f_f" is the external forces applied on the foam element.

3.2.3. Verifying the Reduced-Dimension Finite Element Model:

To verify the assumptions made in reducing the finite element model of the foam from a three- to two-dimensional model, a detailed inspection of a 3-dimensional finite element model for the foam was carried out and the results were compared to the predictions of the reduced-dimension model.

A finite element model is developed, utilizing the 3-dimensional stress-strain relationships and dynamic equations to model the foam as a 3D-object with finite dimensions as shown in Figure 3.7.

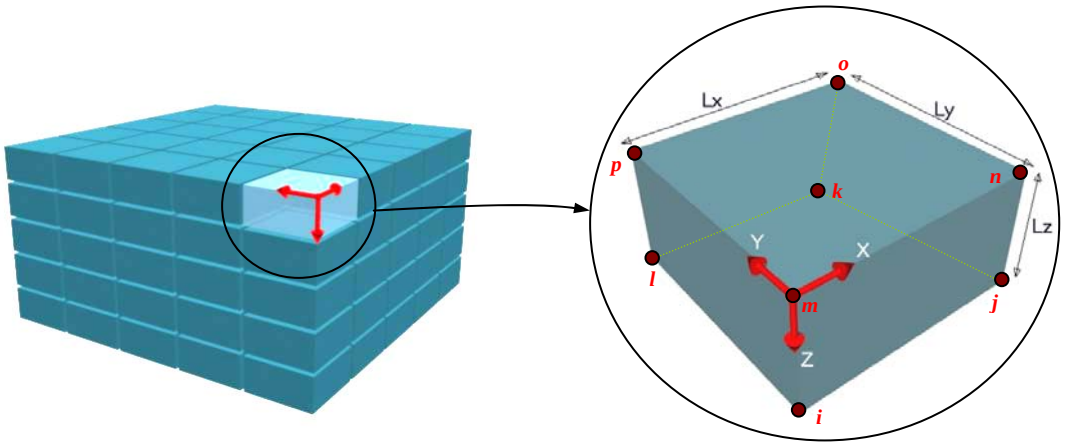

Figure 3.7: Foam brick element.

The foam element is considered to be a brick element with 8 nodes, and 6 degrees of freedom per node. These degrees of freedom include u_f, v_f, w_f describing the solid phase displacements in the x, y and z-direction respectively, and U_f, V_f, W_f describing their fluid

phase counterparts.

The deflection vector for any point (x,y,z) inside the element is defined as:

$$\delta_{f\_xyz} = \begin{pmatrix} u_f & v_f & w_f & U_f & V_f & W_f \end{pmatrix}^T \tag{3.120}$$

Therefore, for the 8-node element, the overall nodal deflection vector is a (48×1) vector $\{\boldsymbol{\delta_f}\}$ defined as:

$$\{\boldsymbol{\delta_f}\} = \begin{pmatrix} \delta_{f\_i} & \delta_{f\_j} & \delta_{f\_k} & \delta_{f\_l} & \delta_{f\_m} & \delta_{f\_n} & \delta_{f\_o} & \delta_{f\_p} \end{pmatrix}^T \tag{3.121}$$

where $i, j, \ldots, p$ are the 8 nodes per element and

$\delta_{f\_nn} = (u_{nn} \quad v_{nn} \quad w_{nn} \quad U_{nn} \quad V_{nn} \quad W_{nn})^T$ represents the deflection vector at node "*nn*".

The corresponding element shape function is chosen to be:

$$N_{foam}(x, y, z) = \begin{pmatrix} 1 & x & y & z & xy & xz & yz & xyz \end{pmatrix} \tag{3.122}$$

Such shape function is the same for all the six DOF's, and it will be denoted as N_{uf}, N_{vf}, N_{wf}, N_{Uf}, N_{Vf} and N_{Wf} corresponding to each DOF of the foam element.

Hence, the spatial distribution of the different displacements are assumed to take the following form,

$$u_f = a_1+a_2\,x+a_3\,y+a_4\,z+a_5\,x.y+a_6\,x.z+a_7\,y.z+a_8\,x.y.z, \quad (3.123)$$

$$v_f = a_9+a_{10}\,x+a_{11}\,y+a_{12}\,z+a_{13}\,x.y+a_{14}\,x.z+a_{15}\,y.z+a_{16}\,x.y.z, \quad (3.124)$$

$$w_f = a_{17}+a_{18}\,x+a_{19}\,y+a_{20}\,z+a_{21}\,x.y+a_{22}\,x.z+a_{23}\,y.z+a_{24}\,x.y.z, \quad (3.125)$$

$$U_f = a_{25}+a_{26}\,x+a_{27}\,y+a_{28}\,z+a_{29}\,x.y+a_{30}\,x.z+a_{31}\,y.z+a_{32}\,x.y.z, \quad (3.126)$$

$$V_f = a_{33}+a_{34}\,x+a_{35}\,y+a_{36}\,z+a_{37}\,x.y+a_{38}\,x.z+a_{39}\,y.z+a_{40}\,x.y.z, \quad (3.127)$$

and $$W_f = a_{41}+a_{42}\,x+a_{43}\,y+a_{44}\,z+a_{45}\,x.y+a_{46}\,x.z+a_{47}\,y.z+a_{48}\,x.y.z \quad (3.128)$$

where the constants $\{a_1, a_2, \ldots, a_{48}\}$ are to be determined in terms of the 48 components of the nodal degrees of freedom vector $\{\delta_f\}$.

Accordingly, the deflection vector $\{\delta_{f\_xyz}\}$ may be expressed in terms of the nodal degrees of freedom vector as follows,

$$\{\delta_{f\_xyz}\} = \begin{bmatrix} N_{uf} & & & & & & \\ & N_{vf} & & & & & \\ & & N_{wf} & & & & \\ & & & N_{Uf} & & & \\ & & & & N_{Vf} & & \\ & & & & & N_{Wf} & \end{bmatrix} [A_{coeff\_f}]\{\delta_f\} \quad (3.129)$$

where $[A_{coeff_f}]$is the (48×48) spatial interpolating matrix corresponding to u_f, v_f, w_f, U_f, V_f and W_f .

The element stiffness and mass matrices are calculated in the same manner as in the reduced-dimension case, taking into consideration that the stress-strain relationship is defined as:

$$\begin{Bmatrix} \sigma_{fx} \\ \sigma_{fy} \\ \sigma_{fz} \\ \tau_{fxy} \\ \tau_{fxz} \\ \tau_{fyz} \\ s_f \end{Bmatrix} = \begin{bmatrix} \frac{E}{(1-\upsilon^2)} & \frac{\upsilon E}{(1-\upsilon^2)} & \frac{\upsilon E}{(1-\upsilon^2)} & 0 & 0 & 0 & Q \\ \frac{\upsilon E}{(1-\upsilon^2)} & \frac{E}{(1-\upsilon^2)} & \frac{\upsilon E}{(1-\upsilon^2)} & 0 & 0 & 0 & Q \\ \frac{\upsilon E}{(1-\upsilon^2)} & \frac{\upsilon E}{(1-\upsilon^2)} & \frac{E}{(1-\upsilon^2)} & 0 & 0 & 0 & Q \\ 0 & 0 & 0 & \frac{E}{2(1+\upsilon)} & 0 & 0 & 0 \\ 0 & 0 & 0 & 0 & \frac{E}{2(1+\upsilon)} & 0 & 0 \\ 0 & 0 & 0 & 0 & 0 & \frac{E}{2(1+\upsilon)} & 0 \\ Q & Q & Q & 0 & 0 & 0 & R \end{bmatrix} \begin{Bmatrix} e_{fx} \\ e_{fy} \\ e_{fz} \\ \gamma_{fxy} \\ \gamma_{fxy} \\ \gamma_{fxy} \\ \varepsilon_{fv} \end{Bmatrix} \quad (3.130)$$

where:

$e_{fx} = \frac{\partial u}{\partial x}$: normal strain of the solid phase in the x-direction,

$e_{fy} = \frac{\partial v}{\partial y}$: normal strain of the solid phase in the y-direction,

$e_{fz} = \frac{\partial w}{\partial z}$: normal strain of the solid phase in the z-direction,

$\gamma_{fxy} = \frac{\partial u}{\partial y} + \frac{\partial v}{\partial x}$: shear strain of the solid phase in the xy plain,

$\gamma_{fxz} = \frac{\partial u}{\partial z} + \frac{\partial w}{\partial x}$: shear strain of the solid phase in the xz plain,

$\gamma_{fyz} = \frac{\partial v}{\partial z} + \frac{\partial w}{\partial y}$: shear strain of the solid phase in the yz plain,

$\varepsilon_{fv} = \nabla \cdot \overline{U}_f$: fluid volumetric strain,

and $\overline{U}_f$: fluid displacement vector.

The 3-dimensional finite element model is used to model a (12" × 12" × 0.5"), (12" ×

12" × 3") and (12" × 12" × 12") foam plates subject to harmonic distributed force acting in the transverse direction. The plates are clamped from all sides and are each divided into 8×8×8 elements. Plotting the transverse displacement of the solid and fluid phases reveals that the displacement field is constant along the transverse direction as long as the foam thickness is relatively small compared to the side lengths regardless of the excitation frequency as shown in Figures 3.8 through 3.10. Hence assuming that ($\partial w_f/\partial z = 0$) and ($\partial W_f/\partial z = 0$) in the reduced-dimension model, was a correct assumption.

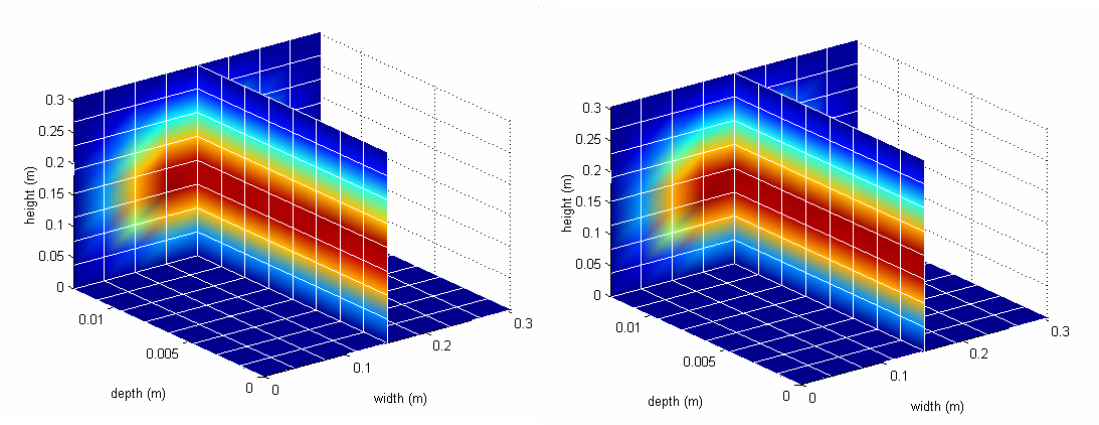

b- transverse displacement field of the solid phase (20 Hz)

a- transverse displacement field of the fluid phase (20 Hz)

d- transverse displacement field of the solid phase (140 Hz)

c- transverse displacement field of the fluid phase (140 Hz)

Figure 3.8: Transverse displacement field for solid and fluid phases for (12" × 12" × 0.5") foam plate.

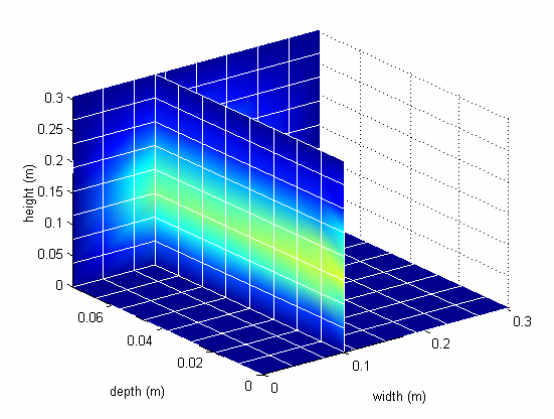

a- transverse displacement field of the solid phase (20 Hz)

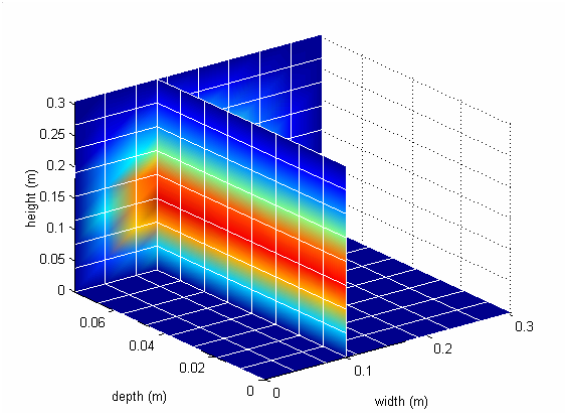

b- transverse displacement field of the fluid phase (20 Hz)

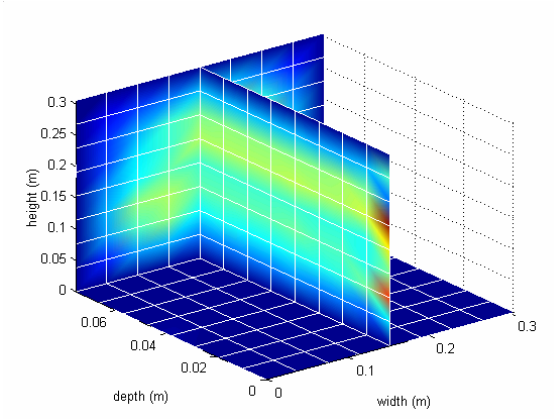

c- transverse displacement field of the solid phase (140 Hz)

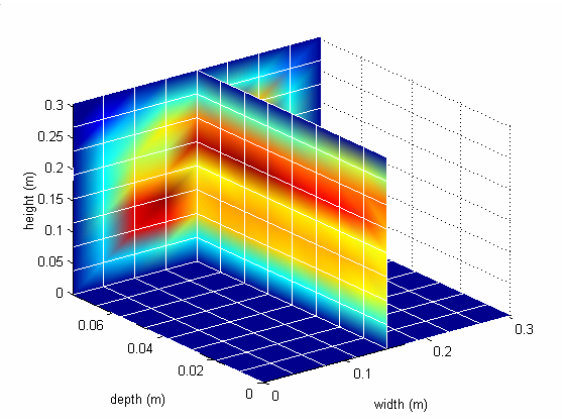

d- transverse displacement field of the fluid phase (140 Hz)

Figures 3.9: Transverse displacement field for solid and fluid phases for (12" × 12" × 3") foam plate.

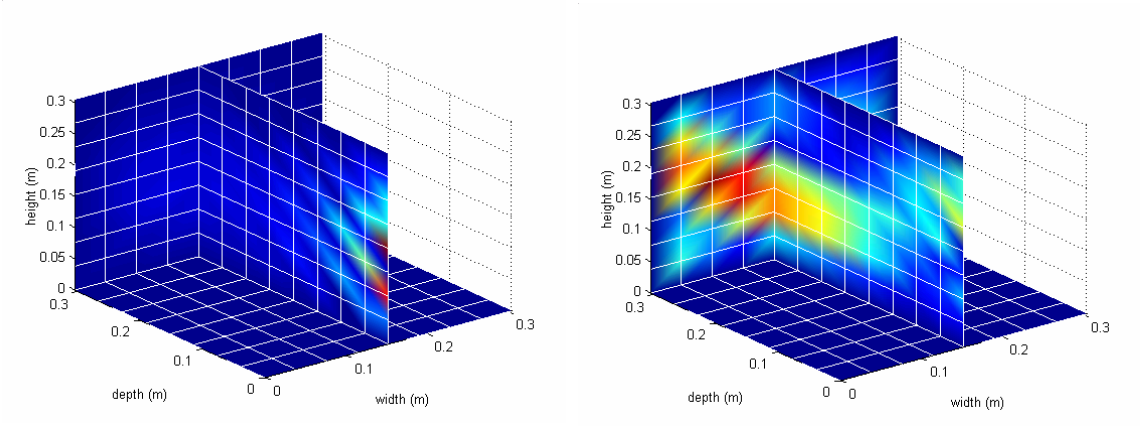

a- transverse displacement field of the solid phase (20 Hz)

b- transverse displacement field of the fluid phase (20 Hz)

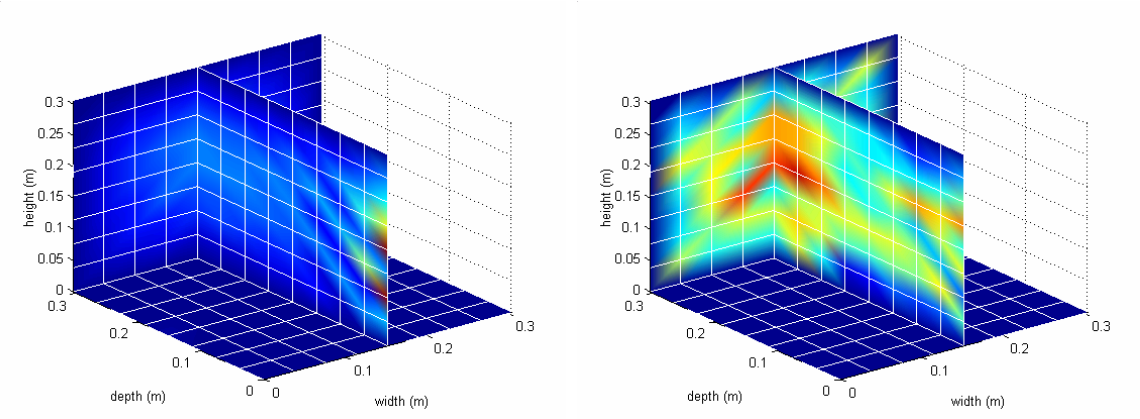

c- transverse displacement field of the solid phase (140 Hz)

d- transverse displacement field of the fluid phase (140 Hz)

Figure 3.10: Transverse displacement field for solid and fluid phases for (12" × 12" × 12") foam plate.

Then by comparing the transverse displacement distribution of the foam for both the 3-dimensional model and reduced-dimension model, a very good match was found as shown in Figures 3.11 and 3.12.

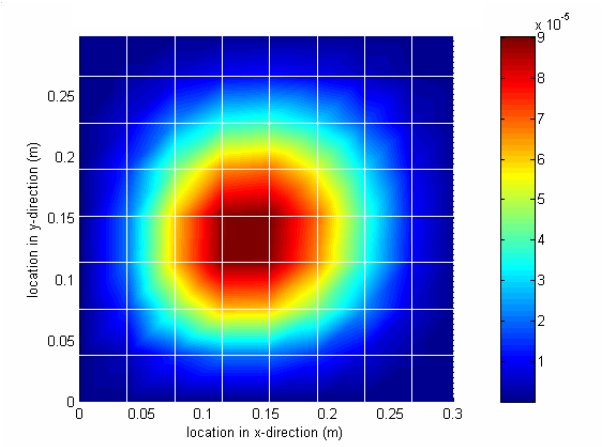

a- transverse displacement field of the 2-dimension model

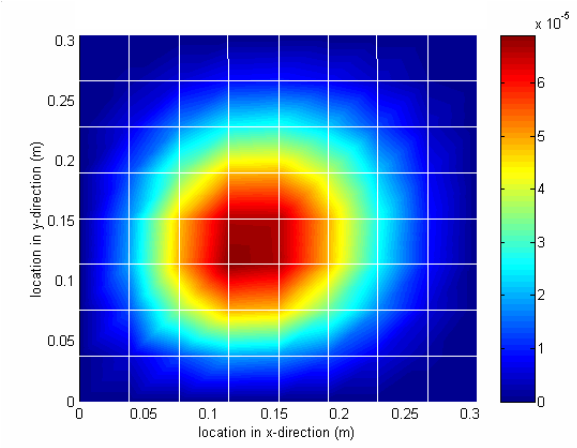

b- transverse displacement field using the 3-dimension model of the solid phase

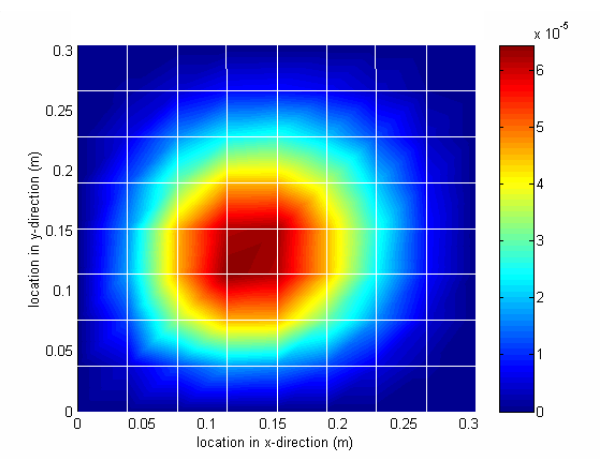

c- transverse displacement field using the 3-dimension model of the fluid phase

Figure 3.11: The transverse displacement fields for both the 3- and reduced-dimension models (20 Hz).

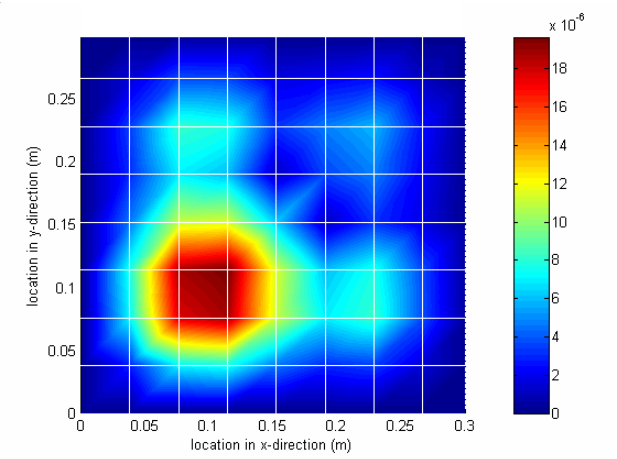

a-transverse displacement field of the 2-dimension model

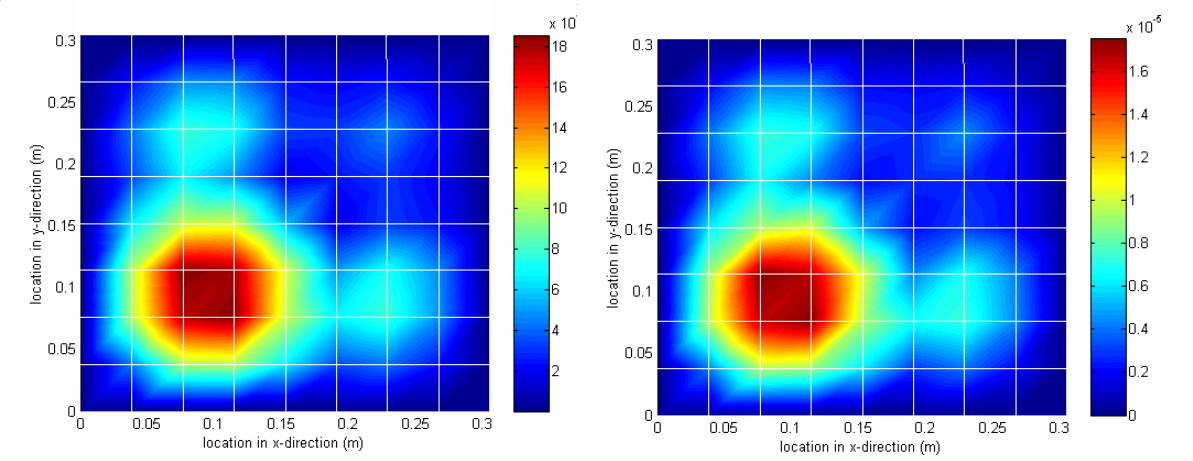

b-transverse displacement field using the 3-dimension model of the solid phase

c-transverse displacement field using the 3-dimension model of the fluid phase

Figure 3.12: The transverse displacement fields for both the 3- and reduced-dimension models (140 Hz).

Finally the transverse and in-plane frequency response for 2 points located at (7" , 7") and (4", 4") were also compared, and a good agreement was also noticed between the 3-dimension and the newly developed reduced-dimension models as shown in Figures 3.13 and 3.14.

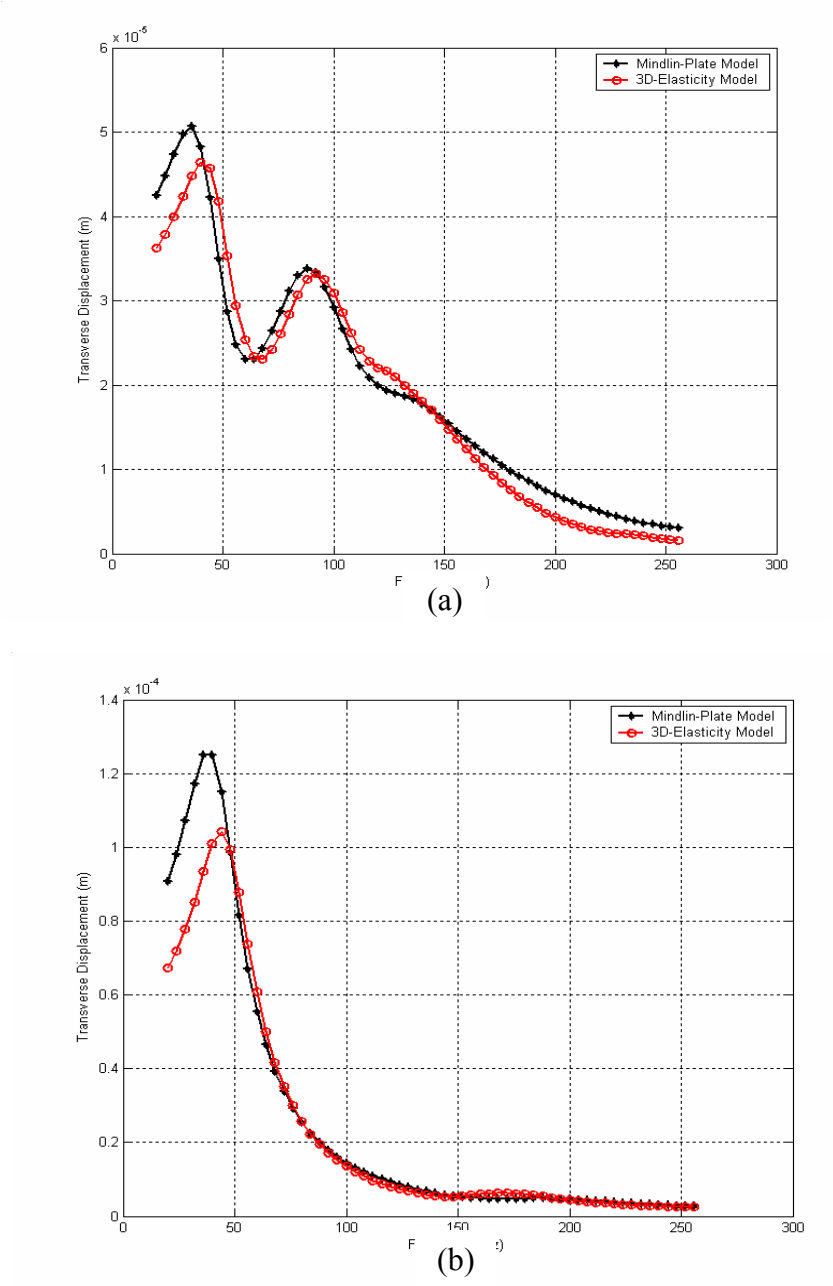

Figure 3.13: The transverse frequency response for both 3 and reduced dimension models(a) point located at (7" , 7") and (b) point located at (4" , 4").

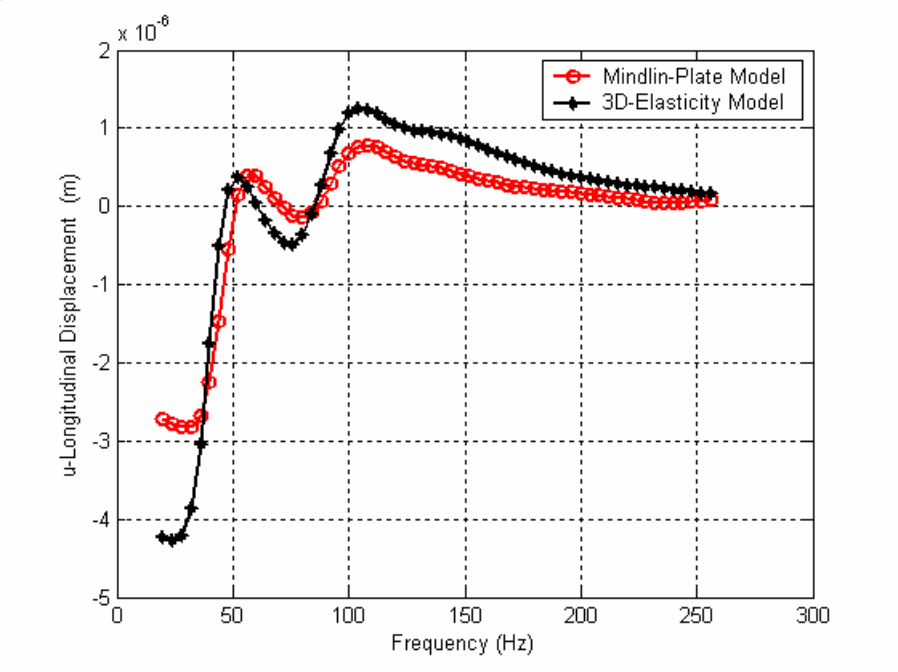

Figure 3.14: The in-plane frequency response for the 3 and reduced dimension models at a point located at (4" , 4").

It can be noticed that at resonance, the response of the reduced-dimension model is slightly higher than that of the 3-dimension model. Also the frequency at which resonance occurs is also slightly higher for the 3-dimension mode. This can be attributed to the fact that by modeling the foam using the 3-dimension model, 8-node brick elements are used, which are considered to be the most stiff brick elements. Using these elements usually results in stiffer structures.

Hence, a good agreement can still be noticed between the two different models, which allows us to use the reduced-dimension model when coupling the foam to any two-dimensional structure.

3.3. FINITE ELEMENT MODEL FOR THE ACOUSTIC CAVITY

Considering a fluid volume "*V*", then the following identities can be defined:

$$\text{Potential Energy } (\mathbf{P.E.}) = \frac{1}{2}\rho_0 c^2 \int_V (div\, u_A)^2\, dV\,, \tag{3.120}$$

$$\text{Kinetic Energy } (\mathbf{K.E.}) = \frac{1}{2}\rho_0 \int_V \dot{u}_A^2\, dV\,, \tag{3.121}$$

The work done on the acoustic cavity by the foam element is given by,

$$(\mathbf{W_F}) = \int_{BoundaryArea} p\left[(1-h_f)w_f + h_f W_f\right] dA, \tag{3.122}$$

The work done on the acoustic cavity by the plate element is given by,

$$(\mathbf{W_P}) = \int_{BoundaryArea} p w_4\, dA \tag{3.123}$$

and the Lagrangian $\mathbf{(J_f) = K.E.-P.E.+W_F}$ (for the foam exposed elements),

$\mathbf{(J_p) = K.E.-P.E.+W_P}$ (for the plate exposed elements)

where, ρ_0 equilibrium density of the acoustic medium,

c sonic speed,

u_A particle displacement in the acoustic medium,

$\dot{u}_A$ particle velocity in the acoustic medium,

p acoustic pressure,

w_f transverse displacement of the solid phase of the foam,

W_f transverse displacement of the fluid phase of the foam,

w_4 transverse displacement of the plate,

and h_f porosity in the foam.

For the sake of simplifying the calculations, the velocity potential φ (a scalar quantity) can be used instead of the acoustic pressure p using the following identities:

- $$p = -\rho_0 \frac{\partial \varphi}{\partial t}, \tag{3.124}$$
- $$\dot{u}_A = -\nabla \varphi = -\left[\frac{\partial \varphi}{\partial x}\vec{i} + \frac{\partial \varphi}{\partial y}\vec{j} + \frac{\partial \varphi}{\partial z}\vec{k} \right], \tag{3.125}$$
- $$\dot{u}_A{}^2 = (-\nabla \varphi)^2 = \left[\left(\frac{\partial \varphi}{\partial x} \right)^2 + \left(\frac{\partial \varphi}{\partial y} \right)^2 + \left(\frac{\partial \varphi}{\partial z} \right)^2 \right], \tag{3.126}$$
- $$div\, u_A = -\frac{1}{c^2}\frac{\partial \varphi}{\partial t}. \tag{3.127}$$

Hence, $$\mathbf{P.E.} = \frac{1}{2}\frac{\rho_0}{c^2}\int_V \varphi^{\bullet 2} dV, \tag{3.128}$$

$$\mathbf{K.E.} = \frac{1}{2}\rho_0 \int_V (\nabla \varphi)^2 dV, \tag{3.129}$$

$$\mathbf{W_F} = -\rho_0 \int_{BoundaryArea} \varphi^{\bullet} \left[(1-h_f) w_f + h_f W_f \right] dA, \tag{3.130}$$

and $$\mathbf{W_P} = -\rho_0 \int_{BoundaryArea} \varphi^{\bullet} w_p \, dA. \tag{3.131}$$

By applying a proper shape function for both the displacements w_f, W_f, w_4 and φ, the resultant DOF become, N_{wf} $\mathbf{w_f}$, N_{Wf} $\mathbf{W_f}$, N_{w4} $\mathbf{w_4}$ and N_ϕ $\boldsymbol{\phi}_\mathbf{e}$.

where, $\mathbf{w_f}$, $\mathbf{W_f}$, $\mathbf{w_4}$ and $\boldsymbol{\varphi}_\mathbf{e}$ represent the nodal displacement of the solid and liquid phases of the foam, the nodal plate transverse displacement and the velocity potential at each node respectively. Also N_{wf}, N_{Wf}, N_{w4} and N_φ represent the corresponding shape functions.

Hamilton's principle, as given in equation (3.132) is then used to extract the differential equation of motion of the acoustic fluid, as influenced by the external forces applied on the exposed foam and the plate.

$$\int_{t_1}^{t_2} \delta\left(\mathbf{K.E.} - \mathbf{P.E.} + \mathbf{W_F}\right) dt = 0\,, \tag{3.132-a}$$

and $$\int_{t_1}^{t_2} \delta\left(\mathbf{K.E.} - \mathbf{P.E.} + \mathbf{W_P}\right) dt = 0\,. \tag{3.132-b}$$

3.3.1. Variation of the Potential Energy (δP.E.)

$$\int_{t_1}^{t_2} \delta\left(\mathbf{P.E.}\right) dt = \frac{\rho_0}{c^2} \int_{t_1}^{t_2} \int_V \left\{\boldsymbol{\delta}\dot{\boldsymbol{\varphi}}_\mathbf{e}\right\}^T \left[\left(N_\varphi\right)^T \left(N_\varphi\right)\right] \left\{\dot{\boldsymbol{\varphi}}_\mathbf{e}\right\} dV dt \tag{3.133}$$

Integrating equation (3.133) by parts to eliminate $\left\{\boldsymbol{\delta}\dot{\boldsymbol{\varphi}}_\mathbf{e}\right\}$ yields:

$$\int_{t_1}^{t_2} \delta\left(\mathbf{P.E.}\right) dt = -\frac{\rho_0}{c^2} \int_{t_1}^{t_2} \int_V \left\{\boldsymbol{\delta}\boldsymbol{\varphi}_\mathbf{e}\right\}^T \left[\left(N_\varphi\right)^T \left(N_\varphi\right)\right] \left\{\ddot{\boldsymbol{\varphi}}_\mathbf{e}\right\} dV dt \quad + (B.C. = 0) \tag{3.134}$$

3.3.2. Variation of the Kinetic Energy (δK.E.)

$$\int_{t_1}^{t_2} \delta(\mathbf{K.E.})dt = \rho_0 \int_{t_1}^{t_2} \int_V \{\boldsymbol{\delta\varphi}_\mathbf{e}\}^T \left[(\nabla N_\varphi)^T (\nabla N_\varphi)\right]\{\boldsymbol{\varphi}_\mathbf{e}\}dVdt \tag{3.135}$$

3.3.3. Variation of the Work done by the Foam (δW_f)

$$\mathbf{W_F} = \mathbf{W_{F1}} + \mathbf{W_{F2}}\,, \tag{3.136}$$

$$\mathbf{W_{F1}} = -\rho_0 \int_A \{\boldsymbol{\varphi}_\mathrm{e}^\bullet\}^T (1-h_f)(N_\varphi)^T (N_{wf})\{\mathbf{w_f}\}dA\,, \tag{3.137}$$

$$\mathbf{W_{F2}} = -\rho_0 \int_A \{\boldsymbol{\varphi}_\mathrm{e}^\bullet\}^T h_f (N_\varphi)^T (N_{Wf})\{\mathbf{W_f}\}dA\,, \tag{3.138}$$

$$\int_{t_1}^{t_2} \delta(\mathbf{W_{F1}})dt = -\rho_0 \int_{t_1}^{t_2} \int_A \{\boldsymbol{\delta\varphi}_\mathrm{e}^\bullet\}^T \left[(1-h_f)(N_\varphi)^T (N_{wf})\right]\{\mathbf{w_f}\}dAdt\,, \tag{3.139}$$

and $$\int_{t_1}^{t_2} \delta(\mathbf{W_{F2}})dt = -\rho_0 \int_{t_1}^{t_2} \int_A \{\boldsymbol{\delta\varphi}_\mathrm{e}^\bullet\}^T \left[h_f (N_\varphi)^T (N_{Wf})\right]\{\mathbf{W_f}\}dAdt \tag{3.140}$$

Using integration by parts gives

$$\int_{t_1}^{t_2} \delta(\mathbf{W_{F1}})dt = -\rho_0 \int_{t_1}^{t_2} \int_A \{\boldsymbol{\delta\varphi}_\mathbf{e}\}^T \left[(1-h_f)(N_\varphi)^T (N_{wf})\right]\{\dot{\mathbf{w}}_\mathbf{f}\}dAdt \;+(B.C.=0)\,, \tag{3.141}$$

and $$\int_{t_1}^{t_2} \delta(\mathbf{W_{F2}})dt = -\rho_0 \int_{t_1}^{t_2} \int_A \{\boldsymbol{\delta\varphi}_\mathbf{e}\}^T \left[h_f (N_\varphi)^T (N_{Wf})\right]\{\dot{\mathbf{W}}_\mathbf{f}\}dAdt \;+(B.C.=0) \tag{3.142}$$

3.3.4. Variation of the Work done by the Plate (δW_P):

$$\text{As } \mathbf{W_P} = -\rho_0 \int_A \{\boldsymbol{\varphi}_e^{\bullet}\}^T (N_\varphi)^T (N_{w4}) \{\mathbf{w_4}\} dA, \tag{3.143}$$

$$\text{then } \int_{t_1}^{t_2} \delta(\mathbf{W_P}) dt = -\rho_0 \int_{t_1}^{t_2} \int_A \{\boldsymbol{\delta\varphi}_e^{\bullet}\}^T \left[(N_\varphi)^T (N_{w4})\right] \{\mathbf{w_4}\} dA dt, \tag{3.144}$$

$$\text{or } \int_{t_1}^{t_2} \delta(\mathbf{W_P}) dt = -\rho_0 \int_{t_1}^{t_2} \int_A \{\boldsymbol{\delta\varphi}_e\}^T \left[(N_\varphi)^T (N_{w4})\right] \{\dot{\mathbf{w}}_4\} dA dt + (B.C. = 0) \tag{3.145}$$

Finally, summing up the terms of $\{\boldsymbol{\delta\varphi}_e\}$ inside the time integral and equating them to zero results in the required equation of motion of the acoustic element.

For the foam-acoustic coupled elements

$$\frac{\rho_0}{c^2} \int_V (N_\varphi)^T (N_\varphi) dV \{\ddot{\varphi}_e\} + \rho_0 \int_V (\nabla N_\varphi)^T (\nabla N_\varphi) dV \{\varphi_e\} =$$

$$\rho_0 \int_A (1 - h_f)(N_\varphi)^T (N_{wf}) dA \{\dot{w}_f\} + \rho_0 \int_A h_f (N_\varphi)^T (N_{Wf}) dA \{\dot{W}_f\} \tag{3.146}$$

For the plate-acoustic coupled elements

$$\frac{\rho_0}{c^2} \int_V (N_\varphi)^T (N_\varphi) dV \{\ddot{\varphi}_e\} + \rho_0 \int_V (\nabla N_\varphi)^T (\nabla N_\varphi) dV \{\varphi_e\} =$$

$$\rho_0 \int_A (N_\varphi)^T (N_{w4}) dA \{\dot{w}_4\} \tag{3.147}$$

Differentiating with respect to time and utilizing the following identities:

$$\dot{\varphi} = -\frac{p}{\rho_0} \quad , \quad \ddot{\varphi} = -\frac{\dot{p}}{\rho_0} , \quad \dddot{\varphi} = -\frac{\ddot{p}}{\rho_0}$$

gives,

$$\frac{1}{c^2}\int_V (N_\varphi)^T (N_\varphi) dV \ \{\ddot{\mathrm{p}}_\mathrm{e}\} + \int_V (\nabla N_\varphi)^T (\nabla N_\varphi) dV \ \{\mathrm{p}_\mathrm{e}\} =$$

$$-\rho_0 \int_A (1-h_f)(N_\varphi)^T (N_{wf}) dA \ \{\ddot{\mathrm{w}}_\mathrm{f}\} - \rho_0 \int_A h_f (N_\varphi)^T (N_{Wf}) dA \ \{\ddot{\mathrm{W}}_\mathrm{f}\} \qquad (3.148)$$

where $\{\mathbf{p_e}\}$ is the nodal pressure vector.

This could also be written as:

$$[\mathbf{M_A}]\{\ddot{\mathbf{p}}_\mathbf{e}\} + [\mathbf{K_A}]\{\mathbf{p_e}\} = -[\mathbf{\Omega}]^T \ \{\ddot{\boldsymbol{\delta}}_\mathbf{p}\} \qquad (3.149)$$

where:

- $\{\boldsymbol{\delta}_\mathbf{p}\}$ represents the structure element set of degrees of freedom,
- $[\mathrm{M_A}] = \frac{1}{c^2}\int_V (N_\varphi)^T (N_\varphi) dV$ represents the acoustic medium mass matrix,
- $[\mathrm{K_A}] = \int_V (\nabla N_\varphi)^T (\nabla N_\varphi) dV$ represents the acoustic medium stiffness matrix,
- $[\mathbf{\Omega}] = (\Omega_f \quad \Omega_p)$ represents the structure-fluid coupling matrix,

  1. $[\Omega_f]^T = \rho_0 \int_A \left[(1-h_f)(N_\varphi)^T (N_{wf}) + h_f (N_\varphi)^T (N_{Wf})\right] dA$ for foam-acoustic coupling,

2. $\left[\Omega_p\right]^T = \rho_0 \int_A \left[\left(N_\varphi\right)^T \left(N_{wp}\right)\right] dA$ for plate-acoustic coupling.

3.4. COUPLING THE ACOUSTIC CAVITY WITH THE PLATE STRUCTURE

Equation of motion of the composite plate is given as:

$$\left[\mathbf{M}_{\mathbf{struct}}\right]\left\{\ddot{\boldsymbol{\delta}}_{\mathbf{struct}}\right\} + \left[\mathbf{C}_{\mathbf{struct}}\right]\left\{\dot{\boldsymbol{\delta}}_{\mathbf{struct}}\right\} + \left[\mathbf{K}_{\mathbf{struct}}\right]\left\{\boldsymbol{\delta}_{\mathbf{struct}}\right\} = F_S \tag{3.150}$$

where: $F_S = F_{S\_f} + F_{S\_p}$ are the forces exerted by the acoustic fluid on the foam and plate elements respectively.

The forcing function "F_{s_f}" and "F_{s_p}" can be calculated from the work done by the acoustic field on the structure as follows:

$$\mathbf{W_F} = \int_{BoundaryArea} \left[(1-h_f)w_f + h_f W_f\right] p\, dA, \tag{3.151}$$

and

$$\mathbf{W_P} = \int_{BoundaryArea} w_4\, p\, dA \tag{3.152}$$

Using the appropriate shape functions, the above equations reduce to:

$$\mathbf{W_{F1}} = \int_A \left\{\mathbf{w_f}\right\}^T (1-h_f)\left(N_{wf}\right)^T \left(N_\varphi\right)\left\{\mathbf{p}\right\} dA, \tag{3.153}$$

and $$\mathbf{W_{F2}} = \int_A \{\mathbf{W_f}\}^T h_f \left(N_{Wf}\right)^T \left(N_\varphi\right)\{\mathbf{p}\} dA \tag{3.154}$$

Their variations are given by:

$$\int_{t_1}^{t_2} \delta(\mathbf{W_{F1}}) dt = \int_{t_1}^{t_2} \int_A \left[\{\boldsymbol{\delta}\mathbf{w_f}\}^T (1-h_f)\left(N_{wf}\right)^T \left(N_\varphi\right)\{\mathbf{p}\} dA\right] dt \tag{3.155}$$

$$\int_{t_1}^{t_2} \delta(\mathbf{W_{F2}}) dt = \int_{t_1}^{t_2} \int_A \left[\{\boldsymbol{\delta}\mathbf{W_f}\}^T h_f \left(N_{Wf}\right)^T \left(N_\varphi\right)\{\mathbf{p}\} dA\right] dt \tag{3.156}$$

Also, $$\mathbf{W_P} = \int_A \{\mathbf{w_4}\}^T \left(N_{w4}\right)^T \left(N_\varphi\right)\{\mathbf{p}\} dA \tag{3.157}$$

Hence, $$\int_{t_1}^{t_2} \delta(\mathbf{W_P}) dt = \int_{t_1}^{t_2} \int_A \left[\{\boldsymbol{\delta}\mathbf{w_4}\}^T \left(N_{w4}\right)^T \left(N_\varphi\right)\{\mathbf{p}\} dA\right] dt \tag{3.158}$$

Since the Work = Force × Displacement, then the forcing term on the plate can be calculated as:

$$F_{S\_f} = \frac{[\Omega_f]\mathbf{p}}{\rho_0} \text{ with } \quad [\Omega_f] = \rho_0 \int_A (1-h_f)\left(N_{wf}\right)^T \left(N_\varphi\right) + h_f \left(N_{Wf}\right)^T \left(N_\varphi\right) dA$$

and $$F_{S\_p} = \frac{[\Omega_p]\mathbf{p}}{\rho_0} \text{ with } \quad [\Omega_p] = \rho_0 \int_A \left(N_{w4}\right)^T \left(N_\varphi\right) dA$$

Thus, the complete differential equation of the composite plate is given as:

$$[\mathbf{M}_{\mathbf{struct}}]\{\ddot{\boldsymbol{\delta}}_{\mathbf{struct}}\}+[\mathbf{C}_{\mathbf{struct}}]\{\dot{\boldsymbol{\delta}}_{\mathbf{struct}}\}+[\mathbf{K}_{\mathbf{struct}}]\{\boldsymbol{\delta}_{\mathbf{struct}}\}=\frac{[\boldsymbol{\Omega}]\{\mathbf{p}\}}{\rho_0} \tag{3.159}$$

The overall coupled system equation of motion is represented in the following matrix-form:

$$\begin{pmatrix} M_{struct} & 0 \\ [\Omega]^T & M_A \end{pmatrix}\begin{Bmatrix} \ddot{\boldsymbol{\delta}}_{\mathbf{struct}} \\ \ddot{\mathbf{p}} \end{Bmatrix}+\begin{pmatrix} C_{struct} & 0 \\ 0 & 0 \end{pmatrix}\begin{Bmatrix} \dot{\boldsymbol{\delta}}_{\mathbf{struct}} \\ \dot{\mathbf{p}} \end{Bmatrix}+\begin{pmatrix} K_{struct} & -[\Omega]/\rho_0 \\ 0 & K_A \end{pmatrix}\begin{Bmatrix} \boldsymbol{\delta}_{\mathbf{struct}} \\ \mathbf{p} \end{Bmatrix}=\begin{Bmatrix} f \\ 0 \end{Bmatrix} \tag{3.160}$$

where, "f" is the externally applied force.

3.5. CONTROL LAW

A simple proportional-derivative feedback control approach is used to reduce the vibration of the plate and reach the required attenuation in the acoustic cavity.

The electric field E_z may be expressed as:

$$E_z = -K_g[C]\{\delta_P\} \tag{3.161}$$

where, K_g is the complex feedback gain. $[C]$ is a vector defining the degrees of freedom upon which control effort is applied.

Introducing the feedback force into the equation of motion, the following closed loop

equation of motion of the system is obtained:

$$\left(\mathbf{M}_{\mathbf{p}}+\mathbf{M}_{\mathbf{c}}+\mathbf{M}_{\mathbf{v}}\right)\left\{\boldsymbol{\delta}_{\mathbf{P}}^{\bullet\bullet}\right\}+\left(\mathbf{K}_{\mathbf{p}}+\mathbf{K}_{\mathbf{c}}+\mathbf{K}_{\mathbf{v}}+\mathbf{K}_{\mathbf{nc\_v}}\right)\left\{\boldsymbol{\delta}_{\mathbf{P}}\right\}+K_g[C]\left\{\boldsymbol{\delta}_{\mathbf{P}}\right\}\left\{\mathrm{F}_{\mathrm{APDC}}\right\}=f \quad (3.162)$$

where, "*f*" is the externally applied force.

Finally combining the equation of motion of the foam with those of the plate, APDC, constraining and viscoelastic layers, the following equation of motion of the entire assembly is expressed as:

$$\left(\mathbf{M}_{\mathbf{p}}+\mathbf{M}_{\mathbf{c}}+\mathbf{M}_{\mathbf{v}}+\mathbf{M}_{\mathbf{1\_s}}+\mathbf{M}_{\mathbf{1\_f}}+\mathbf{M}_{\mathbf{A}}\right)\begin{Bmatrix}\boldsymbol{\delta}_{\mathbf{struct}}^{\bullet\bullet}\\ \mathbf{p}^{\bullet\bullet}\end{Bmatrix}+\left(\mathbf{M}_{\mathbf{2\_s}}+\mathbf{M}_{\mathbf{2\_f}}\right)\left\{\boldsymbol{\delta}_{\mathbf{struct}}^{\bullet}\right\}+$$

$$\left(\mathbf{K}_{\mathbf{p}}+\mathbf{K}_{\mathbf{c}}+\mathbf{K}_{\mathbf{v}}+\mathbf{K}_{\mathbf{nc\_v}}+\mathbf{K}_{\mathbf{f}}+\mathbf{K}_{\mathbf{A}}\right)\begin{Bmatrix}\boldsymbol{\delta}_{\mathbf{struct}}\\ \mathbf{p}\end{Bmatrix}+K_g[C]\begin{Bmatrix}\boldsymbol{\delta}_{\mathbf{struct}}\\ \mathbf{p}\end{Bmatrix}\left\{\mathrm{F}_{\mathrm{APDC}}\right\}=f \quad (3.160)$$

3.6. SUMMARY

In this chapter, a comprehensive derivation of the finite element model of the entire structure-fluid system is presented. Here, expressions for the potential energy of the composite plate as well as its kinetic energy were derived. Expressions for the non-conservative energy of the viscoelastic layer and the non-conservative work done by the APDC were also derived, to finally lead to the set of differential equations of the entire system. The equations governing the dynamics of the acoustic cavity in contact with the composite plate were also developed, for two types of fluid-structure interaction. The first type is that of fluid-foam interaction and the second type is for fluid-plate interaction.

A two-dimensional finite element model for the foam was also presented and its performance was compared with the three-dimensional model. A good agreement between the two models was found, which enables the coupling of the foam to various two-dimensional structure. The validity of the derived finite element model will be presented in chapter 5.

CHAPTER 4

EXPERIMENTAL WORK

The experimental work in this study is divided into three major parts. The function of the first part was to study experimentally the sound absorbing characteristics of the actively controlled foam to be later used in active noise control inside acoustic cavities. The second part involves preliminary investigation of the smart foam inside an acoustic cavity using 90° APDC as the actuating element to determine the potential of such an actuator in active vibration and noise control. Finally, the third and final part of the experimental study was mainly oriented to confirm the theoretical model developed for the smart foam with 45° APDC bonded on an Aluminum plate which is coupled to an acoustic cavity.

4.1 IMPEDANCE TUBE

For the sake of the present study, the impedance tube shown in Figure 4.1, was used to measure the acoustic properties of the smart foam under investigation.

A specially designed auxiliary part was manufactured to allow for the insertion of the smart foam into the impedance tube. The foam consists of the passive porous material, backed with an APDC patch as shown in Figure 4.2.

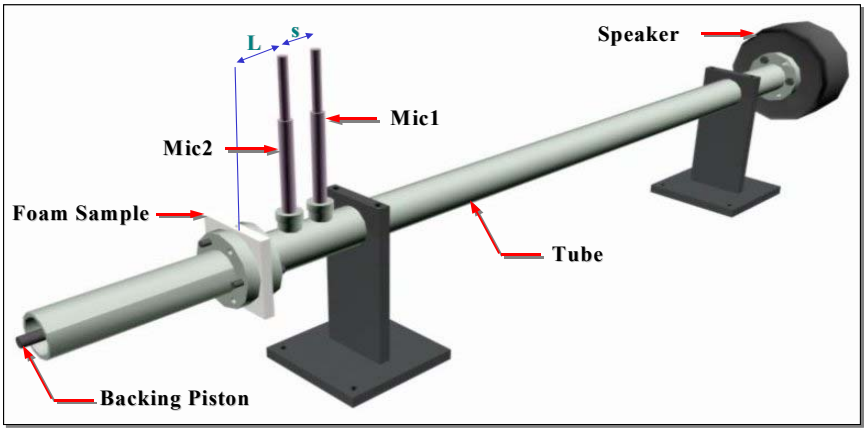

Figure 4.1: Impedance tube used in the experimental investigation.

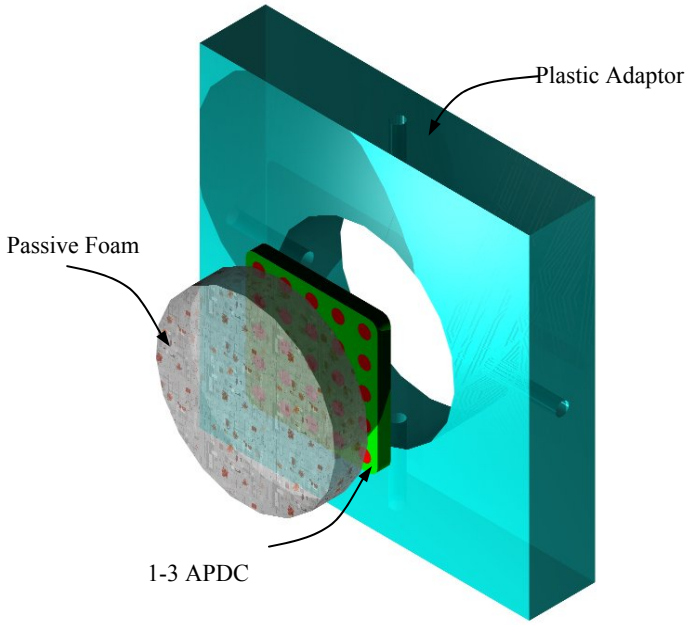

Figure 4.2: Adaptor to install the smart foam inside the impedance tube.

4.1.1 Proposed Smart Foam Configuration

The proposed smart foam used for hybrid vibration and noise control was developed in two versions. The first version, used inside the impedance tube to

monitor the absorption characteristics consists of two parts. The first part is the passive element, which is a regular sound absorbing material and the second part is the active piezo-composite patch. The second version, however, that was used inside an acoustic cavity to control the vibration and sound radiation, consists of a viscoelastic layer, an APDC, passive foam and a proof mass mounted to the foam surface. Both configurations are shown in Figures 4.3 and 4.4.

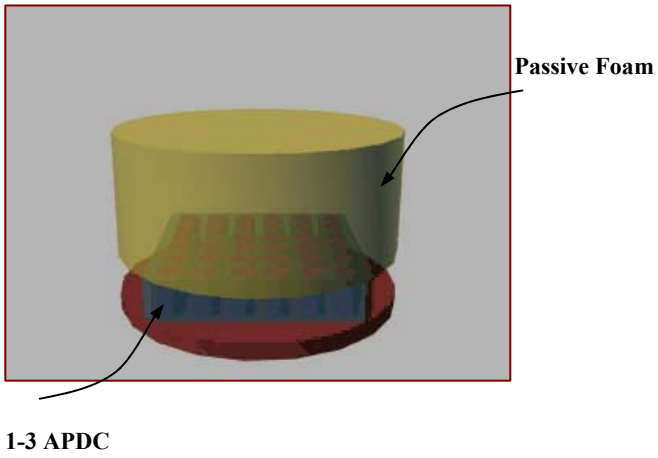

Figure 4.3: Smart foam without proof mass.

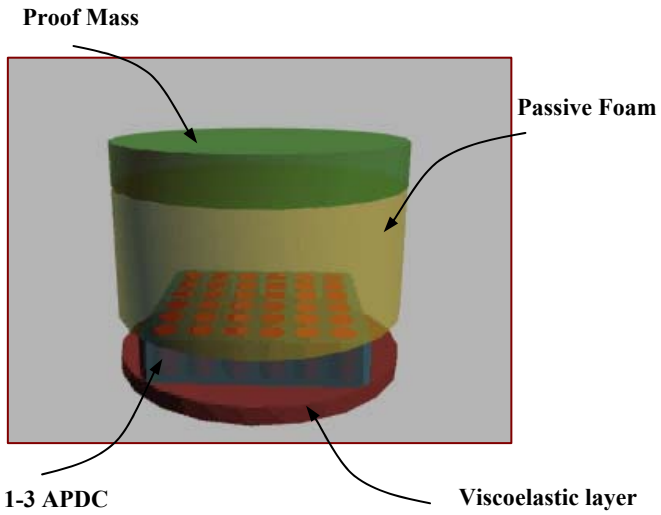

Figure 4.4: Smart foam with proof mass.

4.12. Specifications of the used material

The specifications of the materials used in the experimental investigation are listed in Appendix (A.1).

4.1.3. Absorption Coefficient Characteristics

Two types of piezocomposites were used in this experiment to evaluate the performance of the smart foam with and without control. In the first type, the ceramic rods are embedded perpendicular to the x-y plane of the composite. In the other type, the ceramic rods are embedded obliquely at an angle of 45° to the x-y plane. The objective of using these two types of composites is to study the effect of the direction of the actuation force. The control algorithm used was a simple feedback of the signal of the microphone closest to the specimen. An analog low pass filter was used to eliminate high frequencies contaminations. The controller aims at changing the phase angle of the foam response at the modal frequencies to cancel out the noise radiation into the impedance tube. In other words, the acoustic impedance of the foam itself was altered to closely match that of the fluid medium. To achieve such an objective, the output signal from the microphone was fed through a charge amplifier to the input port of a dSpace® board connected to a PC. The output port of the dSpace® board was connected to a power amplifier to derive the piezocomposites. Using Simulink® toolbox of MATLAB a transfer function between the input and output was generated to achieve the aimed objective.

The effectiveness of the system was evaluated based on changes in the absorption

coefficient of the specimen at the frequencies of interest.

The experimental setup using the impedance tube is shown in Figure 4.5.

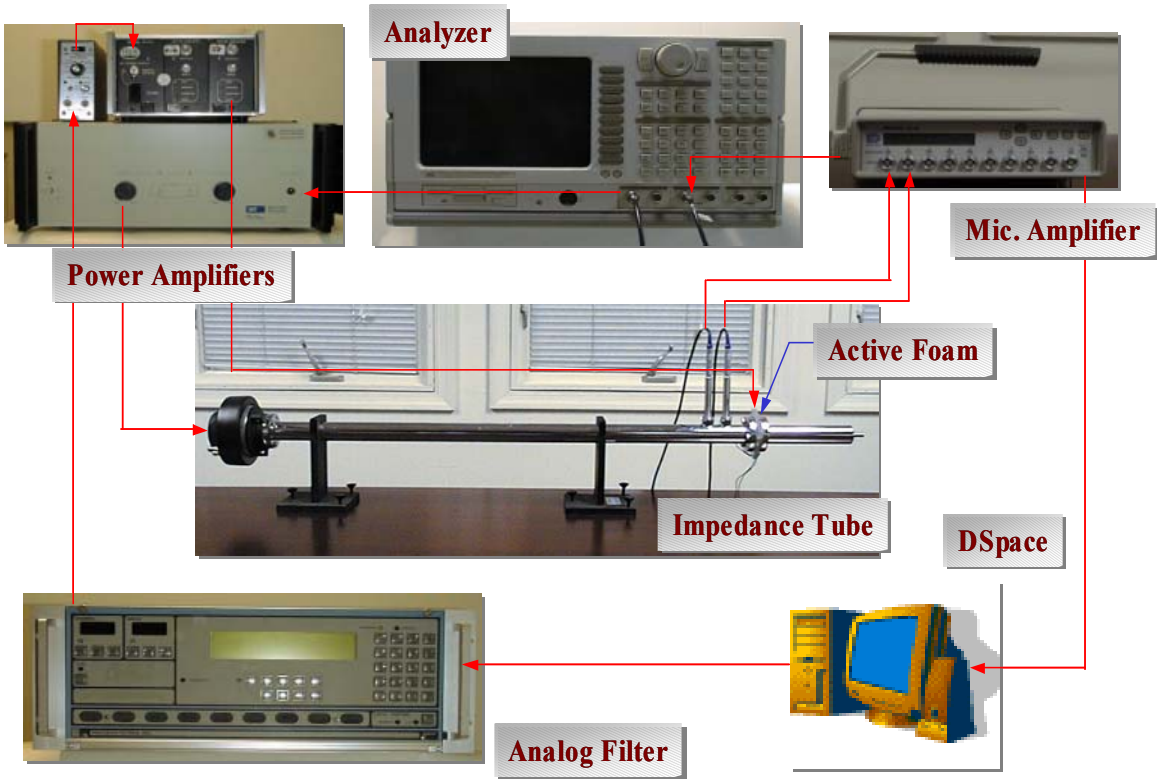

Figure 4.5: Experimental setup used to determine the absorption characteristics of the smart foam.

4.2. 90° APDC SMART FOAM INSIDE ACOUSTIC CAVITY

The proposed smart foam with 90° piezocomposite was installed on an aluminum plate of (0.016 inch) thickness that forms a side of an acoustic cavity made of thick Plexiglas. The rectangular enclosure has the dimensions 12″ × 12″ × 30″ as shown in Figure 4.6. Nine piezocomposite patches were bonded on the surface of a viscoelastic

layer, each of 1"×1". This forms an overall area of 3×3 inch^2 treated area. A rectangular piece of the passive foam of the same dimension was bonded to the top of the active layer. A proof mass was bonded to the other side top of the passive foam.

A microphone was installed in front of the smart foam at a distance of ½" to provide the required feedback signal. Two additional microphones were placed at two other locations inside the cavity to evaluate the global noise attenuation.

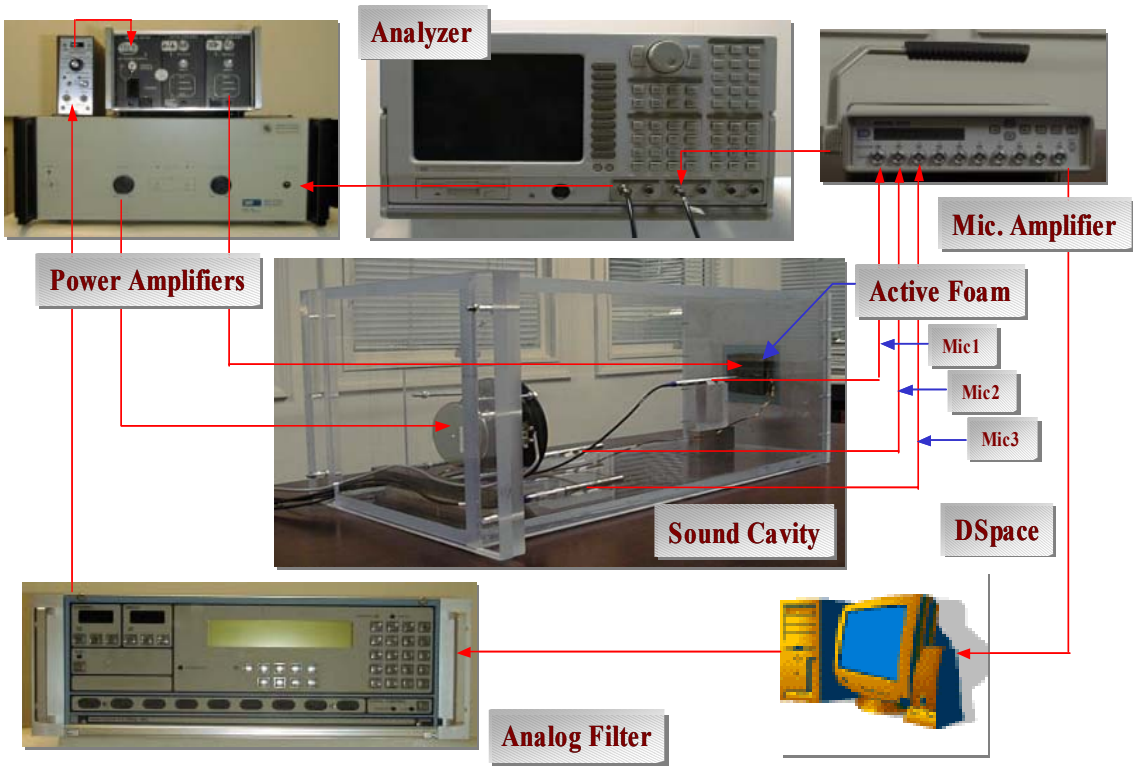

Figure 4.6: The Acoustic cavity experimental Setup.

The experiments inside the cavity were carried out in the following procedure:

- The same setup shown in Figure 4.6 was used and noise inside the enclosure was measured. An additional accelerometer was placed on the back of the

flexible aluminum plate to measure the vibration response of the plate.

- A rigid Plexiglas back-plate was then placed on the back of the aluminum plate as a support to form a rigid enclosure.

In both cases the excitation was carried out through a speaker mounted inside the cavity as shown in Figure4.6. The input to the speaker was in form a sine sweep signal ranging from 50Hz to 1kHz.

4.3. 45° APDC SMART FOAM INSIDE ACOUSTIC CAVITY

The final stage in the experimental work is similar to the second part, except that four 45° APDC actuators were used instead of the nine 90° actuators configured as shown in Figure 4.7. Excitation was carried out using an external speaker outside the acoustic cavity. An aluminum plate of 1/64″ thickness was used as the flexible structure part covering one face of the rigidly sealed acoustic cavity. A microphone was placed at a distance of 2″ away from the aluminum plate. The plate displacement was measured using an accelerometer bonded to the plate at different locations to measure its vibration response. Both the microphone and accelerometer signals are fed to dSpace® board and by using Simulink®, as shown in Figure 4.8, a PD controller was developed for reducing both the structural vibration of the Aluminum plate and the noise level inside the cavity. The setup is illustrated in Figures 4.9 through 4.12.

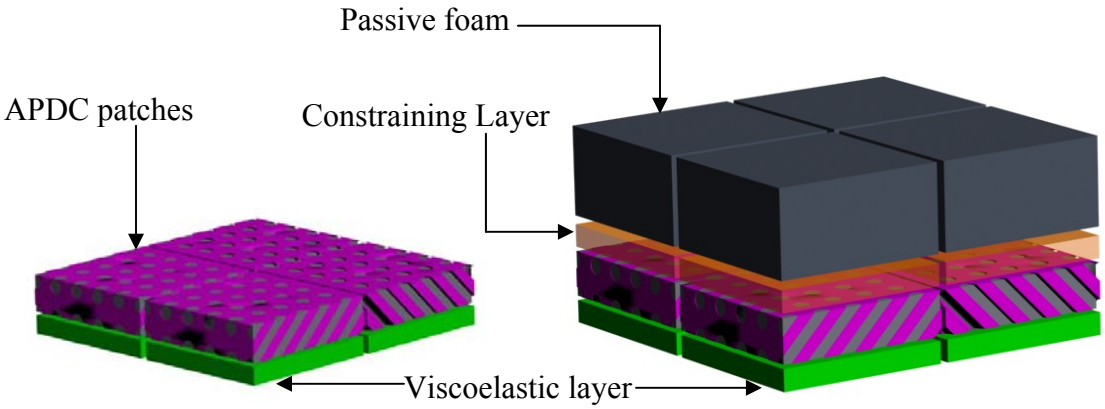

a- Four 45° APDC patches b- Developed smart foam patch

Figure 4.7: Smart foam patch with 45° inclined piezo rods

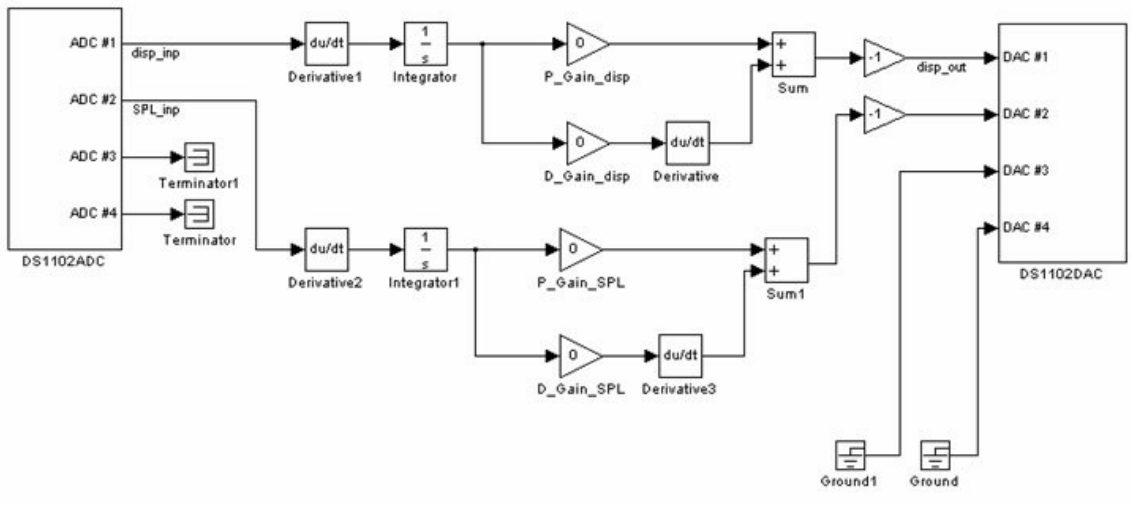

Figure 4.8: Simulink circuit for vibration and sound pressure feedback.

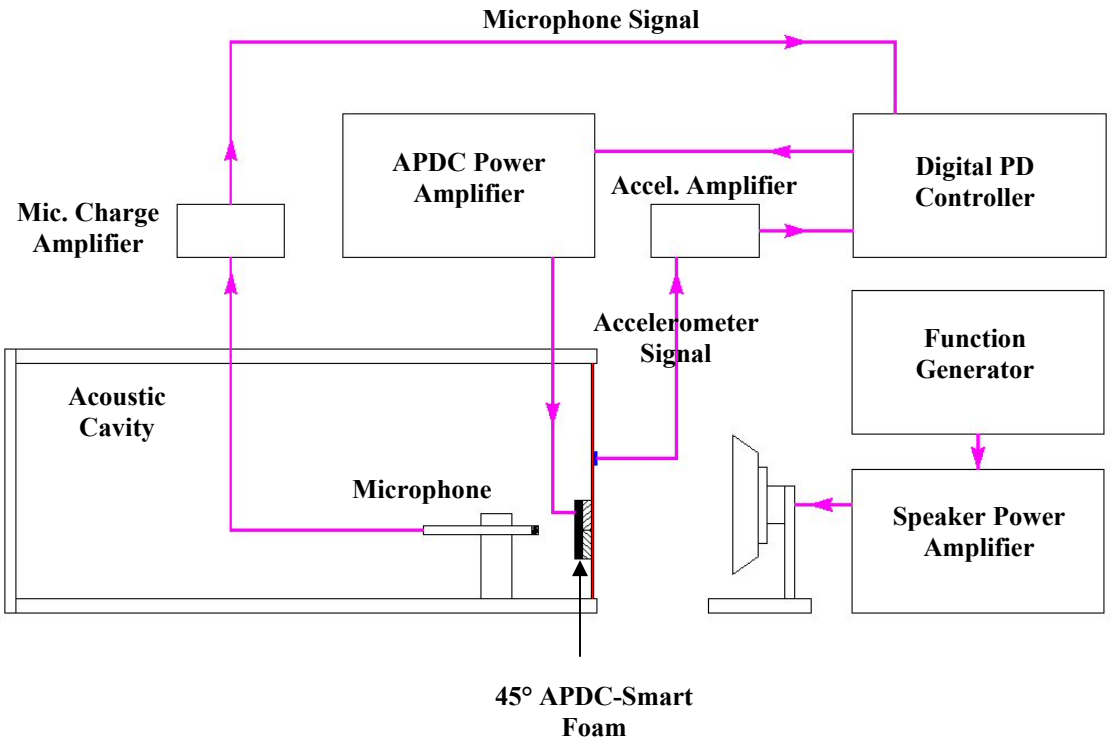

Figure 4.9: Schematic diagram for the experimental setup.

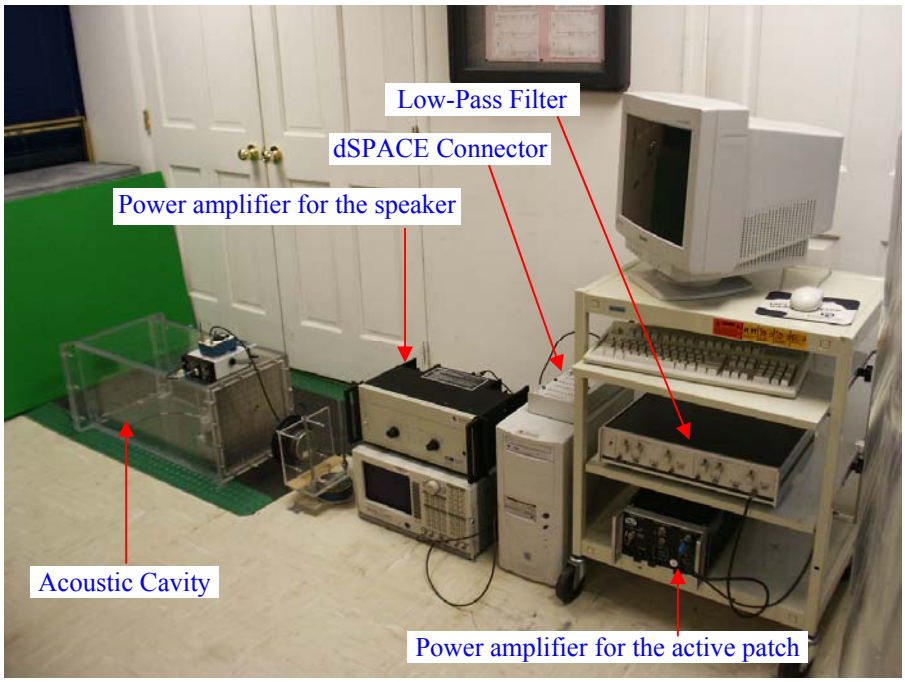

Figure 4.10: Experimental setup for vibration and noise control inside the acoustic cavity using the developed smart foam.

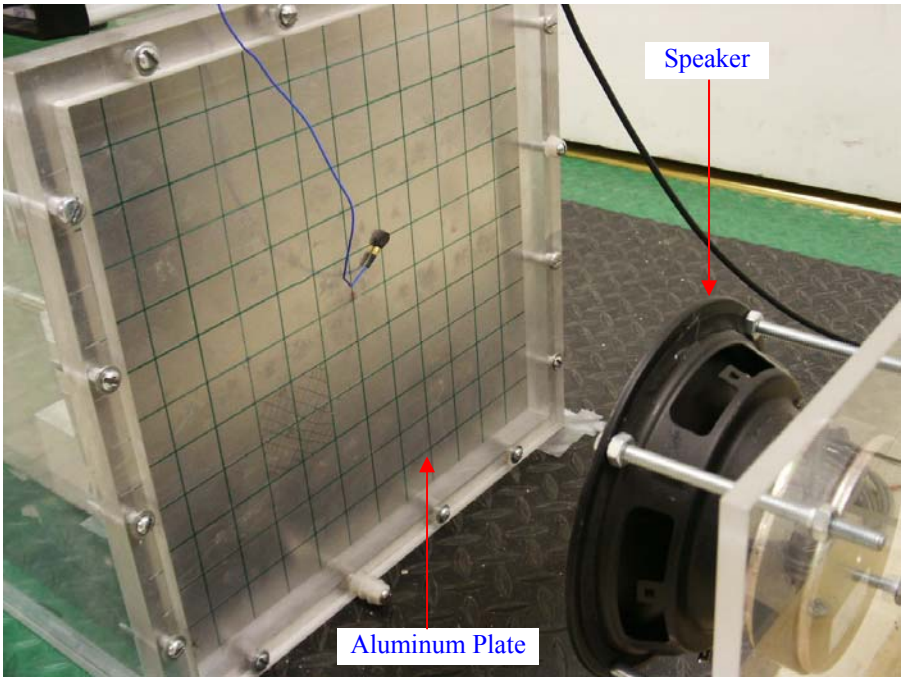

Figure 4.11: The flexible aluminum Plate, which vibration amplitude is controlled using the smart foam.

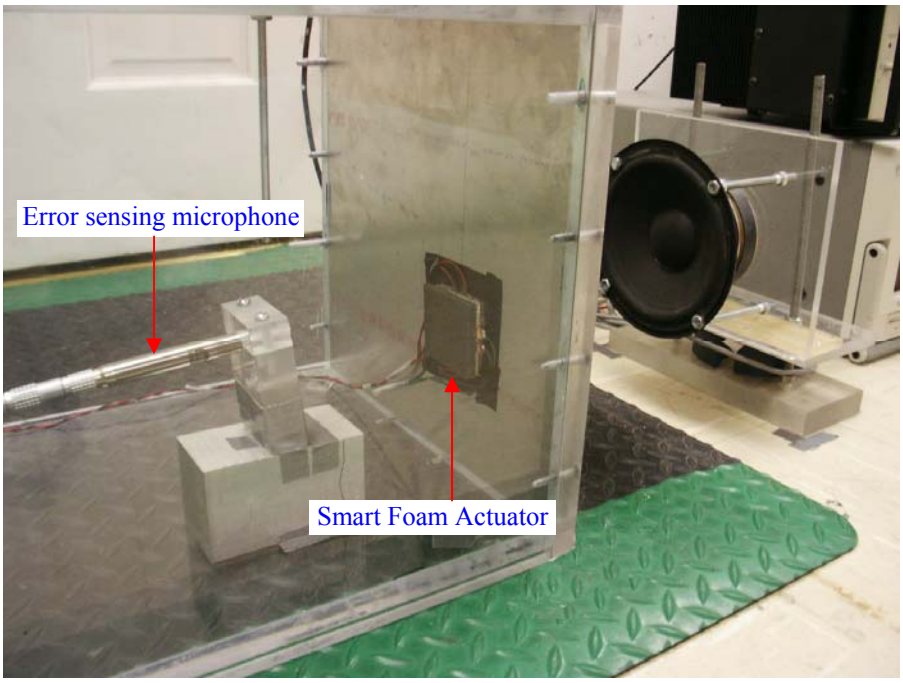

Figure 4.12: The smart foam attached to the flexible aluminum plate coupled with the acoustic cavity.

4.4 SUMMARY:

In this chapter, the experimental setups built for testing the performance of the proposed actuator were described. The absorption coefficient of this actuator was first tested using the impedance tube. The actuator was then bonded to the surface of a flexible aluminum plate coupled with an acoustic cavity, where the vibrations of the plate and noise radiation in the cavity were measured for the controlled and uncontrolled cases. Active piezo damping composites with 45° and 90° were used in this experiment.

CHAPTER 5

RESULTS

The results in this chapter are categorized in the following order:

- Numerical investigation of the effect of feedback control on the absorption coefficient of smart foam.
- Experimental measurement of the absorption coefficient for 90° and 45° APDC smart foam using impedance tube.
- Experimental study of the potential of the newly developed smart foam with 90° APDC inside an acoustic cavity.
- Numerical modeling of 45° APDC smart foam coupled with an acoustic cavity using both vibration and sound pressure feedback to improve the structural vibration as well as reducing the noise level inside the cavity.
- Experimental validation of the numerical model developed for the 45° APDC smart foam.

5.1 EFFECT OF PROPORTIONAL FEEDBACK CONTROL ON THE FOAM ABSORPTION COEFFICIENT

Measuring the reflected acoustical velocity potential in an acoustic cavity, where a polyurethane foam is placed, and feeding it back to the bottom layer of the foam to actively deflect it in both the longitudinal and transverse directions is investigated in this

section.

Based on the aforementioned model for the 2-dimensional foam, proportional feedback control was added, and the increase in absorption coefficient is illustrated in Figures 5.1 through 5.4.

The figures emphasize that such simple proportional feedback control approach has improved the absorption coefficient in the low frequency zones, thus overcoming the limitations of the passive polyurethane foam at those frequency regions.

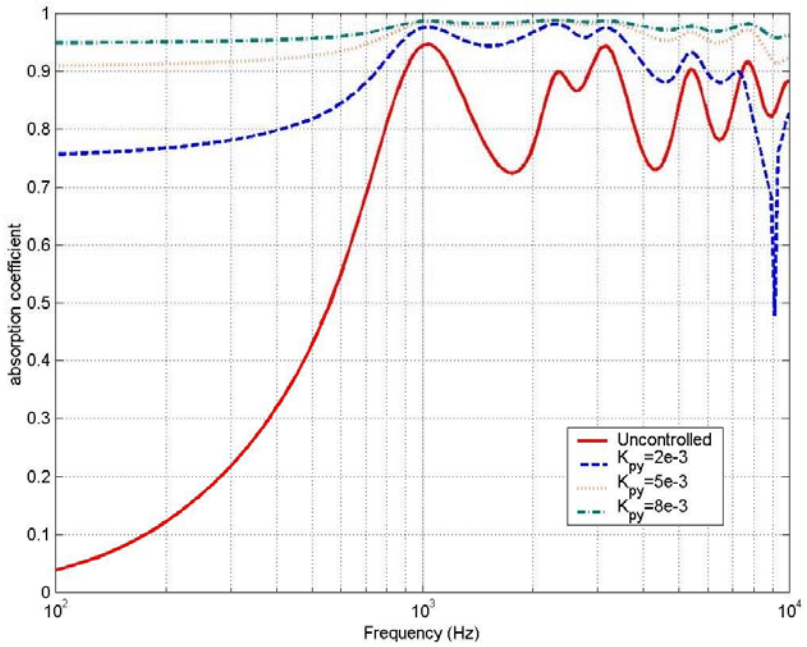

Figure 5.1 Foam directly exposed to incident plane wave; uncontrolled and controlled in the transverse direction only.

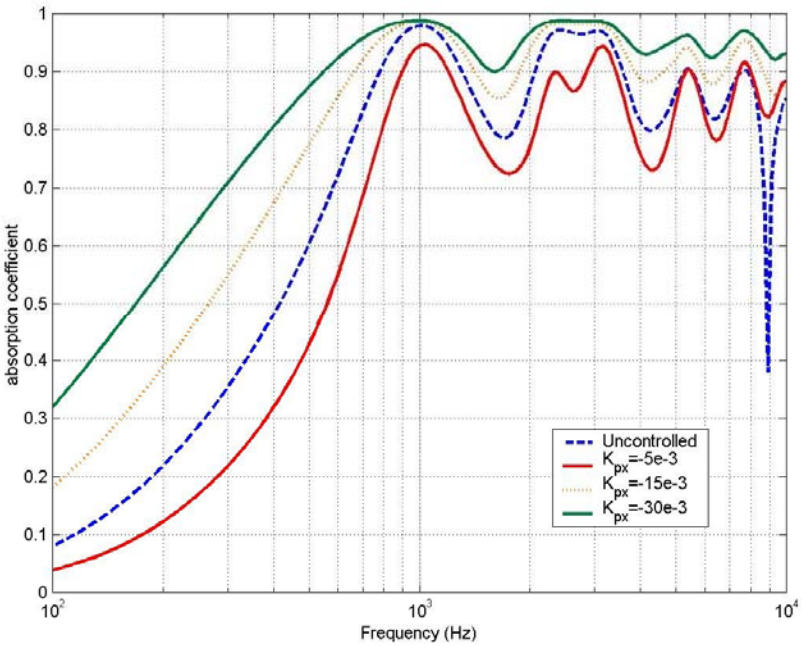

Figure 5.2: Foam directly exposed to incident plane wave; uncontrolled and controlled in the longitudinal direction only.

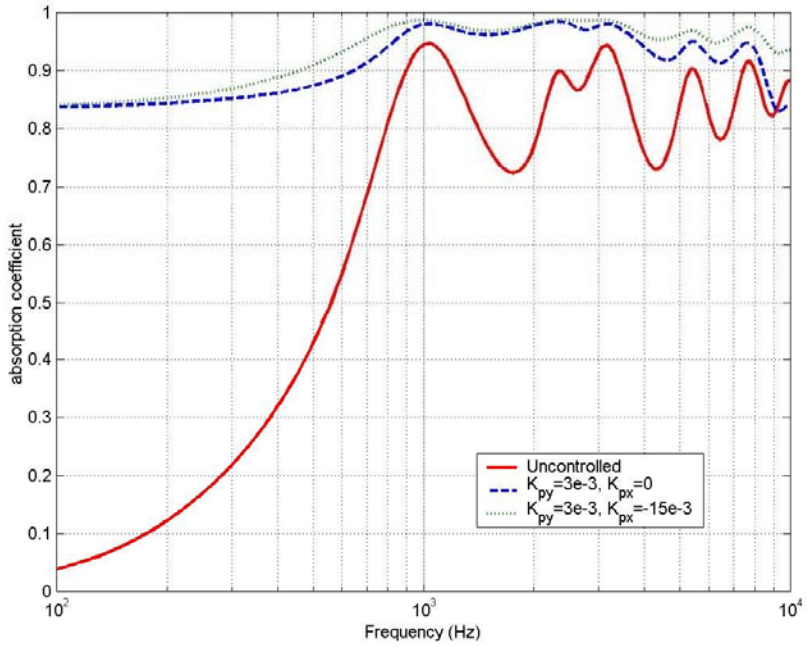

Figure 5.3: Foam directly exposed to incident plane wave; uncontrolled and controlled in the longitudinal and transverse directions.

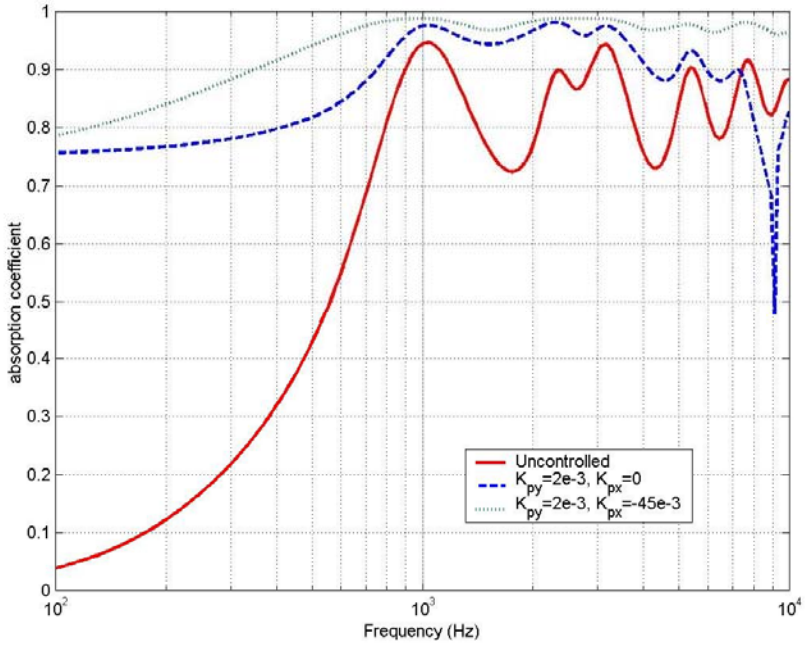

Figure 5.4: Foam directly exposed to incident plane wave; uncontrolled and controlled in the longitudinal and transverse directions.

The obtained results indicate also that the feedback in the transverse direction has been more effective in improving the absorption coefficient of the foam than that in the longitudinal direction

5.2 IMPEDANCE TUBE RESULTS

Figures 5.5 and 5.6 show the effect of using the proposed impedance tube in measuring the improvement of the absorption coefficient at low frequency zones (below 1kHz), which is the zone for which the active elements were added to enhance the absorption characteristics of the passive foam.

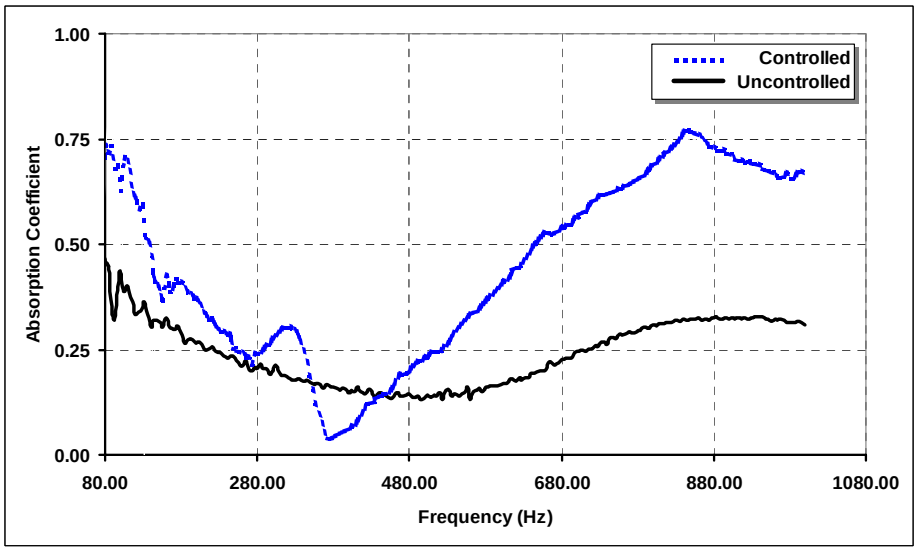

Figure 5.5: Absorption characteristics for smart foam using 90° APDC.

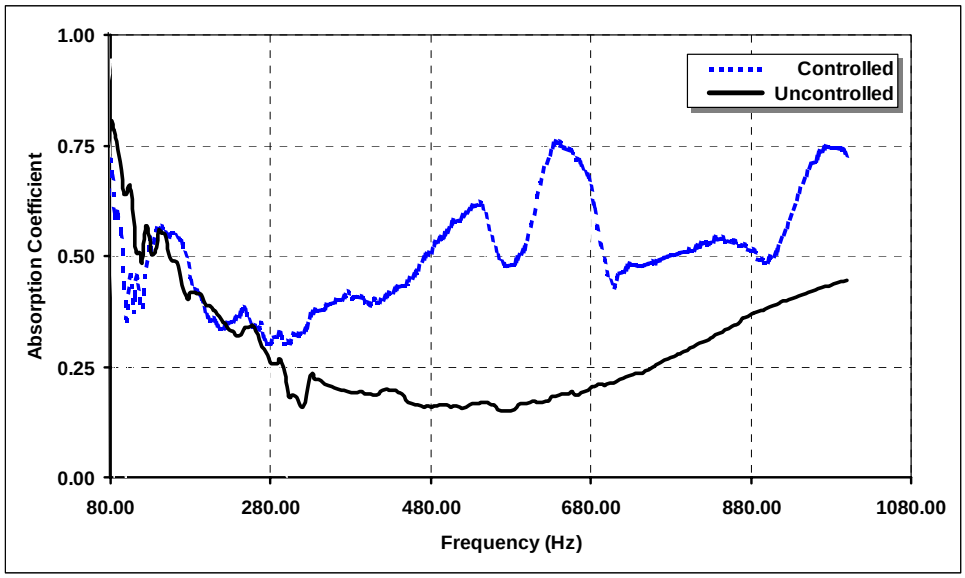

Figure 5.6: Absorption characteristics for smart foam using 45° APDC.

It is evident that using the 90° APDC patch has resulted in improving the absorption characteristics above 480 Hz. However, using the 45° APDC patch has extended this range to above 280 Hz, due to the dual loading of the foam in shear and compression.

Improvement of the absorption coefficient of two to three folds is observed due to the addition of the APDC patches.

5.3 ACOUSTIC CAVITY WITH 90° APDC SMART FOAM

In this stage, a preliminary investigation of the effect of introducing a 90° APDC smart foam inside an acoustic cavity was conducted. The purpose of this investigation was to measure the improvement that can be obtained by using the newly developed actuator. First the acoustic cavity was rigidly sealed except for one face, which was covered with an aluminum flexible plate. The aluminum plate was, later on, supported on a rigid plate to form a completely rigid acoustic cavity.

5.3.1. Acoustic Cavity / Flexible Plate

Figures 5.7 through 5.9 illustrate the acoustic response at the locations of the three microphones. Figure 5.10 shows the response of the accelerometer which is used to measure the corresponding plate vibration. The figures show comparison between the controlled and the uncontrolled smart foam.

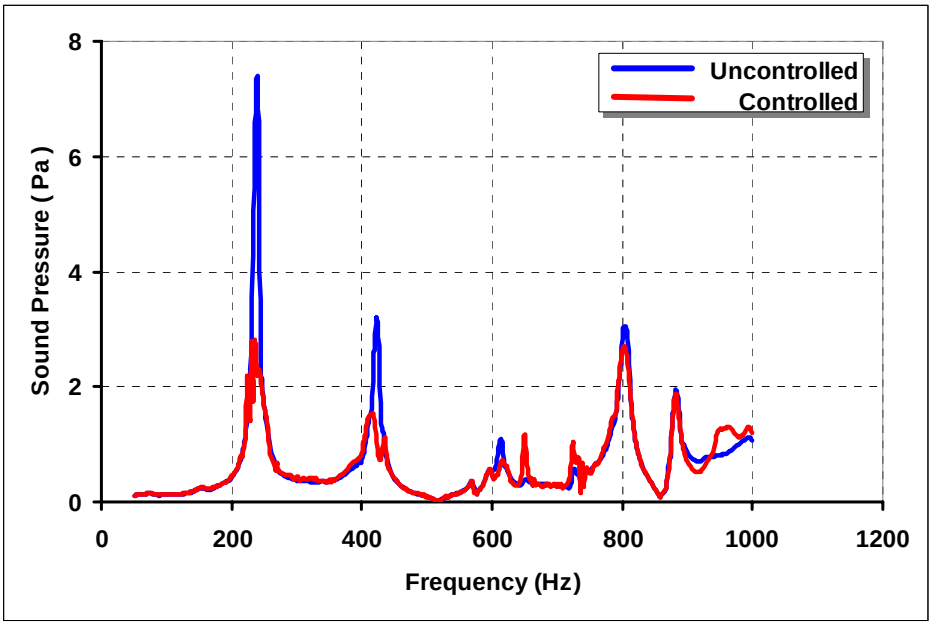

Figure 5.7: Feedback microphone signal (flexible plate)
(———) uncontrolled, (———) controlled.

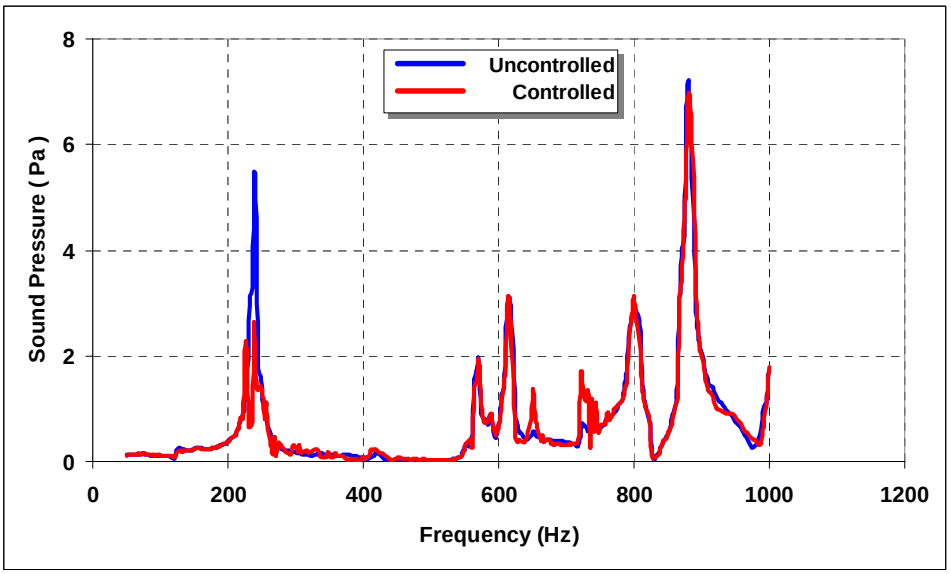

Figure 5.8: second microphone signal (flexible plate)
(———) uncontrolled, (———) controlled.

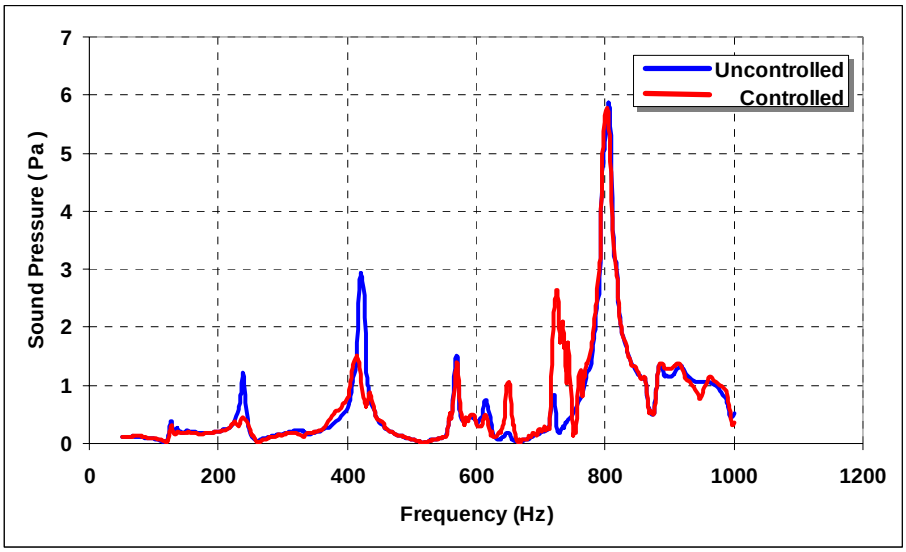

Figure 5.9: Third microphone signal (flexible plate)
(———) uncontrolled, (———) controlled.

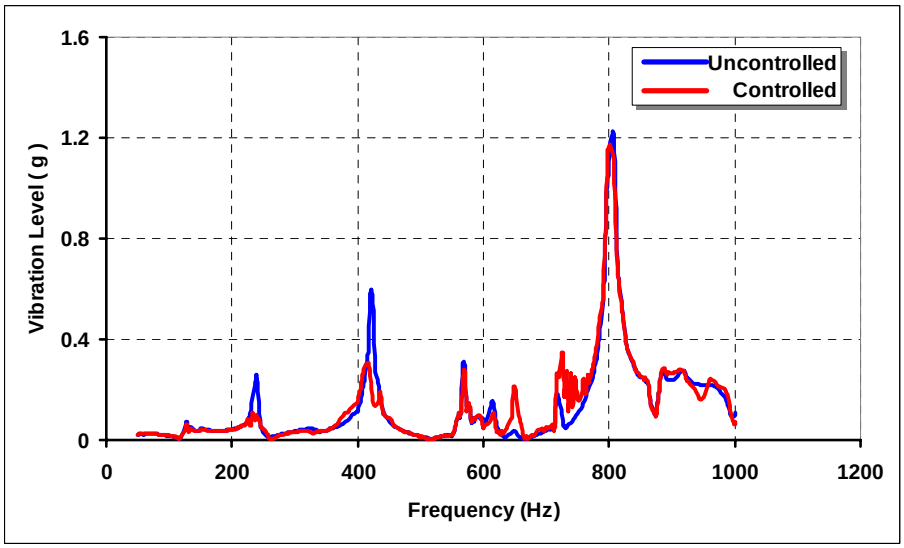

Figure 5.10: Frequency response of the plate vibrations (flexible plate)
(———) uncontrolled, (———) controlled

It can be seen from Figure 5.7 that considerable attenuation of the first acoustics mode, occurring at about 240 Hz, was obtained as measured by the feedback microphone placed in front of the smart foam. Note that attenuation is also achieved at other locations in the acoustic cavity as measured by the other two microphones as shown in Figures 5.8 and 5.9.

In addition to noise attenuation, vibration suppression of the flexible plate was also observed as shown in Figure 5.10.

5.3.2. Acoustic Cavity / Rigid Plate

In this case, only noise attenuation inside the acoustic cavity was investigated, and suppression of the noise inside the enclosure was also observed as demonstrated in Figures 5.11 through 5.13.

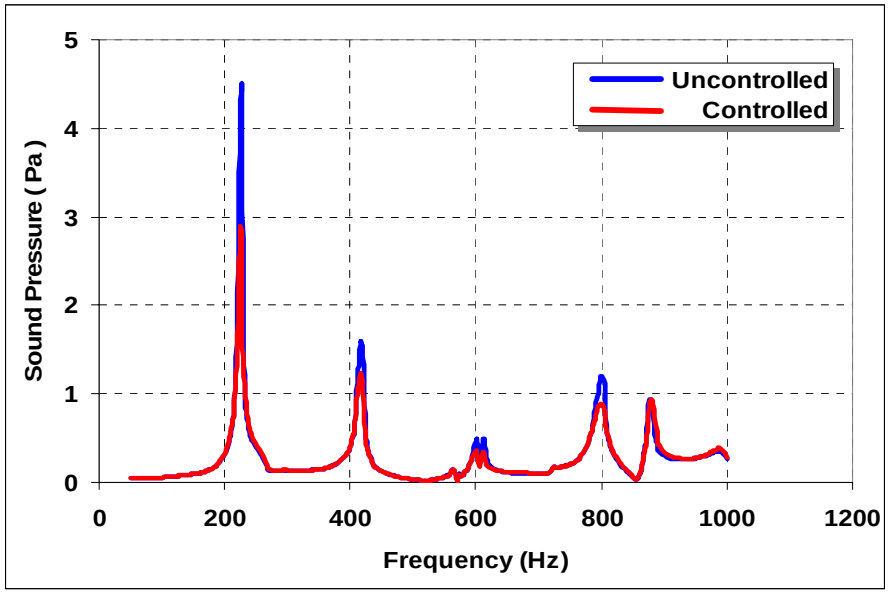

Figure 5.11: Feedback microphone signal (rigid cavity)
(———) uncontrolled, (———) controlled.

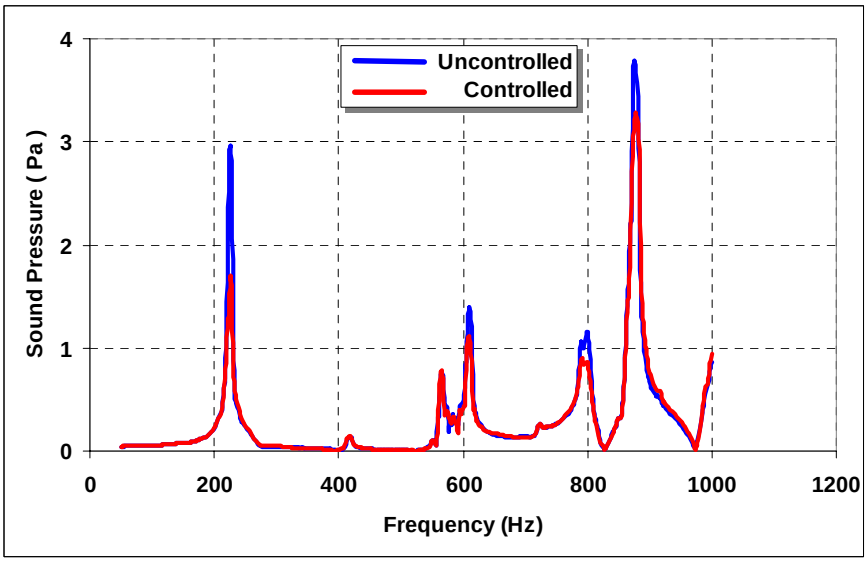

Figure 5.12: Second microphone signal (rigid cavity)
(——) uncontrolled, (——) controlled.

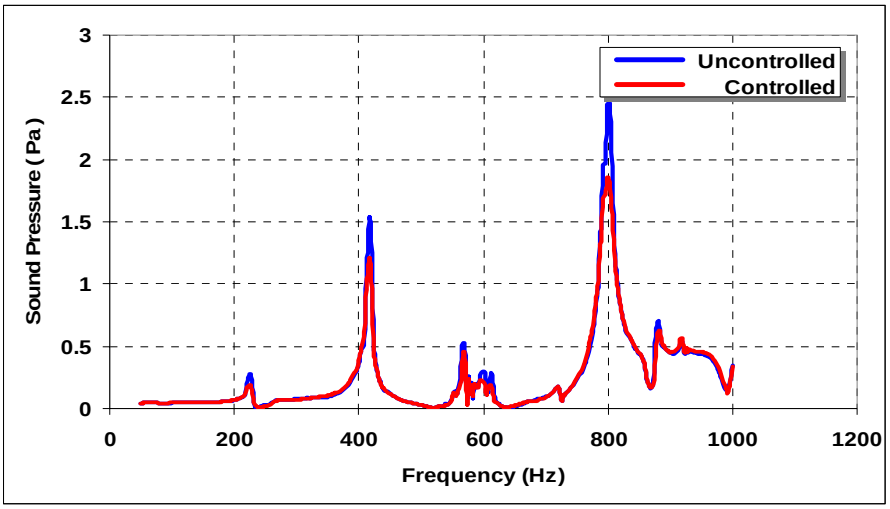

Figure 5.13: Third microphone signal (rigid cavity)
(——) uncontrolled, (——) controlled.

5.4 FINITE ELEMENT MODEL FOR 45° APDC SMART FOAM

In the finite element model developed for the present study, a plate, with 4-node rectangular elements is placed inside an acoustic cavity, which is modeled with 8-node brick elements. The viscoelastic, APDC, constraining, and foam layers were combined in different configurations and bonded to arbitrary locations of the flexible plate. The viscoelastic, APDC, constraining and foam layers were modeled using 4-node rectangular elements. The acoustic cavity is modeled with 12×12×12 elements and the plate is also modeled using 12×12 elements.

The interior acoustic and plate vibration are computed at different locations using PD feedback of the plate transverse vibration and the sound pressure level at predetermined locations

5.4.1 Excitation, Sensing and Control Locations

Figures 5.14 and 5.15 show the location of the vibration and sound pressure feedback points as well as the location of the exciting force, which is evenly distributed over the nodes shown in Figure 5.15.

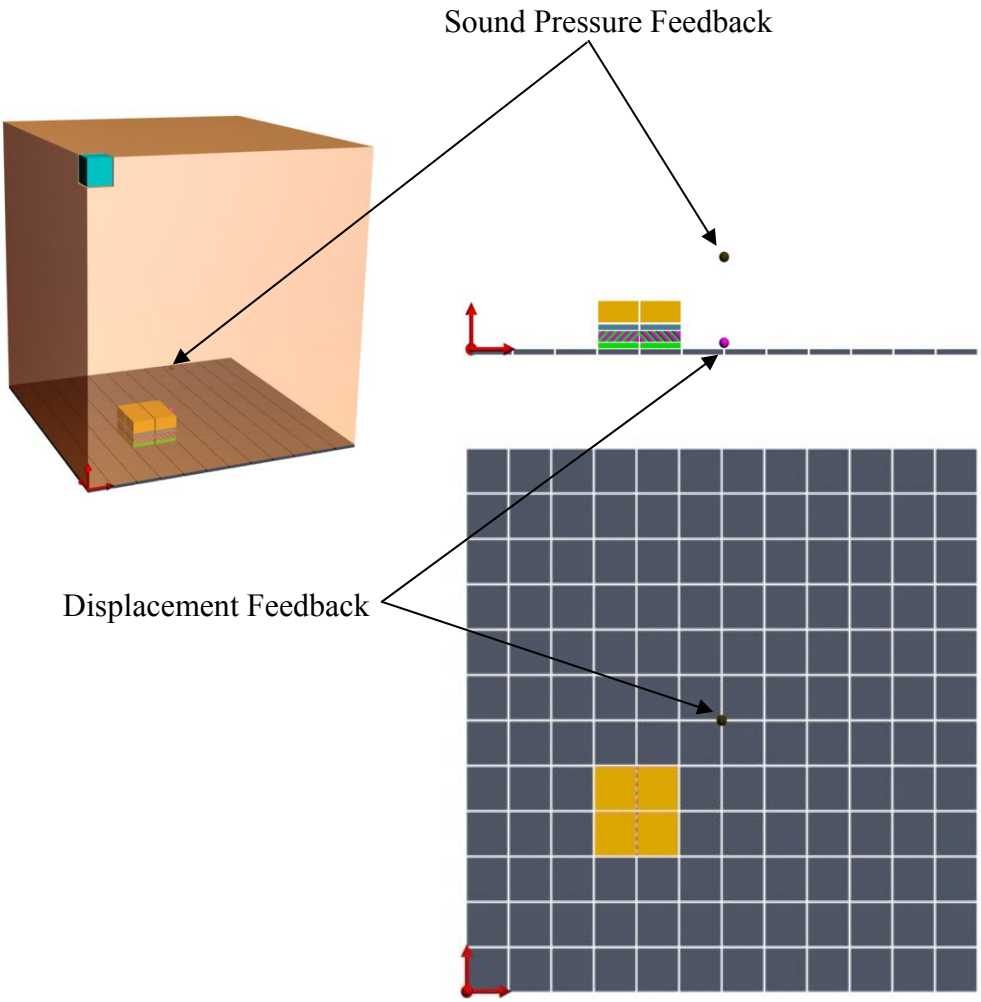

Figure 5.14: Feedback locations.

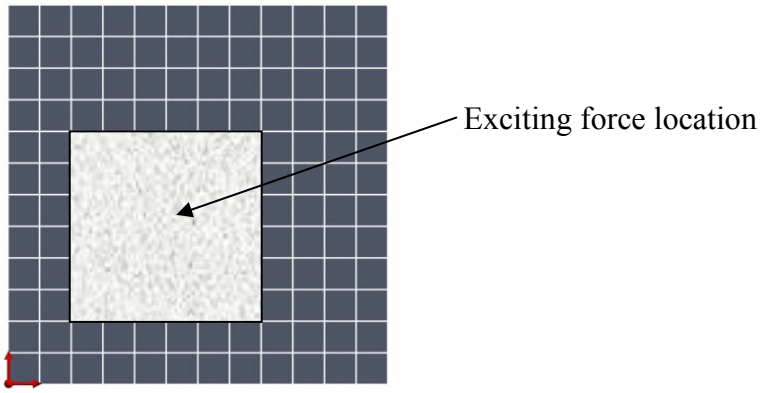

Figure 5.15: Exciting force location.

5.4.2 Results with plate vibration feedback:

Figures 5.16a through 5.16f show the theoretical acoustic and vibration responses at different locations in the acoustic cavity and over the base plate using vibration feedback. Figure 5.16g shows the control voltage required to achieve such attenuation.

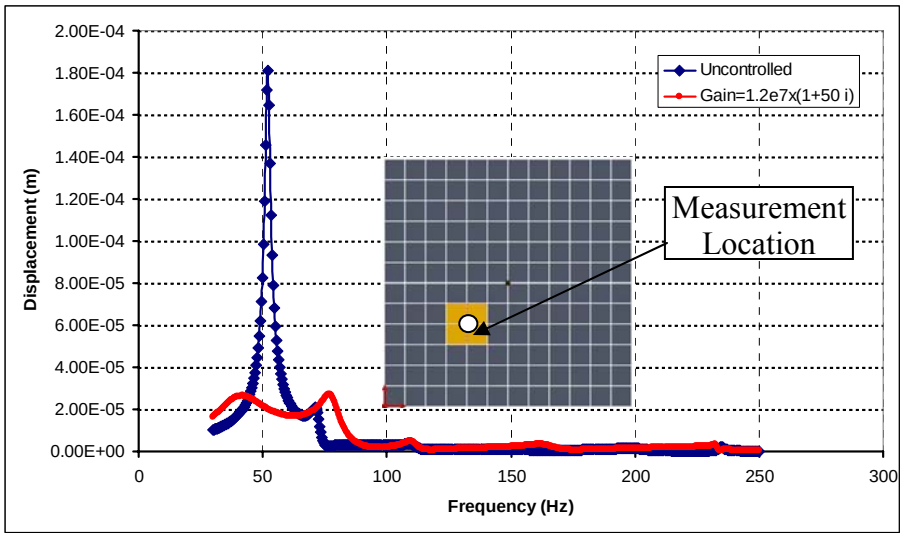

(a)

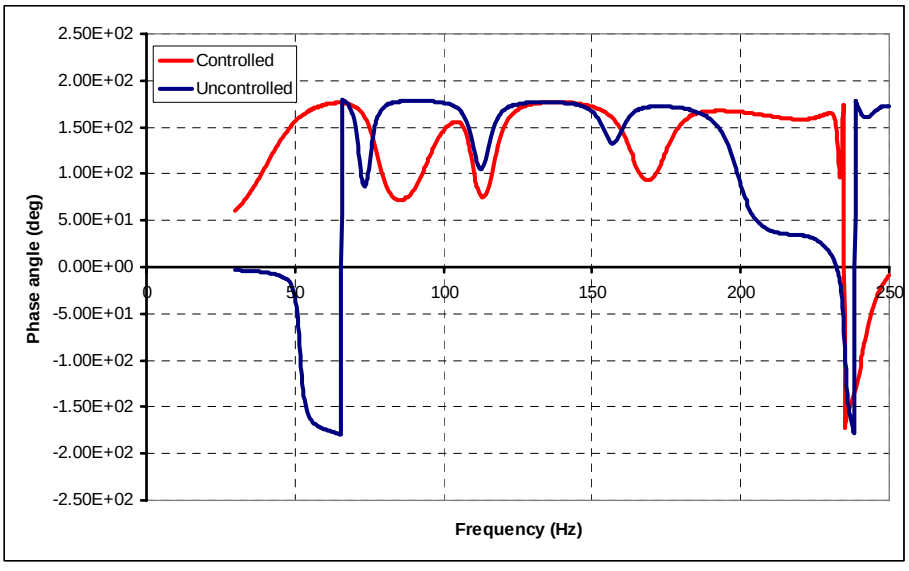

(b)

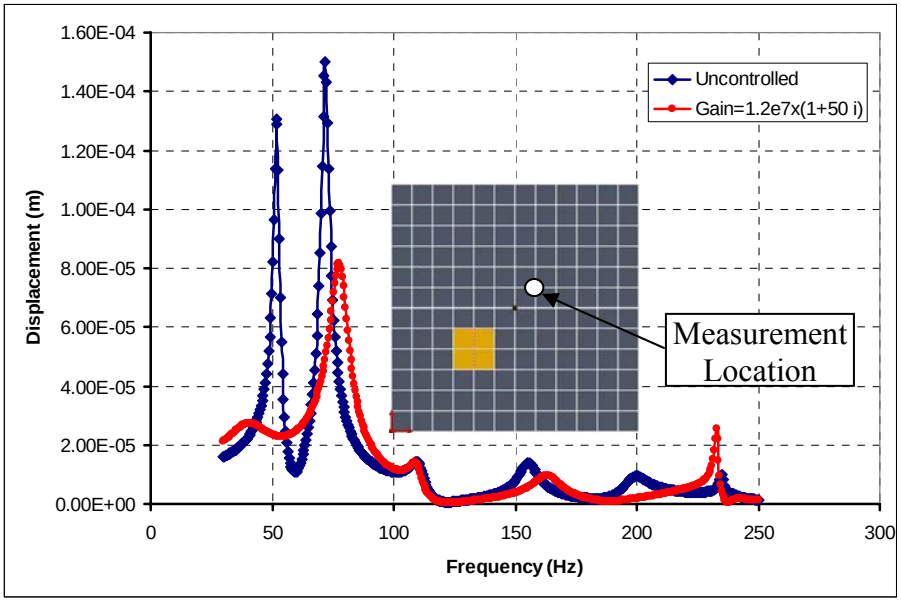
1.60E-04
1.40E-04
1.20E-04
1.00E-04
8.00E-05
6.00E-05
4.00E-05
2.00E-05
0.00E+00
Displacement (m)
0
50
100
150
200
250
300
Frequency (Hz)
Uncontrolled
Gain=1.2e7x(1+50 i)
Measurement Location

(c)

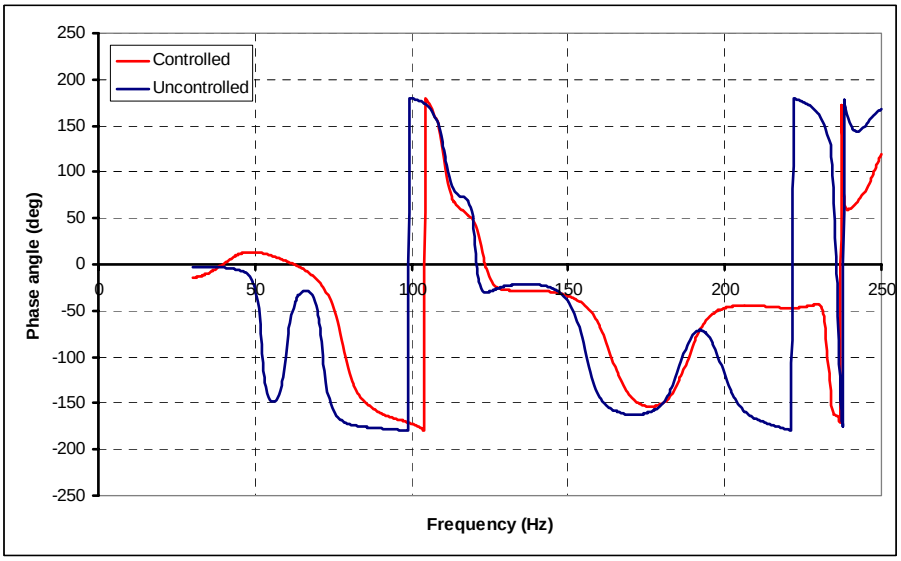
250
200
150
100
50
0
-50
-100
-150
-200
-250
Phase angle (deg)
0
50
100
150
200
250
Frequency (Hz)
Controlled
Uncontrolled

(d)

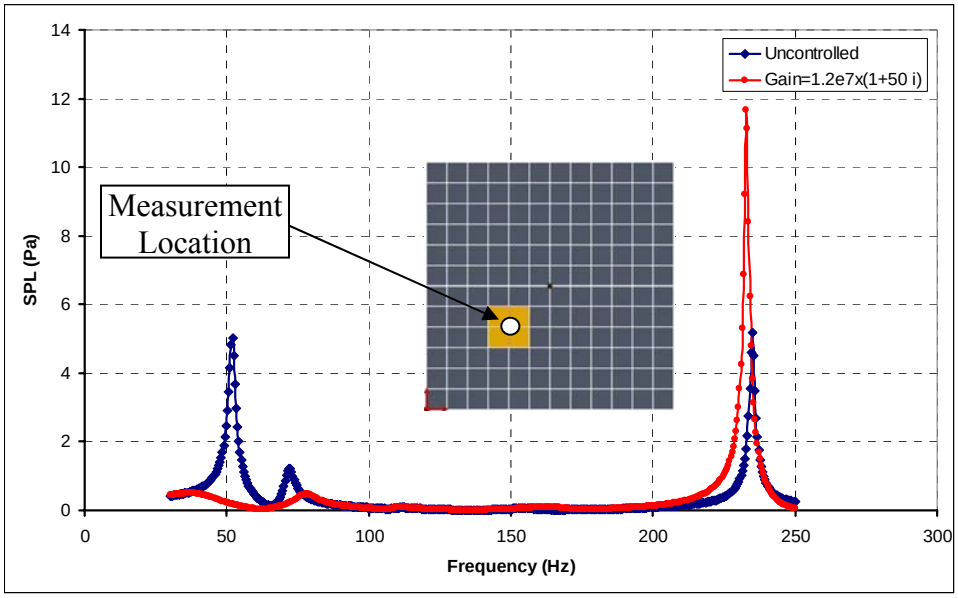
Uncontrolled
Gain=1.2e7x(1+50 i)
Measurement Location
SPL (Pa)
Frequency (Hz)
0
2
4
6
8
10
12
14
0
50
100
150
200
250
300

(e)

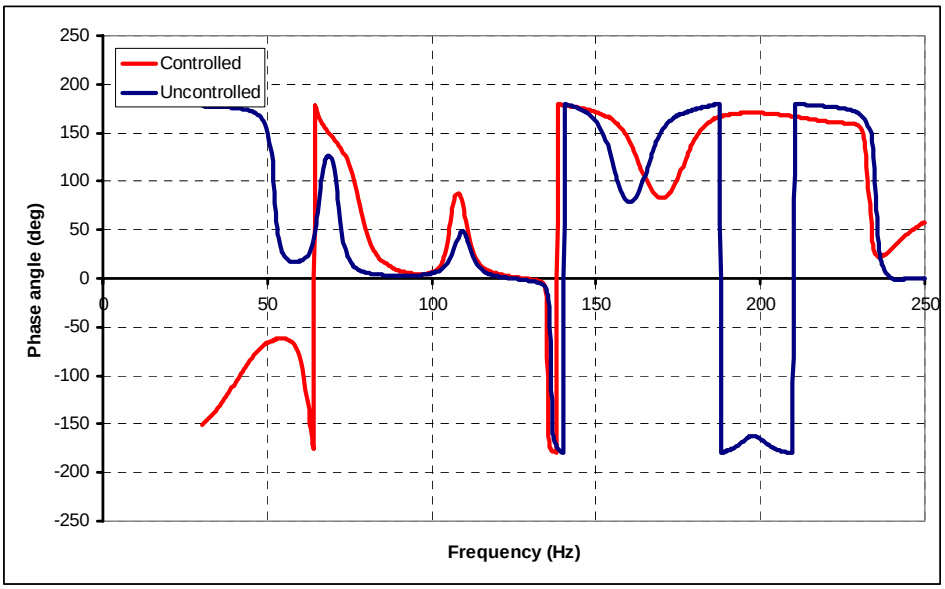
Controlled
Uncontrolled
Phase angle (deg)
Frequency (Hz)
250
200
150
100
50
0
-50
-100
-150
-200
-250
0
50
100
150
200
250

(f)

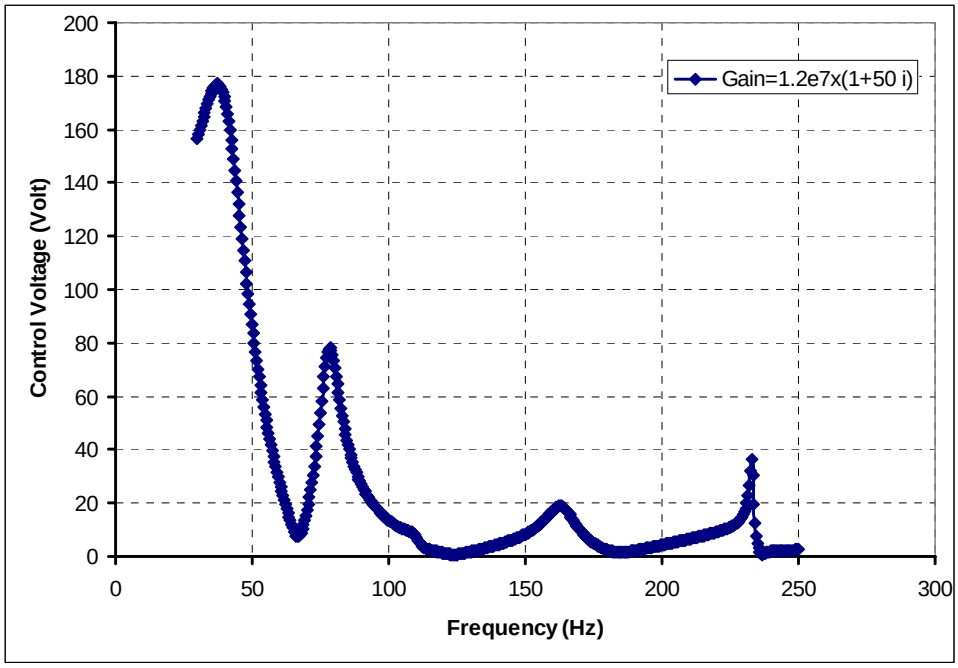

(g)

Figure 5.16: Theoretical performance with vibration feedback, (a-d) Flexural vibration measured at the nodes (5×5×1) and (8×8×1), (e, f) Sound pressure level measured at nodes(5×5×3) and (g) the control voltage.

It is evident from the shown frequency responses, that although a considerable attenuation of the base plate structural vibration and its associated noise was obtained, vibration feedback only couldn't affect the cavity noise modes appearing at 236 Hz.

5.4.3 Results with combined sound pressure and vibration feedback:

To overcome the inefficiency of vibration feedback alone to affect the cavity modes, sound pressure feedback was included in the control system. Figures 5.17a through 5.17d show the theoretical acoustic and vibration responses at different locations in the acoustic

cavity and over the base plate using vibration as well as sound pressure feedback, each with appropriate gain. Figure 5.17e shows the control voltage required to achieve such attenuation.

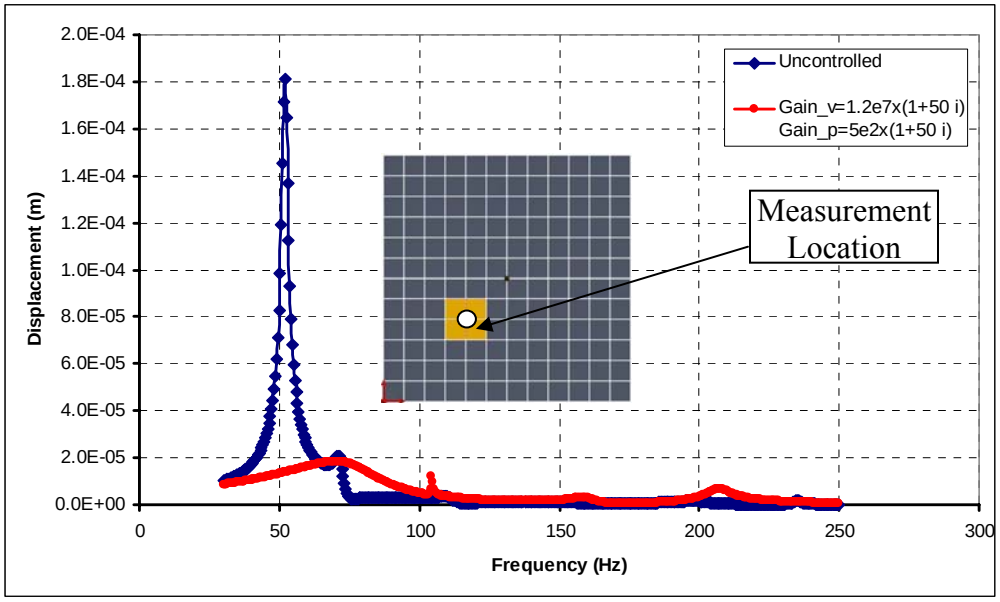

(a)

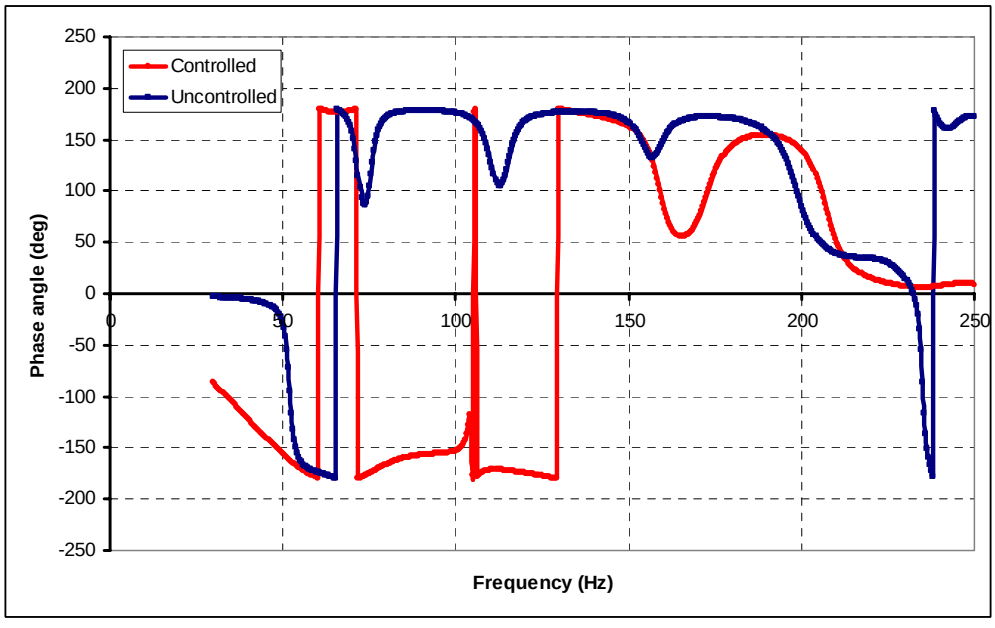

(b)

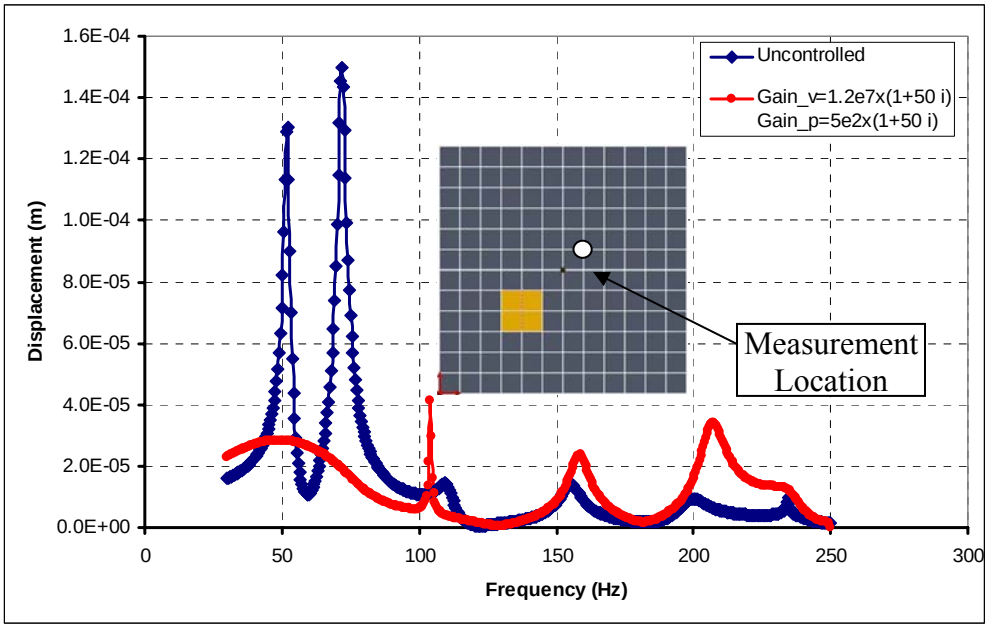
1.6E-04
1.4E-04
1.2E-04
1.0E-04
8.0E-05
6.0E-05
4.0E-05
2.0E-05
0.0E+00
Displacement (m)
0
50
100
150
200
250
300
Frequency (Hz)
Uncontrolled
Gain_v=1.2e7x(1+50 i)
Gain_p=5e2x(1+50 i)
Measurement Location

(c)

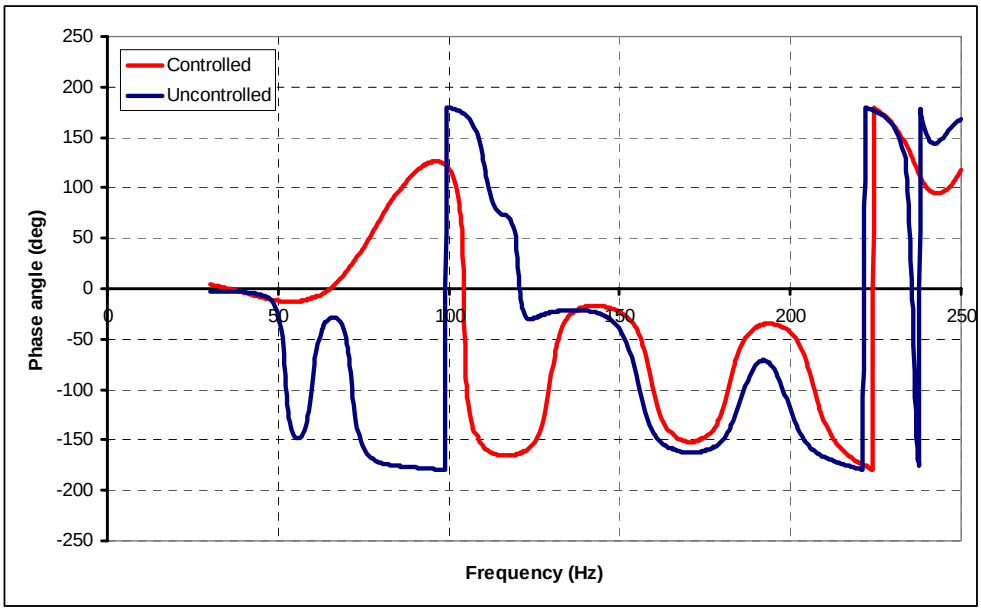
250
200
150
100
50
0
-50
-100
-150
-200
-250
Phase angle (deg)
0
50
100
150
200
250
Frequency (Hz)
Controlled
Uncontrolled

(d)

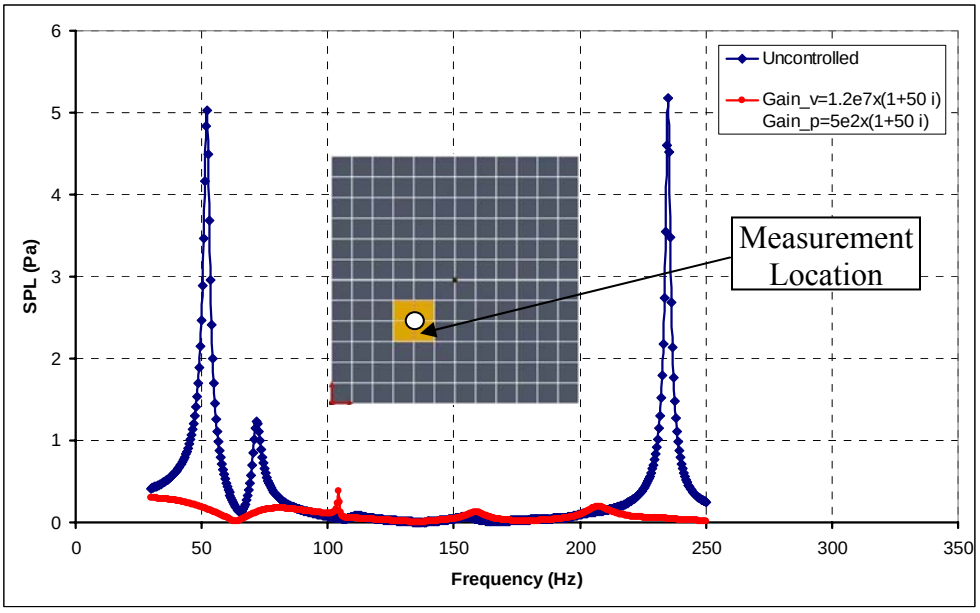
Uncontrolled
Gain_v=1.2e7x(1+50 i)
Gain_p=5e2x(1+50 i)
Measurement Location
SPL (Pa)
Frequency (Hz)
0
1
2
3
4
5
6
0
50
100
150
200
250
300
350

(e)

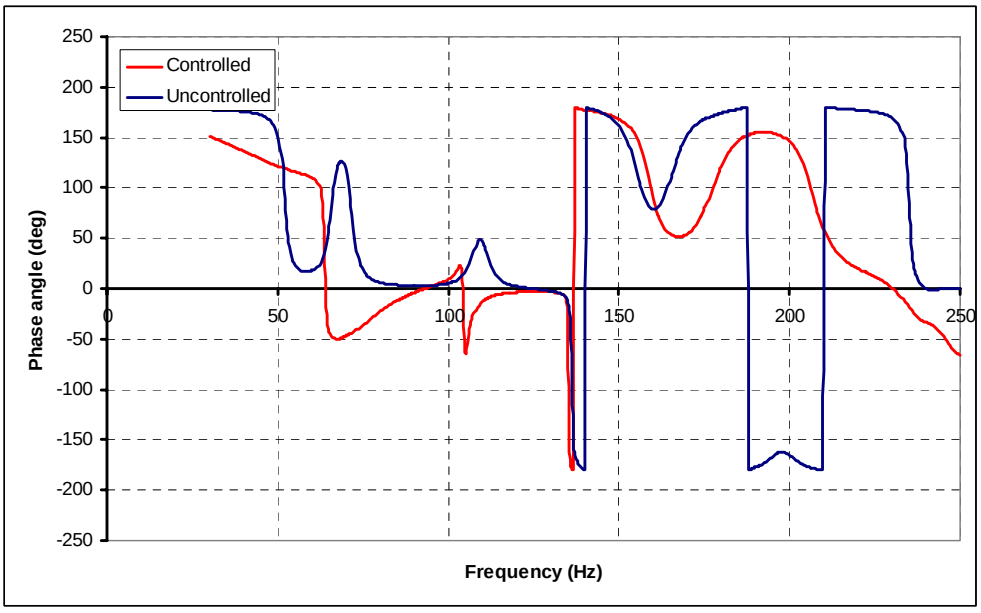
Controlled
Uncontrolled
Phase angle (deg)
Frequency (Hz)
250
200
150
100
50
0
-50
-100
-150
-200
-250
0
50
100
150
200
250

(f)

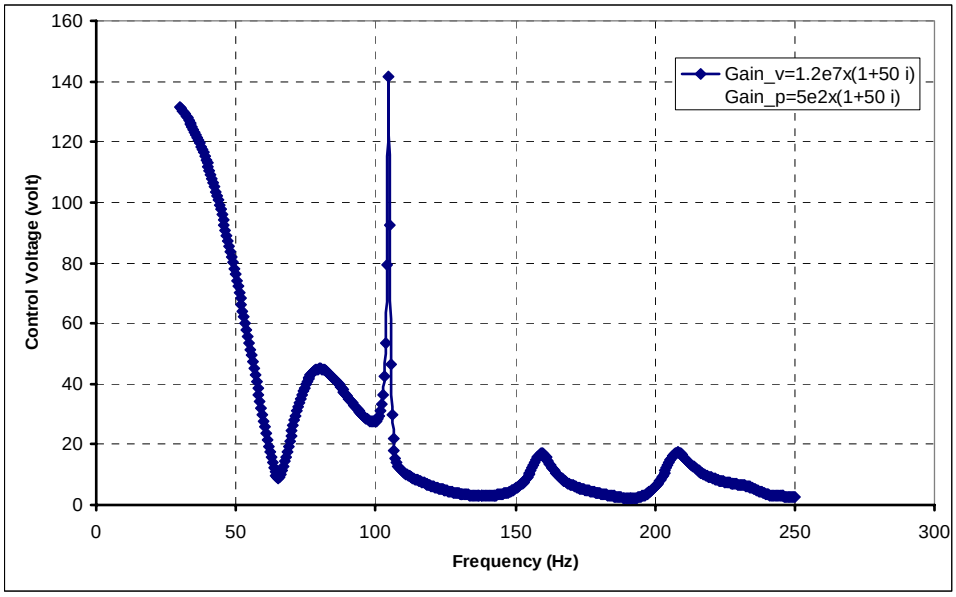

(g)

Figure 5.17: Theoretical performance with vibration and sound pressure feedback, (a-d) Flexural vibration measured at the nodes (5×5×1) and (8×8×1), (e, f) Sound pressure level measured at nodes(5×5×3) and (g) the control voltage.

Combining the vibration and sound pressure feedback signals and using appropriate control gains resulted in considerable attenuation of the flexural vibration of the base plate and the noise levels inside the cavity due to both structural vibration or cavity modes.

5.5 EXPERIMENTAL VALIDATION OF THE FINITE ELEMENT MODEL

The predictions of the aforementioned finite element model for the acoustic cavity coupled with an aluminum plate treated with 45° APDC smart foam patches was verified

against the experimental results.

5.5.1 Results with plate vibration feedback

The experimental plate flexural vibration as well as the sound pressure level measured inside the cavity are presented in Figures 5.18a through 5.18e for the uncontrolled and controlled cases. The displayed results are obtained with vibration feedback only.

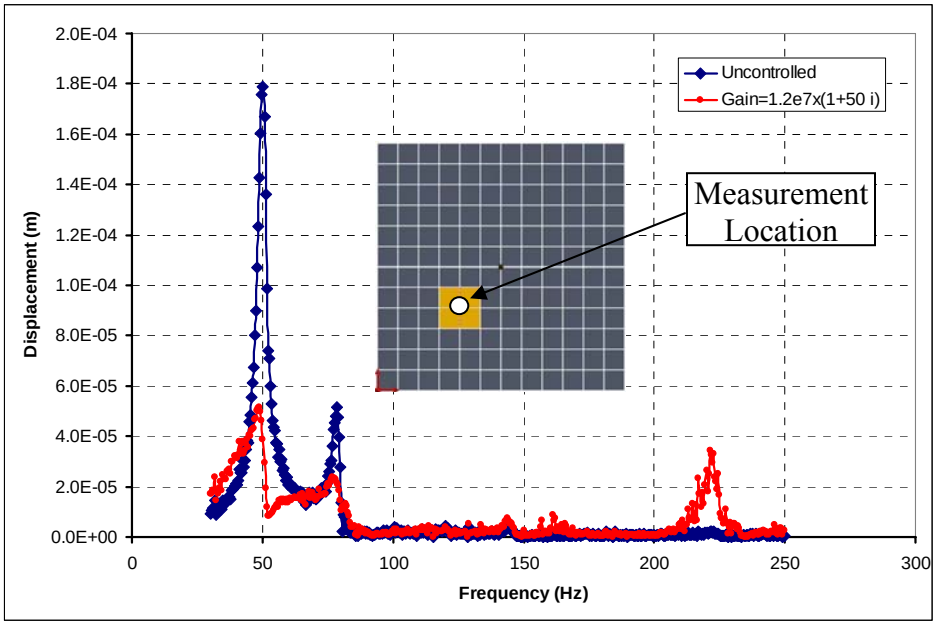

(a)

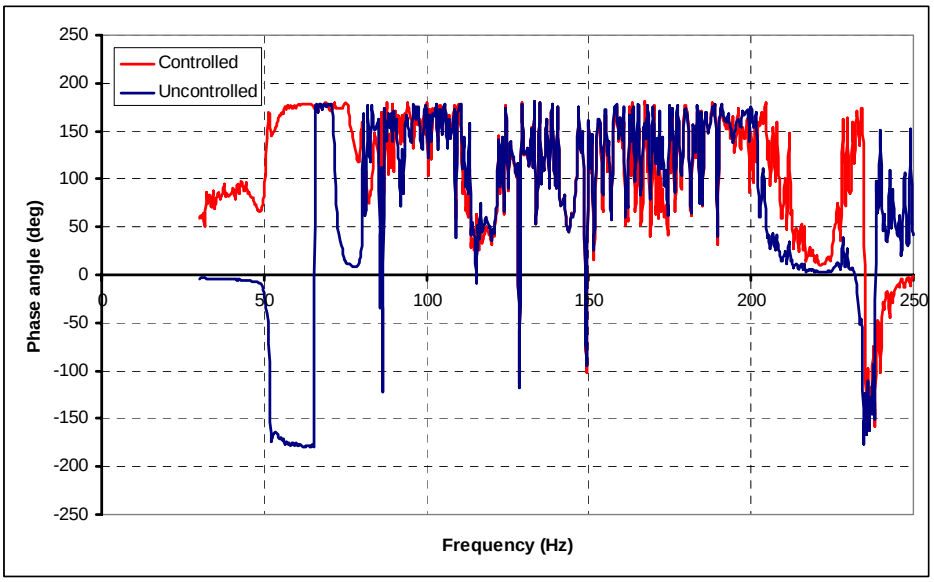
Controlled
Uncontrolled
Phase angle (deg)
Frequency (Hz)
250
200
150
100
50
0
-50
-100
-150
-200
-250
0
50
100
150
200
250

(b)

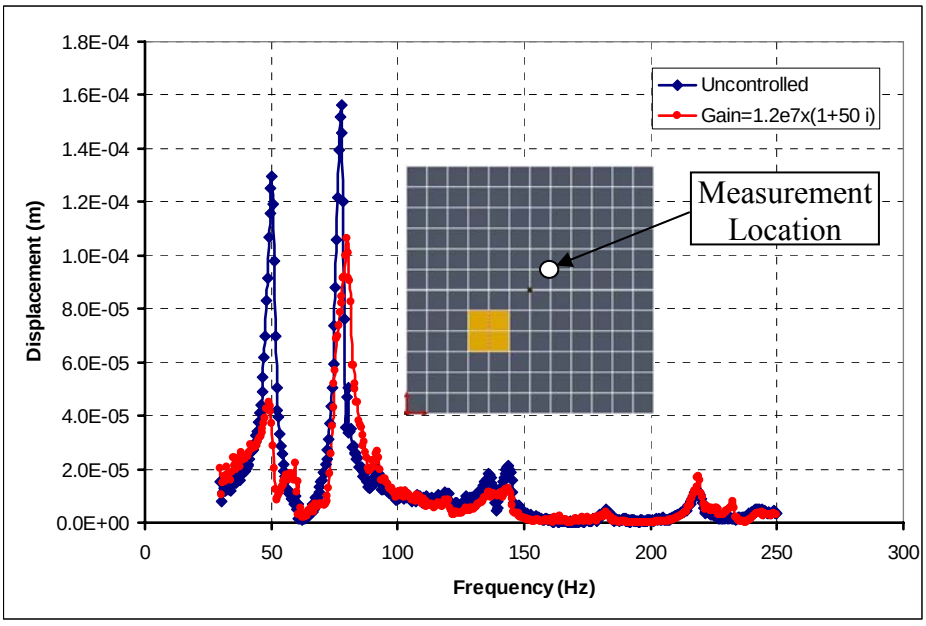
Uncontrolled
Gain=1.2e7x(1+50 i)
Measurement Location
Displacement (m)
Frequency (Hz)
1.8E-04
1.6E-04
1.4E-04
1.2E-04
1.0E-04
8.0E-05
6.0E-05
4.0E-05
2.0E-05
0.0E+00
0
50
100
150
200
250
300

(c)

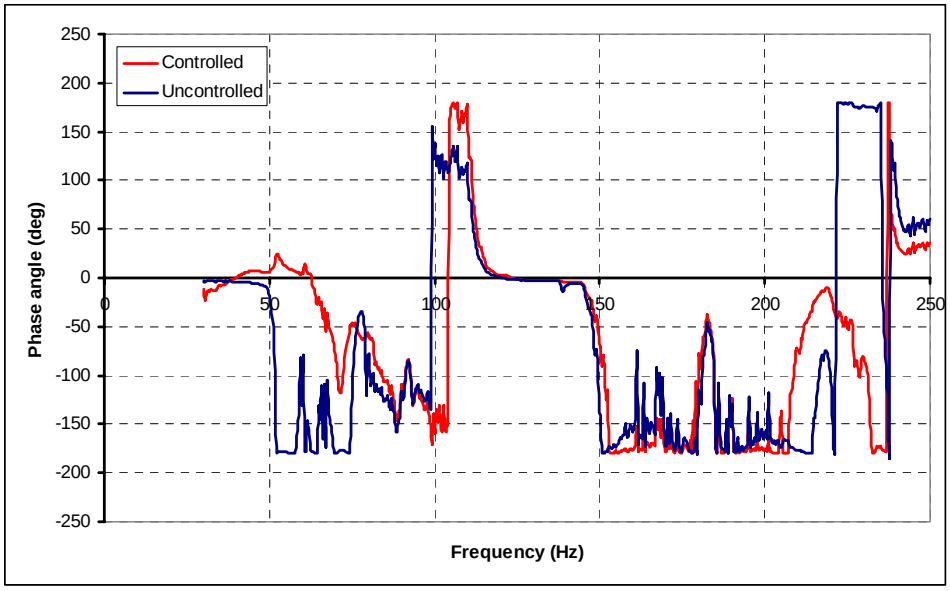
Controlled
Uncontrolled
Phase angle (deg)
Frequency (Hz)
250
200
150
100
50
0
-50
-100
-150
-200
-250
0
50
100
150
200
250

(d)

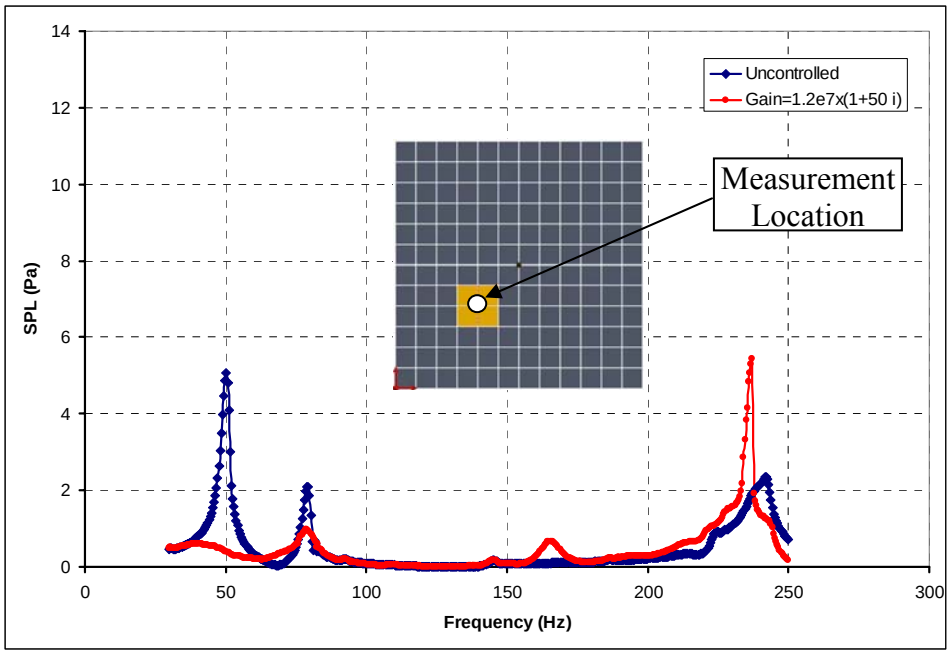
Uncontrolled
Gain=1.2e7x(1+50 i)
Measurement Location
SPL (Pa)
Frequency (Hz)
14
12
10
8
6
4
2
0
0
50
100
150
200
250
300

(e)

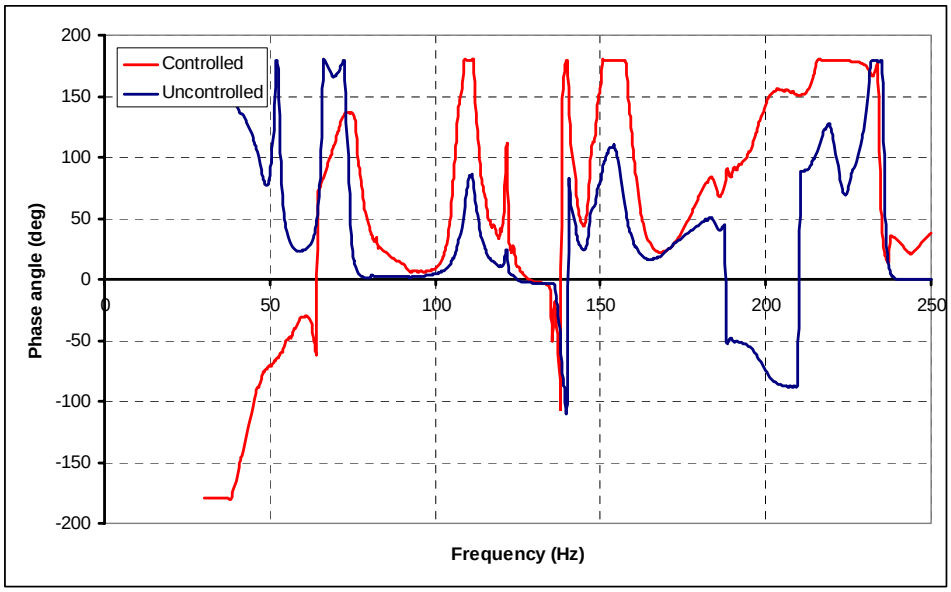

(f)

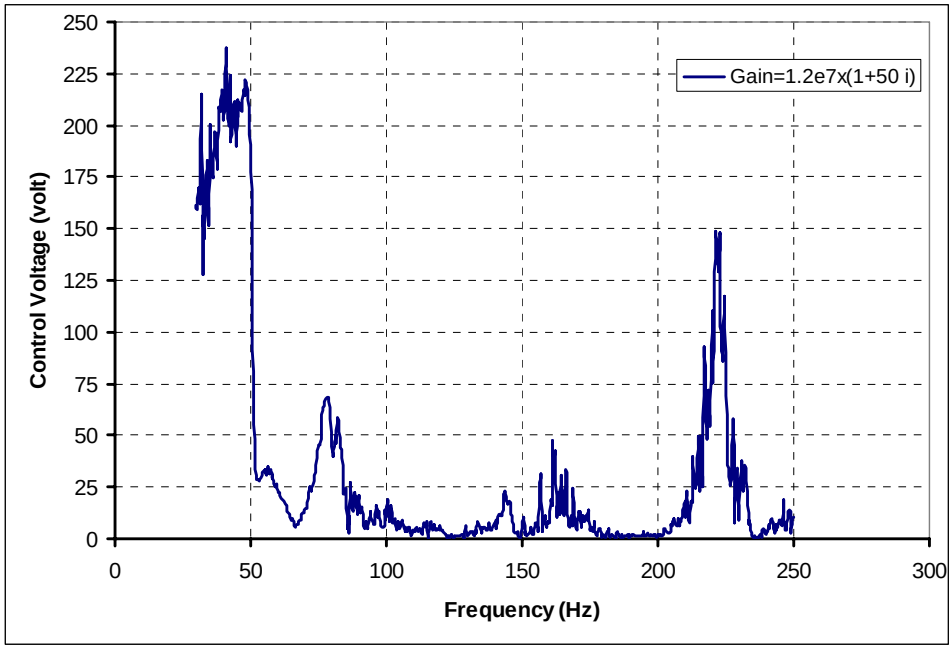

(g)

Figure 5.18: Experimental performance with vibration feedback, (a-d) Plate displacement measured at (4″,4″) and (7″,7″) from the lower left corner, (e, f) Sound Pressure Level measured at (4″,4″,2″) from the lower left corner of the plate and (g) the control voltage.

5.5.2 Results with combined sound pressure and vibration feedback

The experimental vibration response of the aluminum plate and the noise level inside the acoustic cavity are measured for the uncontrolled and controlled cases using vibration as well as sound pressure feedback.

Figures 5.19a through 5.19f show the experimental vibration and acoustic responses at different locations inside the acoustic cavity and over the base plate. Figure 5.19g shows the corresponding control voltage required to achieve such attenuation.

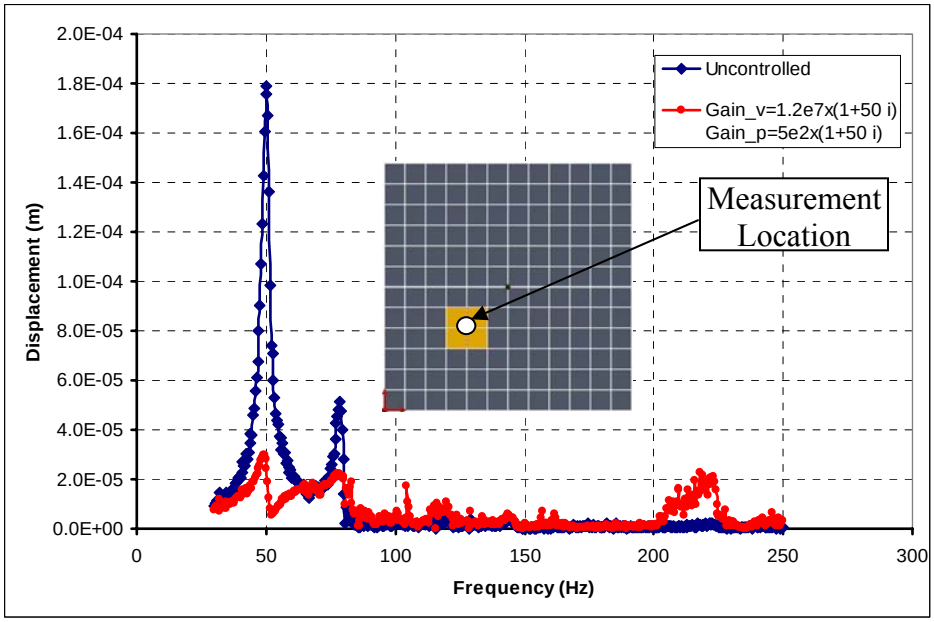

(a)

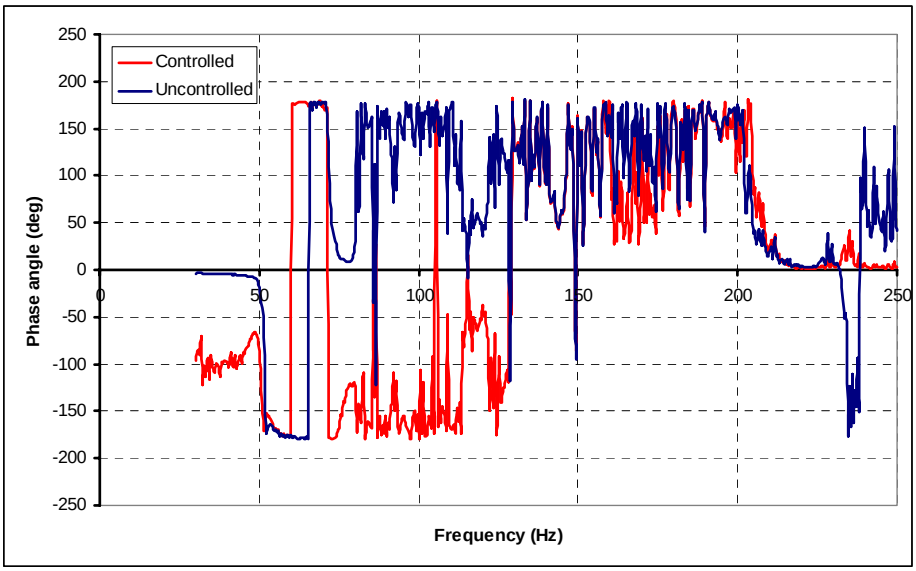
Controlled
Uncontrolled
Phase angle (deg)
Frequency (Hz)
250
200
150
100
50
0
-50
-100
-150
-200
-250
0
50
100
150
200
250

(b)

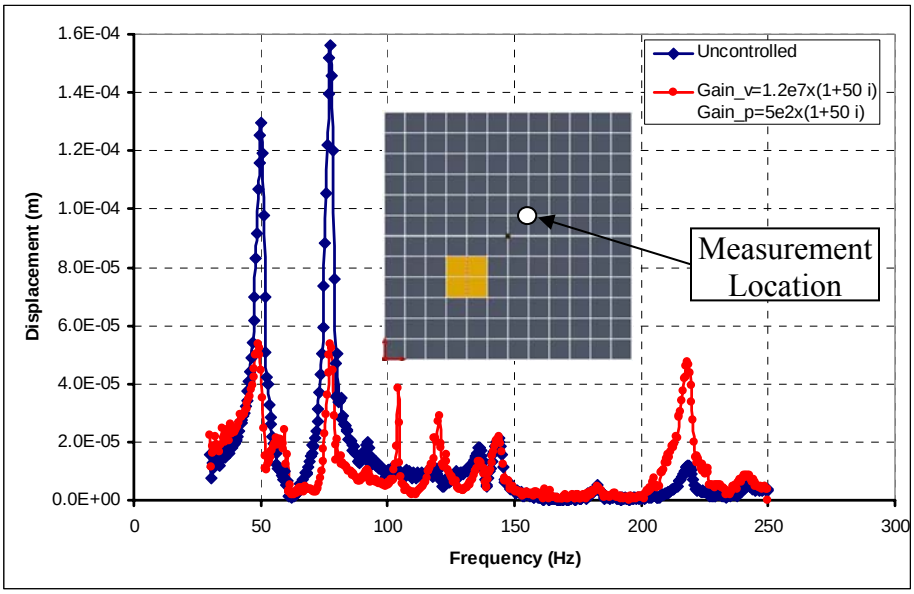
Uncontrolled
Gain_v=1.2e7x(1+50 i)
Gain_p=5e2x(1+50 i)
Measurement Location
Displacement (m)
Frequency (Hz)
1.6E-04
1.4E-04
1.2E-04
1.0E-04
8.0E-05
6.0E-05
4.0E-05
2.0E-05
0.0E+00
0
50
100
150
200
250
300

(c)

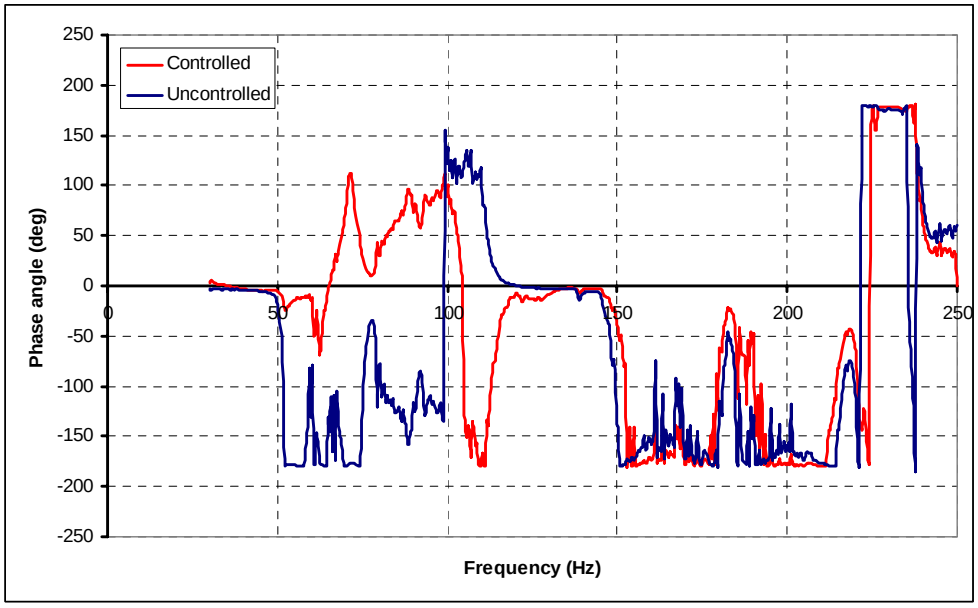
Controlled
Uncontrolled
Phase angle (deg)
Frequency (Hz)
250
200
150
100
50
0
-50
-100
-150
-200
-250
0
50
100
150
200
250

(d)

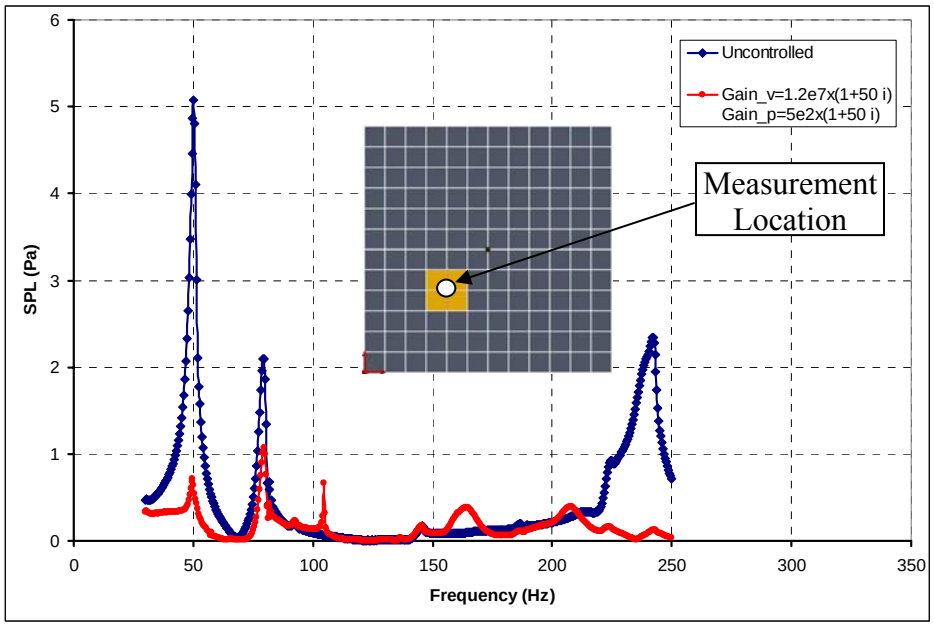
Uncontrolled
Gain_v=1.2e7x(1+50 i)
Gain_p=5e2x(1+50 i)
Measurement Location
SPL (Pa)
Frequency (Hz)
6
5
4
3
2
1
0
0
50
100
150
200
250
300
350

(e)

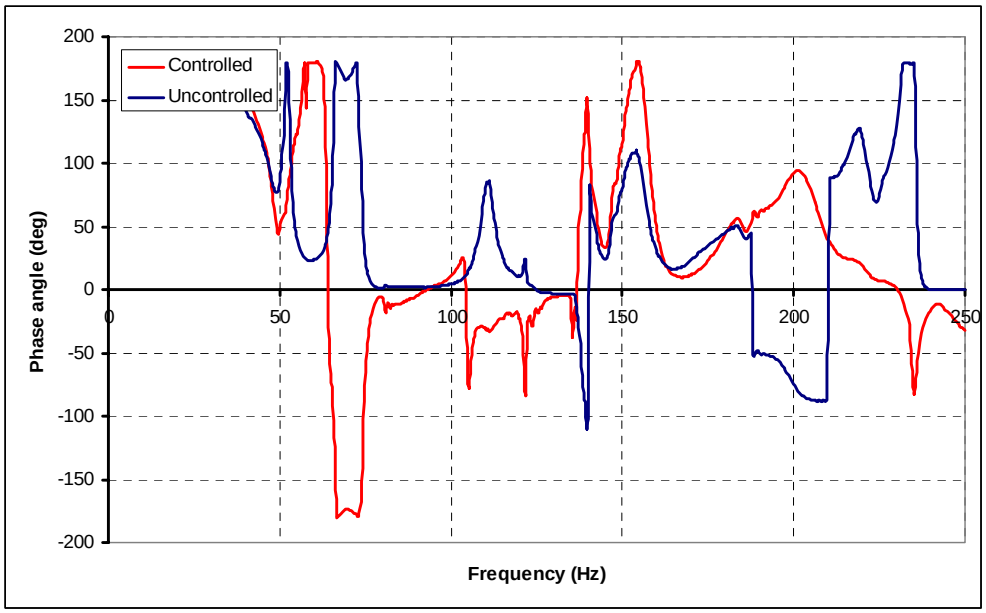

(f)

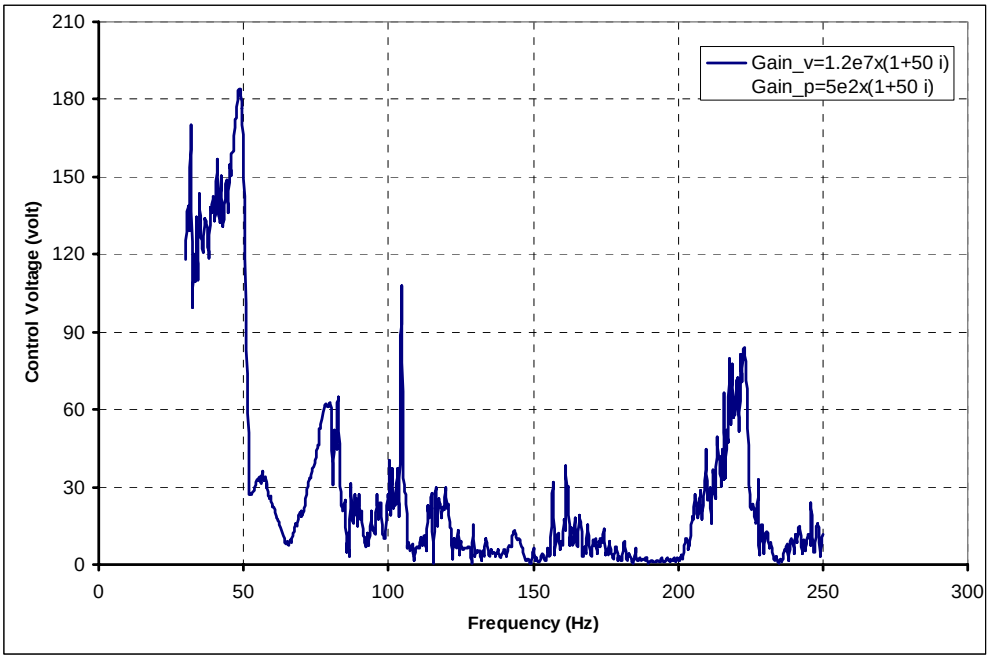

(g)

Figure 5.19: Experimental performance with vibration and sound pressure feedback, (a-d) Plate displacement measured at (4″,4″) and (7″,7″) from the lower left corner, (e, f) Sound Pressure Level measured at (4″,4″,2″) from the lower left corner of the plate and (g) the control voltage.

Comparisons between the theoretical predictions shown in Figures 5.16 and 5.17 as well as the experimental results shown in Figures 5.18 and 5.19 suggest a good agreement between the theoretical and experimental models. With only plate displacement feedback, it is observed that the controller is ineffective in controlling the first acoustic mode which is measured at 236 Hz. Using the combined plate displacement and sound pressure feedback has resulted in attenuation of both the plate flexural vibration as well as the noise inside the acoustic cavity.

5.6 SUMMARY

In this chapter, numerical evaluation of the absorption coefficient with feedback control was carried out, and high improvement of the absorption characteristics of the active foam was observed particularly at low frequencies. Both experimental and numerical results for evaluating the performance of the proposed hybrid passive / active actuator are presented. Tests for measuring the absorption characteristics of the foam using the impedance tube have been conducted, and considerable improvement in the absorption characteristics have been recorded. Using the hybrid actuator for simultaneous vibration and noise control has demonstrated promising results particularly over the low frequency regions. Finite element model of the entire system was developed and the vibration and acoustic responses of the plate/cavity system were calculated. The predictions of the model are validated experimentally and a good agreement is shown between theory and experiments.

CHAPTER 6

CONCLUSIONS AND RECOMMENDATIONS

6.1 CONCLUSIONS

This dissertation has presented a new class of smart foams that can be used to simultaneously control the vibration and noise radiation from vibrating plates coupled with acoustic cavities. The theoretical bases governing the operation of this class of smart foams are presented. Detailed 3-dimensional and 2-dimensional finite element models of the smart foam have been developed. The development of the 2-D model constitutes a major contribution of this study as it enables its integration with models of 2-D structural members as plates. Such compatible integration enhances the computational effort and makes it a very effective predictive tool.

The absorption characteristics of the smart foam are determined theoretically and experimentally, when the foam is controlled actively using Active Piezoelectric Damping Composites (APDC) in various configurations. It was concluded that controlling the transverse deformation of the smart foam is very effective in improving its absorption characteristics as compared to controlling its in-plane deformation.

Finite element models have also been developed to model the interaction between the smart foam and vibrating plates and acoustic cavities. The predictions of the models are validated experimentally by using appropriate feedback of the plate vibration and/or the sound pressure inside the cavity; both proportional and derivative feedback control strategies are used.

The obtained results indicate that feeding back both the plate vibration and cavity pressure is very effective in attenuating both structural vibration and the acoustic cavity modes. Such effectiveness is attributed to the fact that the actuator has the APDC component to influence directly the structural vibration and the foam to attenuate the acoustics of the cavity. It is mentioned that the proposed actuator configuration as it is bonded directly on the structure makes it very suitable for many practical applications. This practicality is attractive, since the actuator does not have any components that can take space inside the acoustic cavity as is the case when speakers are used as actuators.

The obtained theoretical and experimental results demonstrate the feasibility of the concept of smart foam as an effective tool for simultaneous control of vibration and noise. For example, with both vibration and sound pressure feedback, vibration and noise attenuations of about 90% are obtained with control voltages of less than 180 volts.

The developed theoretical and experimental techniques can be invaluable tools for the design and application of the smart foam to a wide variety of systems such as passenger cars, helicopters, and aircraft cabins.

6.1 RECOMMENDATIONS

Although this dissertation has presented a comprehensive investigation of the new class of smart foams, there are many issues that remain to be addressed. Important among these issues is the optimization and sizing of the design parameters of the actuator. Development of appropriate optimization strategies will be essential to the adoption of

the actuator in various practical applications. Along the same lines, optimal placement and number of the actuators on the vibrating structures is important to realize the effective attenuation of the vibration and noise over broad frequency bands. Another important issue that has not been considered is the effect of the operating temperature on the performance of the actuator. Issues related to performance degradation with temperature and the use of the appropriate control strategies to compensate for such degradation must be considered.

A natural extension of this work is to consider the use of the smart foam in controlling the vibration and noise radiation from shells. This extension will be invaluable because of the importance of the shells in many applications such as aircraft cabins and payload fairings.

Also, although our emphasis has been placed on combining passive foam with APDC, it is natural to consider making the foam itself active by making it from a piezoelectric material, for example, or any other smart material. In this manner, the control of the sound absorption can be envisioned to be direct and more efficient. Other modifications of the configuration of the smart foam are only limited by our imagination.

APPENDIX A.1

PROPERTIES OF THE ELEMENTS USED IN THE EXPERIMENTAL STUDY

IMPEDANCE TUBE EXPERIMENT

Passive foam:

Table A.1: Passive foam properties

Diameter (m)	0.0508
thickness (m)	0.00635
Bulk density of solid phase (kg/m^3)	30
In vacuo Young's Modulus (N/m^2)	8×10^5
In vacuo loss factor	0.265
Bulk Poisson's Ratio	0.4
Flow resistivity (MKS Rayls/m)	25×10^3
Structure factor	7.8
Porosity	0.9

Table A.2: APDC properties

Width (m)	0.0254
Length (m)	0.0254
Polymer matrix thickness (mm)	3.175
Volume fraction (%)	15

Table A.3 Physical properties of the piezoelectric rods

Parameter	**PZT-5**	**PZT-5H**
c_{11}^{E} $(10^{10}\ \mathrm{N/m^2})$	12.1	15.1
c_{12}^{E} $(10^{10}\ \mathrm{N/m^2})$	7.54	9.8
c_{13}^{E} $(10^{10}\ \mathrm{N/m^2})$	7.52	9.6
c_{33}^{E} $(10^{10}\ \mathrm{N/m^2})$	11.1	12.4
c_{23}^{E} $(10^{10}\ \mathrm{N/m^2})$	2.11	1.4
c_{22}^{E} $(10^{10}\ \mathrm{N/m^2})$	2.16	2.65
e_{33} $(\mathrm{C/m^2})$	15.8	27
e_{15} $(\mathrm{C/m^2})$	12.3	20
e_{13} $(\mathrm{C/m^2})$	-5.4	-5.1
$e_{33}^{s} / \varepsilon_0$	830	1500
$e_{11}^{s} / \varepsilon_0$	916	1700

Table A.4 Physical properties of polymer matrix

Parameter	**Hard Polyurethane**	**Soft Polyurethane**
c_{11} $(10^{10}\ \mathrm{N/m^2})$	0.3	0.001667
c_{12} $(10^{10}\ \mathrm{N/m^2})$	0.29	0.001664

ACOUSTIC CAVITY

Table A.5 Physical properties of the acoustic cavity / aluminum plate

Acoustic cavity length (m)	0.3048
Acoustic cavity width (m)	0.3048
Acoustic cavity depth (m)	0.762
Aluminum plate width (m)	0.3048
Aluminum plate length (m)	0.3048
Aluminum plate thickness (m)	3.97×10^{-4}
Aluminum plate Young's modulus ($\mathrm{N/m^2}$)	70×10^{9}
Aluminum plate density ($\mathrm{kg/m^3}$)	2700
Aluminum plate Poisson's ratio	0.3
Aluminum plate loss factor	0.03

REFERENCES

1. **Alam, N. and Asnani, N. T.,** "Vibration and Damping Analysis of Multilayered Rectangular Plates with Constrained Viscoelastic Layers" , *Journal of Sound and Vibration*, Vol. 97, pp. 597-614, 1984.

2. **Arafa, M. and Baz, A.** "Dynamics of Active Piezoelectric Damping Composites" , *Journal of Composites*, Part B, Vol. 31, pp. 255-264, 2000.

3. **ASTM Standards** "Standard Test Method for Impedance and Absorption of Acoustical Materials by the Impedance Tube Method", Designation: C 384-98, 1998.

4. **ASTM Standards** "Standard Test Method for Impedance and Absorption of Acoustical Materials using a Tube, Two Microphones and a Digital Frequency Analysis System", Designation: E 1050-98, 1998.

5. **Atalla, N., Panneton, R. and Debergue, P.,** "A mixed displacement-pressure formulation for poroelastic materials" , *Journal of the Acoustical Society of America*, Vol. 104, No. 3, pp. 1444-1452, September 1998.

6. **Avellaneda, M. and Swart, P. J.,** "Calculating the Performance of 1-3 Piezoelectric Composites for Hydrophone Applications: An Effective Medium Approach" , *Journal of the Acoustical Society of America*, Vol. 103, No. 3, pp. 1449-1467, March 1998.

7. **Balamurugan, V. and Narayanan, S.,** "Active Vibration Control of Smart Shells using Distributed Piezoelectric Sensors and Actuators" , *Journal of Smart Materials and Structures*, Vol. 10, pp. 173-180, 2001.

8. **Baruh, H.**, *Analytical Dynamics*, McGraw-Hill, 1998.

9. **Baz, A.,** "Active Constraint Layer Damping", US patent (5,485,053), 1996.

10. **Baz, A. and Ro, J.,** "Vibration Control of Rotating Beams with Active Constrained Layer Damping" , *Journal of Smart Materials and Structures,* Vol. 10, pp. 112-120, 2001.

11. **Baz, A. and Ro, J.,** "The Concept and Performance of Active Constrained Layer Damping Treatments" , *Sound and Vibration*, Vol. 28, pp. 18-21, March 1994.

12. **Baz, A. and Ro, J.,** "Vibration Control of Plates with Active Constrained Layer Damping" , *Journal of Smart Materials and Structures*, Vol. 5, pp. 272-280, 1996.

13. **Baz, A. and Tempia, A.,** "Active Piezoelectric Damping Composites", *accepted in Journal of Sensors and Actuators B,* 2004.

14. **Biot, M. A.**, "Theory of propagation of elastic waves in a fluid-saturated porous solid" , *Journal of the Acoustical Society of America*, Vol 28, pp. 168-191, 1956.

15. **Blanguernon, A., Léné, F. and Bernadou, M.,** "Active Control of a Beam using a Piezoceramic Element" , *Journal of Smart Materials and Structures*, Vol. 8, pp. 116-124, 1999.

16. **Bolton, J. and Green, E.,,** "Smart Foams for Active Absorption of Sound", *Second Conference on Recent Advances in Active Noise Control of Sound and Vibration, Blacksburg, VA*, pp. 139-149, 1993.

17. **Chan, H. L. W. and Unsworth, J.,** "Simple Model for Piezoelectric Ceramic/Polymer 1-3 Composites Used in Ultrasonic Transducer Applications" , *IEEE Transactions on Ultrasonics, Ferroelectrics and Frequency Control*, Vol. 36, No. 4, pp. 434-441, January 1989.

18. **Chen, T. and Baz, A.,** "Performance Characteristics of Active Constrained Layer Damping Versus Passive Constrained Layer Damping" , SPIE, vol. 2715, pp. 256-268, 1996.

19. **Chung, J. and Blaser, D.,** "Transfer Function Method of Measuring In-duct Acoustic Properties. I. Theory" , *Journal of the Acoustical Society of America*, Vol. 68, No. 3, pp. 907-913, Sept. 1980.

20. **Chung, J. and Blaser, D.,** "Transfer Function Method of Measuring In-duct Acoustic Properties. I. Experiment" , *Journal of the Acoustical Society of America*, Vol. 68, No. 3, pp. 914-921, Sept. 1980.

21. **Clark, R. and Fuller, C.,** "Experiments on Active Control of Structurally Radiated Sound using Multiple Piezoceramic Actuators" , *Journal of the Acoustical Society of America*, Vol. 91, No. 6, pp. 3313-3320, June 1992.

22. **Conover, W. B. and Ringlee, R. J.,** "Recent contributions to transformer audible noise control" , *Transactions of the AIEE Part III, Power apparatus and systems*, Vol. 74, pp. 77-90, 1955.

23. **Dauchez, N., Sahraoui, S. and Atalla, N.,** "Investigation and Modeling of Damping in a Plate with a bonded Porous Layer" , *Journal of Sound and Vibration,* Vol. 265, pp. 437-449, 2003.

24. **Elliot, S., Nelson, P., Stothers, I., and Boucher, C.,** "In-flight Experiments on the Active Control of Propeller-Induced Cabin Noise" , *Journal of Sound and Vibration*, Vol. 140, No. 2, pp. 219-238, 1990.

25. **Fuller C. R., Elliot S. J. and Nelson P. A.**, *Active control of vibration*, Academic Press publisher, 1997.

26. **Fuller, C., Hansen, C., and Snyder, S.,** "Active Control of Sound Radiation from a Vibrating Rectangular Panel by Sound Sources and Vibration Inputs: An Experimental Comparison" , *Journal of Sound and Vibration*, Vol. 145, No. 2, pp. 195-215, 1991.
27. **Fuller, C., Hansen, C. and Snyder, S.,** "Experiments on Active Control of Sound Radiation from a Panel using a Piezoceramic Actuator" , *Journal of Sound and Vibration*, Vol. 150, No. 2, pp. 179-190, 1991.

28. **Furstoss, M., Thenail, D. and Galland, M.,** " Surface Impedance Control for Sound Absorption: Direct and Hybrid Passive/Active Strategies" , *Journal of Sound and Vibration*, Vol. 203, pp. 219-236, 1997.

29. **Gentry, C., Guigou, C. and Fuller, C.,** "Smart Foam for Applications in Passive-Active Noise Radiation Control" , *Journal of the Acoustical Society of America*, Vol. 101, No. 4, pp. 1771-1778, April 1997.

30. **Gu, Y., Clark, R.L., Fuller, C. R. and Zander, A.C.**, "Experiments on Active Control of Plate Vibration Using Piezoelectric Actuators and Polyvinylidine Fluoride (PVDF) Modal Sensors" , *Journal of Vibration and Acoustics*, Vol. 116, pp. 303-308, July 1994.

31. **Guicking, D. and Lorenz, E.,** "An Active Sound Absorber with Porous Plate" , *Journal of Vibration, Acoustics, Stress and Reliability in Design*, Vol. 106, pp. 389-392, 1984.

32. **Guigou, C. and Fuller, C.,** "Adaptive Feedforward and Feedback Methods for Active/Passive Sound Radiation Control using Smart Foam" , *Journal of the Acoustical Society of America*, Vol. 104, No. 1, pp. 226-231, July 1998.

33. **Hagood N. W. and von Flotow, A.,** "damping of Structural Vibrations with Piezoelectric Materials and Passive Electrical Networks" , *Journal of Sound and Vibration*, Vol. 146, No. 2, pp. 243-268, 1991.

34. **Hull, A.,** "The Modal Decomposition of an Impedance Tube" , *Structural Acoustics, NUWC Division Newport Technical Digest*, pp. 82-92, June 1995.

35. **Kang, Y. J. and Bolton, J. S.,** "Finite Element Modeling of Isotropic Elastic Porous Materials Coupled with Acoustical Finite Elements" , *Journal of the Acoustical Society of America*, Vol. 98, No. 1, pp. 635-643, July 1995.

36. **Kang, Y. J. and Bolton, J. S.,** "A finite element modeling for sound transmission through foam-lined double-panel structures" , *Journal of the Acoustical Society of America*, Vol. 99, No. 5, pp. 2755-2765, May 1996.

37. **Kang, Y. J., Gardner, B. K. and Bolton, J. S.,** "An axisymmetric poroelastic finite element formulation" , *Journal of the Acoustical Society of America*, Vol. 106, No. 2, pp. 565-574, August 1999.

38. **Kim, Y., Kim, G. and Roh, C.,** "Active Noise Control with a Hybrid Control Algorithm using an Active/Passive Smart Foam Actuator" , *Smart Structures and Materials 2002, Proceedings of SPIE*, Vol. 4701, pp.413-425.

39. **Kinsler, L., Frey, A., Coppens, A. and Sanders, J.,** *Fundamentals of Acoustics*, 4th edition, John Wiley & Sons Inc, 1999.

40. **Lueg, P.**, "Process of silencing sound oscillations", US Patent No. 2043416, 1936.

41. **Meyer, J. L., Harrington, W. B., Agrawal, B. N. and Song, G.,** "Vibration Suppression of a Spacecraft Flexible Appendage using Smart Material" , *Journal of Smart Materials and Structures*, Vol. 7, pp. 95-104, 1998.

42. **Oh, J., Poh, S., Ruzzene, M. and Baz, A.,** "Vibration Control of Beams Using Electro-Magnetic Compressional Damping Treatment" , *Journal of Vibration and Acoustics*, Vol. 122, pp. 235-243, July 2000.

43. **Orsagh, R. and Ghoneim, H.,** "Experimental Investigation of Electro-mechanical Surface Damping" , Smart Materials and Structures Conference in Damping, 3672, pp. 234-241, 1999.

44. **Pan, J. and Hansen, C.,** "Active Control of Noise Transmission through a Panel into a Cavity. II: Experimental Study" , *Journal of the Acoustical Society of America*, Vol. 90, No. 3, pp. 1488-1492, September 1991.

45. **Pan, J., Hansen, C. and Bies, D.,** "Active Control of Noise Transmission through a Panel into a Cavity. II: Analytical Study" , *Journal of the Acoustical Society of America*, Vol. 87, pp. 2098-2108, 1990.

46. **Poh, S., Baz, A. and Balachandran, B.,** "Experimental Adaptive Control of Sound Radiation from a Panel into an Acoustic Cavity using Active Constrained Layer Damping" , *Journal of Smart Materials and Structures*, Vol. 5, pp. 649-659, 1996.

47. **Portis, B. L.,** "Piezoelectric Composites for Use in Adaptive Damping Concepts" , Proceedings of Damping 1993, Vol. 2 of 3. pp. GBB1-GBB18.

48. **Ro, J. and Baz, A.** "Control of Sound Radiation from a Plate into an Acoustic Cavity using Active Constrained Layer Damping" , *Journal of Smart Materials and Structures*, Vol. 8, pp. 292-300, 1999.
49. **Ruzzene, M., Oh, J. and Baz, A.,** "Finite Element Modeling of Magnetic Constrained Layer Damping" , *Journal of Sound and Vibration*, Vol. 236, No. 4, pp. 657-682, 2000.

50. **Shen, I. Y.,** "Hybrid Damping through Intelligent Constrained Layer Treatments" , *Journal of Vibration and Acoustics*, Vol. 116, pp. 341-349, 1994.

51. **Shiau, N.,** "Multi-dimensional wave propagation in elastic porous materials with applications to sound absorption, transmission and impedance measurement" , *PhD Thesis, Purdue University*, May-1991.

52. **Shields, W., Ro, J. and Baz, A.,** "Control of Sound Radiation from a Plate into an Acoustic Cavity using Active Piezoelectric-Damping Composites" , *Journal of Smart Materials and Structures*, Vol. 7, pp. 1-11, 1998.

53. **Simon, B., R., Wu, J., S., S., Zienkiewicz, O., C. and Paul, D. K.,** "Evaluation of u-w and u-π finite element methods for the dynamic response of saturated porous media using one-dimensional models" , Int. J. Num. Analytical Methods Geomech., Vol. 10, pp 461-482, 1986.

54. **Smith, W. A.,** "Modeling 1-3 Composite Piezoelectrics: Hydrostatic Response" , *IEEE Transactions on Ultrasonics, Ferroelectrics and Frequency Control*, vol. 40, No. 1, pp. 41-49, January 1993.

55. **Smith, W. A. and Auld, B. A.,** "Modeling 1-3 Composite Piezoelectrics: Thickness Mode Oscillation" , *IEEE Transactions on Ultrasonics, Ferroelectrics and Frequency Control*, Vol. 38, No. 1, pp. 40-47, January 1991.

56. **Smith, J., Johnson, B. and Burdisso, R.,** "A Broadband Passive-Active Sound Absorbing System" , *Journal of the Acoustical Society of America*, Vol. 106, No. 5, pp. 2646-2652, April 1999.

57. **Swart, P. J. and Avellaneda, M.,** "The Role of Matrix Porosity and Poisson's Ratio on the Design of High-Sensitivity Piezocomposite Transducers" , *Adaptive Structures and Composite Materials: Analysis and Applications, ASME*, AD-Vol. 45/MD-Vol. 54, pp. 59-66, 1994.

58. **Yang, S. M. and Chiu, J. W.,** "Smart Structures-Vibration of Composites with Piezoelectric Materials" , *Journal of Composite Structures*, Vol. 25, pp. 381, 1993.

59. **Zienkiewicz, O., C., "**Numerical methods in Geomechanics", edited by J. B. Martins (Reidel, Dordrecht, The Netherlands, 1982), pp. 39-55.